Brush-Modified Materials: Control of Molecular Architecture, Assembly Behavior, Properties and Applications

Jiajun Yan[a,c], Michael R. Bockstaller[b], Krzysztof Matyjaszewski*[a]*

[a] Department of Chemistry and [b] Department of Materials Science & Engineering, Carnegie Mellon University, Pittsburgh, Pennsylvania 15213, United States.

[c] Present address: Materials Sciences Division, Lawrence Berkeley National Laboratory, Berkeley, California 94720, United States.

KEYWORDS: polymer brush, hybrid materials, inorganic nanoparticles, reversible deactivation radical polymerization, ATRP

Abstract

Recent progress in surface-initiated polymerization enables the deliberate polymer modification of nanoscopic surfaces with high levels of precision. This has given rise to the development of brush particle-based materials (sometimes referred to as 'hairy nanoparticles') that are formed by tethering of polymer chains to the surface of nanoparticle-like objects. Brush particles have attracted interest as model systems to understand the effect of surface modification on the structure and interactions in polymer modified colloidal systems (which play a role across fields as diverse as functional coatings, cosmetics, foods or pharmaceuticals) but also as building blocks for the assembly of 'one-component hybrid materials' that exhibit unprecedented property combinations, not realizable in classical composite materials. This review presents a summary and analysis of the developments in the field of 'particle brush materials'. The evolution of synthetic methodologies from the original pioneering work to emerging trends and opportunities in the field

of brush synthesis is presented first. Subsequently, the effect of brush architecture on the structure, interaction and assembly of brush particles both with and without a matrix is discussed. Finally, recent advances in the development of functional hybrid materials with applications in energy, catalysis, sensing and other areas is presented.

Graphical Abstract

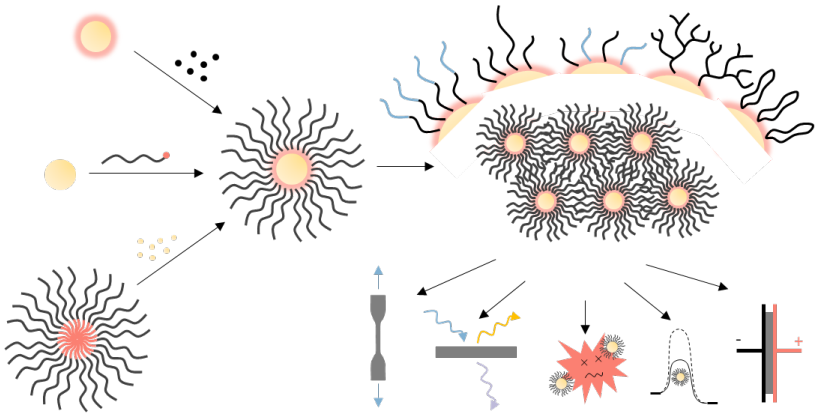

Table of Contents

Nomenclature

a	length of a repeat
AFM	atomic force microscopy
AP	anionic polymerization
A(R)GET	activator (re)generation by electron transfer
ATRP	atom transfer radical polymerization
-b-	*-block-*
bcc	body-centered cubic
BCP	block copolymer
BiBADA	12-(2-bromoisobutyramido)dodecanoic acid
BMWD	bimodal molecular weight distribution
BSA	bovine serum albumin
CB	conduction band
CD	cyclodextrin
CPB	concentrated polymer brush
CPDB	4-(4-cyanopentanoic acid) dithiobenzoate
CRP	controlled radical polymerization
CT	computed tomography
CTA	chain-transfer agent
CuAAC	copper-catalyzed azide-alkyne cycloaddition
d	diameter OR brush height
Đ	dispersity
dc	diamond cubic
DC	Daoud and Cotton
DEPN	*N*-*tert*-butyl-*N*-(1-diethylphosphono-2,2-dimethylpropyl) nitroxide

DFT	density functional theory
d_{ip}	interparticle distance
DLS	dynamic light scattering
DMSO	dimethyl sulfoxide
DNA	deoxyribonucleic acid
DOTA	1,4,7,10-Tetraazacyclododecane-1,4,7,10-tetraacetic acid
DP	degree of polymerization
*e*ATRP	electrochemically-mediated atom transfer radical polymerization
EGaIn	eutectic gallium-indium alloy
E_{pc}	cathodic peak potential
f	number of chains
f_x	weight fraction of x
fcc	face-centered cubic
FRP	(conventional) free radical polymerization
h	(brush) height
hcp	hexagonal close packed
HOMO	highest occupied molecular orbital
$h\nu$	photoirradiation
ICAR	initiator for continuous activator regeneration
IgG	immunoglobin G
K_{Ic}	stress intensity factor for mode I fracture
l	segment length
LAP	living anionic polymerization
LC	liquid crystal
LCP	living cationic polymerization

LCST	lower critical solution temperature
LED	light-emitting diode
MADIX	macromolecular design via interchange of xanthates
Me_6TREN	tris(2-(dimethylamino)ethyl)amine
M_n	number-average molecular weight
MRI	magnetic resonance imaging
M_w	weight-average molecular weight
MW	molecular weight
MWC	Millner, Witten, and Cates
MWD	molecular weight distribution
n	refractive index
N	degree of polymerization
N_A	Avogadro number
NHS	*N*-hydoxysuccinimide
NIR	near infrared
NMP	nitroxide-mediated polymerization
NP	nanoparticle
OEGA	oligo(ethylene glycol acrylate)
OMRP	organometallic-mediated radical polymerization
P2VP	poly(2-vinylpyridine)
P4VP	poly(4-vinylpyridine)
PAA	poly(acrylic acid)
PAAm	polyacrylamide
PAN	polyacrylonitrile
PAPTAC	poly(3-(acrylamido)propyl(trimethyl)ammonium chloride)

PBA	poly(*n*-butyl acrylate)
PBiBEM	poly(2-(2-bromoisobutyryloxy)ethyl methacrylate)
PDMAEMA	poly(2-(dimethylamino)ethyl methacrylate)
PDMS	poly(dimethylsiloxane)
PEA	poly(ethyl acrylate)
PEDOT	poly(3,4-ethylenedioxythiophene)
PEG	poly(ethylene glycol)
PEGMA	poly(ethylene glycol) methacrylate
PenG	penicillin G
PEO	poly(ethylene oxide)
PET	photoinduced electron transfer
PGMA	poly(glycidyl methacrylate)
PHEMA	poly(2-hydroxyethyl methacrylate)
photoATRP	photochemically-mediated atom transfer radical polymerization
PIMP	photoiniferter-mediated polymerization
PMA	poly(methyl acrylate)
PMAA	poly(methacrylic acid)
PMDETA	*N*,*N*,*N*',*N*'',*N*''-pentamethyldiethylenetriamine
PMMA	poly(methyl methacrylate)
PNIPAM	poly(*N*-isopropylacrylamide)
POSS	polyhedral oligomeric silsesquioxane
PPE	poly(phenylene ethynylene)
PPG	poly(propylene glycol)
PRISM	polymer reference interaction site model
PS	polystyrene

PSS	poly(4-styrene sulfonate)
PSAN	poly(styrene-*co*-acrylonitrile)
P*t*BA	poly(*tert*-butyl acrylate)
PVP	poly(*N*-vinyl-2-pyrrolidone)
QD	quantum dot
QLED	quantum dot light emitting diode
R	radius
RAFT	reversible addition-fragmentation chain-transfer
RDRP	reversible deactivation radical polymerization
R_g	radius of gyration
RITP	reversible iodine transfer polymerization
RNA	deoxyribonucleic acid
ROMP	ring-opening metathesis polymerization
ROP	ring-opening polymerization
SAM	self-assembled monolayer
SARA	supplemental activator and reducing agent
SCFT	self-consistent field theory
SCVP	self-condensing vinyl polymerization
SDPB	semidilute polymer brush
SEC	size-exclusion chromatography
SFRP	stable free radical mediated polymerization
SI-	surface-initiated
SPIO	superparamagnetic nanoparticles
S-RAFT	surface reversible addition-fragmentation chain-transfer
St	styrene

TEM	transmission electron microscopy
TERP	organotellerium-mediated radical polymerization
TFA	trifluoroacetic acid
T_g	glass transition temperature
TGA	thermogravimetric analysis
THF	tetrahydrofuran
TMS	trimethylsilyl
TPMA	tris(2-pyridinylmethyl)amine
TSI	thermal self-initiation
UCL	upconversion luminescence
$U(r)$	repulsion potential
VB	valence band
WZ	Wijmans and Zhulina
ε	permittivity
λ	wavelength
v	excluded volume parameter
$V(r)$	effective pair interaction potential
$\xi(r)$	size of a thermal blob
χ	Flory Huggins interaction parameter
ϱ	(bulk) density
ϱ_s	grafting density (on surface)
σ	grafting density
ϕ	volume fraction

1. Introduction

Future advancements in areas such as electronics, transportation, bioengineering, and energy will depend on polymer science to develop materials that combine light weight, high mechanical stability with novel optical, electronic or thermal transport properties. To accomplish this task, hybrid materials, *i.e.* materials combining a polymeric with other (organic, inorganic, or biological) material constituents play an important role. Inspiration for how complex property combinations can be realized in hybrid materials can be drawn from structural biology. A well-known example is nacre that forms the inner shell of certain molluscs. Here, the combination of proteins and ceramic platelets (*i.e.* materials that are individually weak or brittle) into a layered nanocomposite structure results in a high-performance structural material with order of magnitude increase of strength and toughness.[1] During the past 25 years, polymer nanocomposite materials, in which a polymer matrix is admixed with nanoparticle fillers have attracted significant attention to address the need for novel functional materials. The addition of nanofillers offers the opportunity to augment the properties of the matrix without sacrificing the economic formability characteristics of the polymer host. The potential to design polymeric materials with tailored or improved optical, electronic or mechanical properties as well as wear or thermal resistance has rendered 'polymer nanocomposites' one of the most active areas in current polymer science and engineering. However, despite the advances in the field of polymer nanocomposites, synthetic materials often fall short of the complex functional features of their natural counterparts. Natural materials (such as nacre) often display property amplifications that are beyond rule-of-mixture predictions and also exhibit the ability to dynamically respond, self-heal or adapt in changing environments. 'Learning from nature' thus implies developing the ability to design and synthesize complex structured hybrid materials in which the connectivity and interactions between

components gives rise to novel and synergistic property combinations. One aspect, critical to achieving these functionalities, is the control or the structure and interactions across interfaces between the distinct components.

Recent advances in the field of surface-initiated polymerization provide a tool set to realize 'polymer canopies' on surfaces with precisely controlled molecular characteristics, composition and hierarchical internal microstructure. Applied to the surface of nanoparticles, this has given rise to the field of 'particle brush materials' – a novel class of hybrid materials that promise unprecedented property combinations. This review highlights recent developments and concepts in the field of particle-brush hybrid materials, emphasizing synthetic approaches that facilitate the precise tailoring of the architecture of polymer canopies, current understanding of the role of architecture on the interaction and the assembly behavior of brush particles as well as emerging applications of particle brush-type materials across areas such as electronics, optics, energy and biomedical engineering. We also point out existing challenges in this area and discuss the needs and opportunities for future research in the field. However, to provide context for the subsequent discussion, and to acknowledge the significance of the milestones accomplished by pioneers in the field, we begin this review with a brief summary of the historical evolution of the field of surface-initiated polymerization.

2. A Brief History of Surface Polymerization

The important milestones in the evolution of the preparation of polymer-based hybrid materials are summarized in **Fig. 1**.

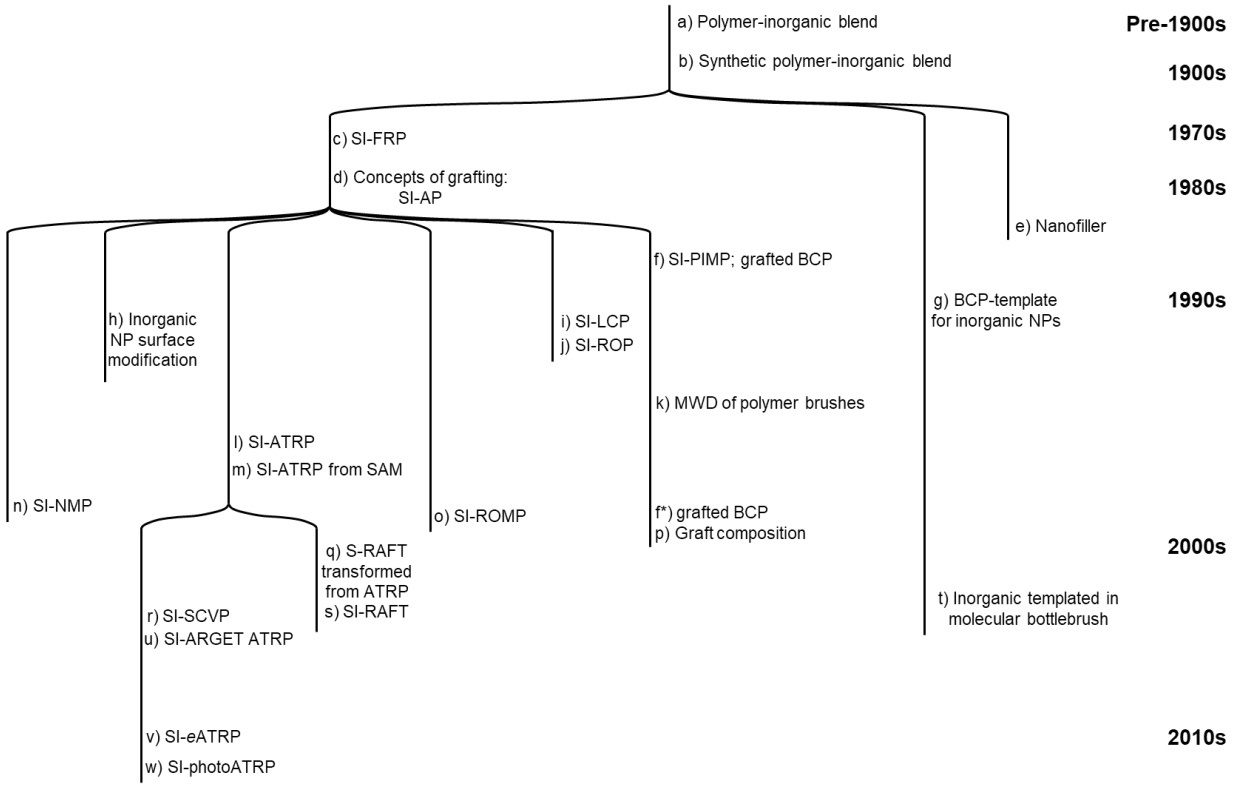

Fig. 1. Development of polymer-based hybrid materials. (a) Inorganic-reinforcement of natural rubber; Goodyear 1856.[2]. (b) Inorganic-reinforcement of synthetic polymer; Baekeland 1907.[3] (c) Free-radical polymerization from a silica surface; Laible and Hamann 1975.[4] (d) Concepts of grafting and surface-initiated anionic polymerization; Laible and Hamann 1980.[5] (e) Silica nanoparticles used as filler in poly(dimethylsiloxane) network; Mark and Pan 1982.[6] (f) Surface-initiated photoiniferter-mediated polymerization and (claimed) grafted block copolymer *without* evidence; Otsu, et al. 1986.[7] * Grafted block copolymer with *chromatographic* evidence. Matyjaszewski, et al. 1999.[8] (g) Inorganic nanoclustered templated in block copolymer self-assembly; Möller, et al. 1991.[9] (h) Surface modification of inorganic nanoparticles; Alivisatos, et al. 1992.[10] (i) Surface-initiated living cationic polymerization from silica surfaces; Spange, et al. 1992. [11] (j) Surface-initiated ring-opening polymerization; Whitesell, et al. 1993.[12] (k) Bimodal polymer brushes on air-liquid surface; Kent, et al. 1996.[13] (l) Surface-initiated atom

transfer radical polymerization (SI-ATRP) from porous silica; Wirth, et al. 1997.[14] (m) SI-ATRP from self-assembled monolayer of initiator on surface; Fukuda, et al. 1998.[15] (n) Surface-initiated nitroxide-mediated polymerization; Russell and Hawker, et al. 1999.[16] (o) Surface-initiated ring-opening metathesis polymerization; Grubbs, et al. 1999.[17] (p) Binary polymer grafts from surface; Minko and Stamm, et al. 1999.[18] (q) Surface reversible addition-fragmentation chain-transfer polymerization by transformation from a SI-ATRP chain end; Fukuda, et al. 2001.[19] (r) Surface-initiated self-condensing vinyl polymerization; Müller, et al. 2002.[20] (s) Surface-initiated reversible addition-fragmentation chain-transfer polymerization; Brittain, et al. 2002.[21] (t) Polymer-gold hybrid nanorods synthesized from molecular bottlebrush templates; Schmidt, et al. 2002.[22] (u) SI ATRP by activator regeneration by electron transfer (ARGET); Matyjaszewski, et al. 2007.[23] (v) Surface-initiated electrochemically-mediated atom transfer radical polymerization; Zhou, et al. 2012.[24] (w) Surface-initiated photochemically-mediated atom transfer radical polymerization; Zhou, et al. 2013.[25, 26]

The first demonstration of growing polymer chains from an inorganic surface was not accomplished until the 1970s.[4] In 1980, the three most commonly adopted grafting approaches, 'grafting-from', 'grafting-onto', and 'grafting-through' were demonstrated, **Fig. 2**.[5] This pioneering contribution was also the first report of surface-initiated anionic polymerization (SI-AP) and immobilization of azo-initiator on a surface.

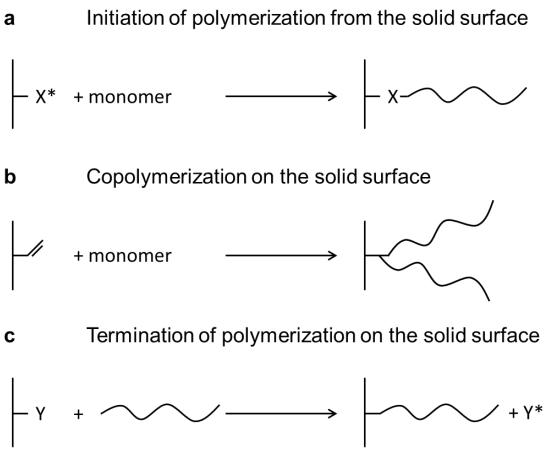

Fig. 2. Principles of polymerization reactions on solid surfaces, often termed as (a) 'grafting-from', (b) 'grafting-through' and (c) 'grafting-onto'. [5], Copyright 1980. Adapted with permission from Elsevier Science Ltd.

After these initial contributions, an outburst of research on new concepts and methodologies in several relevant areas took place during the 1980s. A series of reports and patents on polymer incorporation on exfoliated single layers of silicates by researchers from Toyota around 1990 were generally accepted as the origin of application-driven research in polymer-inorganic hybrid materials.[27-31] Photoiniferter-mediated polymerization (PIMP) belongs to a general class of reversible addition-fragmentation chain transfer (RAFT) polymerization. In fact, the first example of surface-initiated reversible deactivation radical polymerization (SI-RDRP)[32] was SI-PIMP.[7] This was also the first report of moderate control of molecular weight (MW) and arguably the first architecture control of surface-grafted polymers. Although successful grafting of block copolymer (BCP) was claimed, no solid evidence was provided other than demonstration of monomer conversion and an increase in molecular weight. A better defined BCP grafted from inorganic surfaces was reported more than a decade later.[8]

Nanoparticle surface modification and the pursuit of controlled/living polymerization procedures provide the current foundation for the synthesis of polymer-inorganic hybrid materials. Surface initiated living cationic polymerization (SI-LCP), reported in 1992, brought 'livingness' to surface-initiated polymerization.[11] In the same year, surface-modification was used to attach semiconductor NPs to flat surfaces.[10] Two years later, a more robust sol-gel method was demonstrated.[33] Surface-initiated ring-opening polymerization (SI-ROP) was developed during the same time period, although no livingness was discussed in the first report.[12] RDRP procedures developed around the 1990s, especially atom transfer radical polymerization (ATRP),[34] significantly enriched the toolbox of controlled polymerization. Although the first example of SI-ATRP was reported in 1997,[14] no control over the polymerization was demonstrated as the primary goal was to graft polymer onto porous silica for the production of chromatographic fillers. A controlled polymerization was achieved by treating a surface with self-assembled monolayer (SAM) of initiators one year later, **Fig. 3**.[15] Later, better controlled SI-ATRP with good chain-end fidelity was demonstrated in the absence of untethered sacrificial initiator.[8] This approach was subsequently used for the development of well-defined, high-density polymer grafts from (nano)particles.[35-39] Living cationic SI-ROP,[40] surface-initiated nitroxide-mediate polymerization (SI-NMP),[16] surface-initiated ring-opening metathesis polymerization (SI-ROMP)[17] were developed in late 1990s. In addition to macroscopic flat

surfaces and spherical particles, surface-initiated polymerization was also demonstrated from concave surfaces.[41]

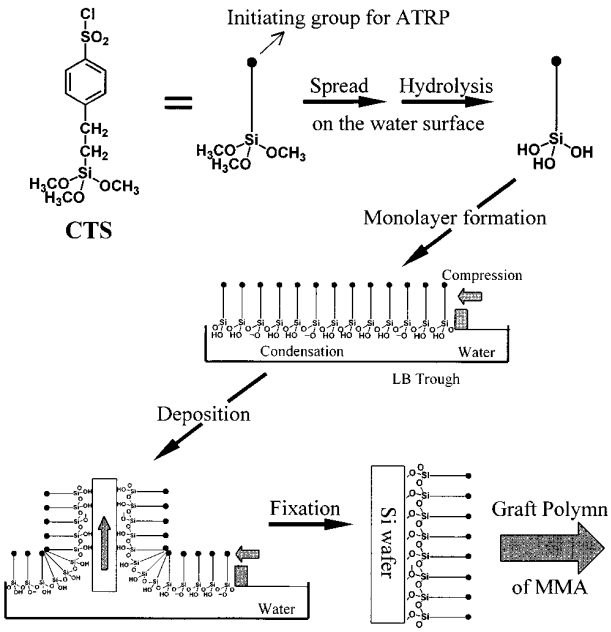

Fig. 3. Illustration of immobilization of ATRP initiator self-assembled monolayer on surface using the Langmuir-Blodgett technique. [15], Copyright 1998. Reproduced with permission from American Chemical Society.

In addition to MW and chain architecture, the molecular weight distribution (MWD) and composition of polymer grafts became tunable. The first experimental study on the effect of MWD of polymer brushes was performed on the interface of air and ethyl benzoate[13] with an earlier theoretical discussion.[42] However, tailored MWDs, or more specifically bimodal MWDs, of polymer grafts on solid surfaces were not demonstrated until two decades later.[43, 44] A challenging topic, *i.e.* the grafting of miktoarm/binary polymer brushes, received more attention. The first report relied on the stepwise activation of azo-initiators immobilized on surface and thus two different monomers were polymerized in two SI-FRP stages.[18] Indeed, a similar result, yet

with better control of the polymerization, can be achieved by performing the reaction under a reverse ATRP condition.[45] Binary polymer brushes were also obtained by grafting a Y-shaped polymer onto a surface[46] or by conducting a two-step ATRP-NMP from the surface.[47, 48]

A preparation of hybrid NPs was developed in the same period as an alternative approach to 'grafting-from', 'grafting-onto', or 'grafting-through', which all start with a solid surface. In this case, hybrid NPs were prepared via a 'polymer-first' approach, *i.e*. using BCP self-assembly as a template.[9] This approach was initially based on BCP phase-separation of a film on a solid surface and later evolved to BCP micelles in a liquid phase.[49] This approach later developed to incorporate covalently bonded polymer brushes with more complex architectures, such as molecular bottlebrushes[22, 50, 51] and star polymers,[52] as templates to synthesize better-defined polymer-inorganic hybrid materials.

Surface(-initiated) RAFT (S/SI-RAFT) polymerizations were reported later, due to their intrinsic challenges, although preceded by SI-PIMP.[53] The first SI-RAFT polymerization was performed by mechanistic transformation of a SI-ATRP reaction, *i.e*. adding the chain-transfer agent (CTA) into a SI-ATRP reaction.[19] Another way to perform RAFT polymerization is to initiate the reaction from immobilized azo initiators on the surface and modulate the reaction via free CTA in solution. This approach was termed SI-RAFT polymerization.[21] Polymerizations were also conducted by direct immobilization of CTAs on surface with radical initiators in solution.[54]

Among the diverse range of methods, SI-ATRP and its derivative procedures have become by far the most popular approach for grafting polymer brushes from surfaces.[32, 39, 55, 56] In addition to conventional monomers, polymerization of a monomer bearing an initiating group

(inimer), termed self-condensing vinyl polymerization (SCVP), led to hyperbranched polymer brushes grafted from a surface.[20] Emergence of activator regeneration by electron transfer (ARGET) ATRP not only reduced the copper catalyst concentration to a ppm level, but also made the reaction far less susceptible to oxygen exposure.[57, 58] This new technique ensured that SI-ATRP is more amenable to large scale applications on macroscopic surfaces.[23, 59, 60] Similarly, when a copper plate was used a reducing agent, *i.e*. supplemental activator and reducing agent (SARA) ATRP, similar large grafting was accessible.[61, 62]

Based on a concept similar to ARGET ATRP, catalyst activation by external stimuli, such as electrochemical reduction or light irradiation, was introduced to SI-ATRP.[24-26] The presence of the external stimuli allows temporal and spatial control of polymer growth on surfaces enabling top-down patterning of polymer brushes and more precise control over MW, **Fig. 4**.

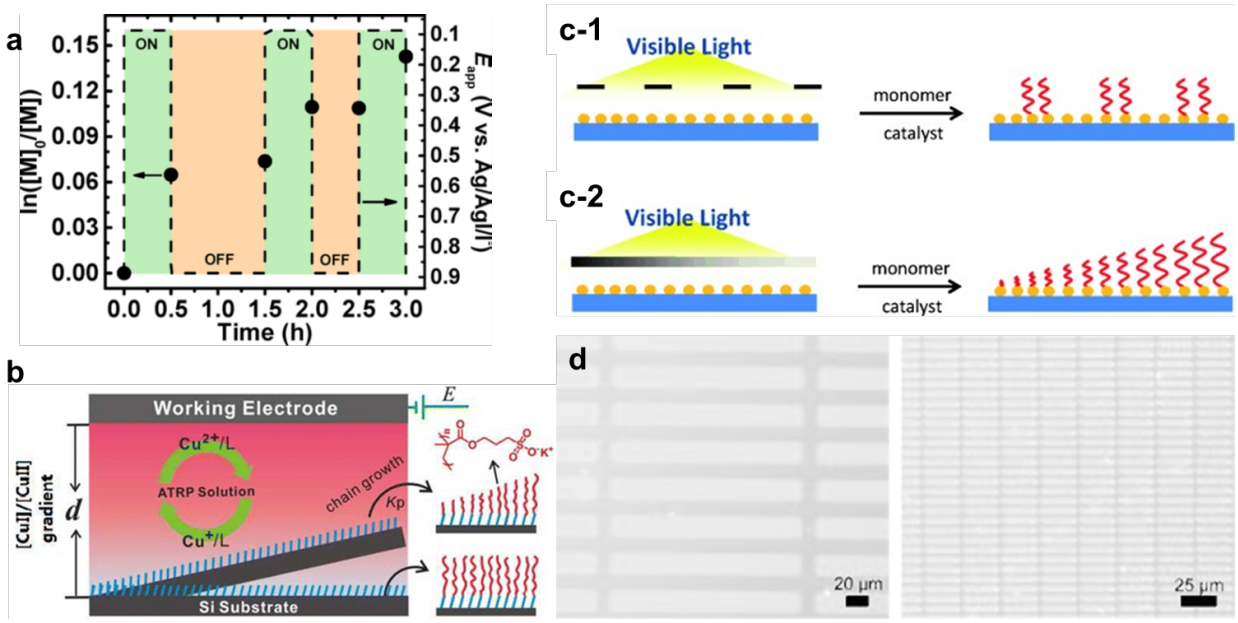

Fig. 4. Temporal and spatial control of SI-ATRP with external stimuli. Panel a shows first-order kinetic plot of simplified SI-*e*ATRP with periodically applied different values of potential. ON

potential = E_{pc} – 80 mV; OFF potential = E_{pc} + 720 mV. [63], Copyright 2017. Reproduced with permission from American Chemical Society. Panel b illustrates gradient polymer brush growth by tuning the distance of working electrode from the substrate in SI-*e*ATRP. [64], Copyright 2013. Reproduced with permission from American Chemical Society. Panel c describes polymer brushes patterning by SI-photoATRP using patterned (c-1) or gradient (c-2) photomasks. Panel d exemplified optical microscopy image of patterned PMMA brushes (converted to grayscale to enhance contrast). [26], Copyright 2013. Adapted with permission from John Wiley & Sons Inc.

The subsequent sections will describe how the techniques presented in this section have been adopted to enable the precision synthesis of brush particle materials that are the subject of this review.

3. Preparation of Polymer-Inorganic Hybrid Materials

In the past three decades, diverse methodologies have been developed to prepare polymer-inorganic hybrid materials. Here the term 'hybrid material' is used to denote a heterogeneous material in which primary or strong secondary chemical bonds are established between the constituents. This is a differentiating feature from classical composite materials which encompass mixed systems such as particle-in-polymer dispersions (although composite fabrication might involve 'hybrid material concepts' to achieve, for example, miscibility between filler and matrix). This section reviews methodologies for the synthesis of polymer hybrid materials from surface-functionalization and immobilization to three grafting techniques and templated synthesis, *i.e.* the 'polymer-first' approach. The capabilities and limitations of each method will be discussed.

3.1 Surface Functionalization

Immobilization of functional groups or polymer chains is the basis of polymer-inorganic hybrid materials. In this section, the coupling agents/groups and their respective scope for attachment on surfaces are discussed.

3.1.1 Surface Anchoring

Selection of suitable anchoring groups is the key to creating a stable bond between polymer and inorganic constituents. A variety of coupling agents with different anchoring groups were developed to match the surface chemistry of respective targeted inorganics. **Table 1** shows several common anchoring groups and their applicable targeting surfaces. Examples of coupling agents bearing each of the anchoring groups are provided.

Table 1. Surface Anchoring Groups and Applicable Surfaces.

Anchoring group	**Surface**	**Examples**	**Ref.**
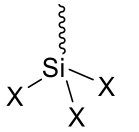 X = halogen or RO trihalo/alkoxysilane	silica, metal oxide, metal, etc.	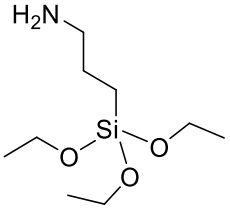	[59]
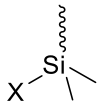 X = halogen or RO halo/alkoxydimethylsilane	silica	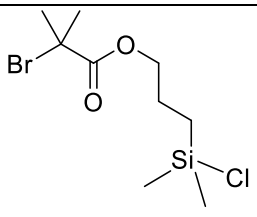	[65, 66]

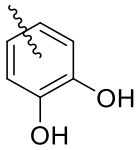 catechol	metal, metal oxide, carbon, etc.	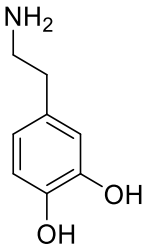	[67-69]
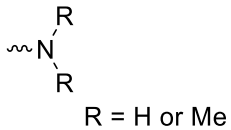 amino	metal, metal oxide, carboxylic acid-functionalized surface	PSAN-NH_2	[70]
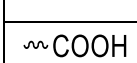 carboxylic acid	metal, metal oxide, amino-functionalized surface	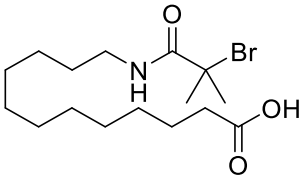	[71]
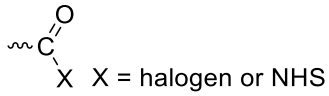 activated acyl	hydroxy/amino-functionalized surface, cellulose	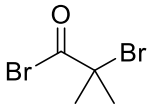	[72-74]
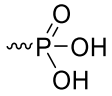 phosphonic acid/phosphates	metal oxide	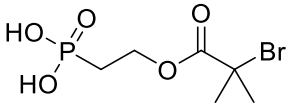	[75, 76]
radical	metal, metal oxide, carbon	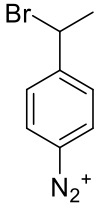	[77, 78]
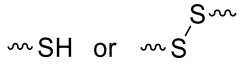 thiol/disulfide	metal	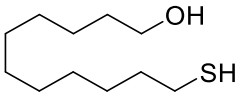	[54, 79, 80]
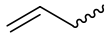 allyl	hydrogen-treated silicon	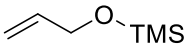	[66]

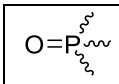 phosphine oxide	quantum dots	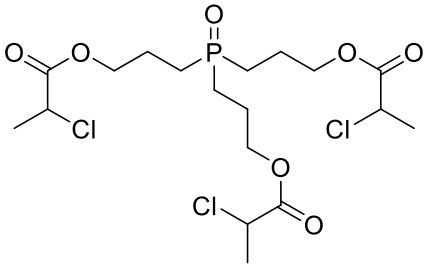	[81, 82]

Silane-based coupling agents are the most often used chemicals for surface modification, because many common functional silanes, such as trialkoxy(vinyl)silane, (3-aminopropyl)trialkoxylsilane, (3-mercaptopropyl)trialkoxylsilane, (3-chloropropyl)trialkoxylsilane, (3-glycidyloxypropyl)trialkoxylsilane, 3-(trialkoxylsilyl)propyl (meth)acrylate, and others are commercially available at a relatively low cost from the silicone industry. The incorporated amino groups are then further converted to various functionalities such as ATRP initiating moieties. More complicated functionalities can also be introduced by hydrosilylation. Silane-based coupling agents can possess 1-3 halide or alkoxy functionalities. Each of the functionalities can react with one silanol group on the surface or a functionality on another silane-based coupling agent. Therefore, a coupling agent with three functionalities forms a more stable covalent linkage to the surface but at the same time it tends to self-polymerize into multiple layers.[83] The formation of the layered structure enables the coupling agents with three functionalities to enclose the substrate, thus making them appropriate for a large variety of surfaces.

Catechol derivatives, especially dopamine and polydopamine, have attracted increased research attention in recent years.[68, 84] Catechol was initially known to form stable adhesion to metal oxide surfaces via a five-member ring chelate.[85] However, the discovery of dopamine-like peptides in byssus of mussels inspired the utilization of dopamine as a universal coupling agent. In a simple biocompatible procedure (pH 8.5, room temperature, exposure to air), dopamine

self-polymerizes into multiple layers covering the surface of the substrate.[68] Polydopamine provides a broad range of surface functionalities, including amino, hydroxy, aromatics, conjugated carbonyl (via *o*-quinone), etc., ready for further modifications. Beyond (poly)dopamine, other natural or artificial structures based on catechol/phenols were used as surface coupling agents, such as tannic acid and catechol-bearing peptides.[86, 87] The amino acid residue in the catechol-bearing peptide was the same as found in byssus of mussels.

The use of fatty acids for the modification of metal or metal oxide surfaces can be traced back to the beginning of organic modification of inorganic surfaces.[88] Later, fatty acids, or amines, were used for the stabilization of inorganic NPs in organic colloids.[89-91] Both carboxylates and amines may covalently coordinate with the metal elements on the surface in addition to generating noncovalent interactions.[91-93] However, inexpensive fatty acids or amines, such as oleic acid, oleyl amine, or octylamine, originally served merely for compatibilization. No reactive functionality was introduced. Recent studies demonstrated incorporation of initiating groups or even polymer chains with a carboxylic acid or amino end-group onto the surface. [70, 71] A carboxylate-based initiator was found to be efficient for a broad range of inorganic surfaces and surface modifications methods, **Fig. 5**.[71, 94] Introduction of ATRP initiating functionalities enabled the use of these anchoring groups for the preparation of polymer-inorganic hybrid materials. In addition to aliphatic amines, deposition of aniline or pyrrole is another convenient approach for modification of inorganic surfaces.[95] However, their anchoring and control of surface functionality is overall not as facile as with silane or dopamine, *vide supra*.[96]

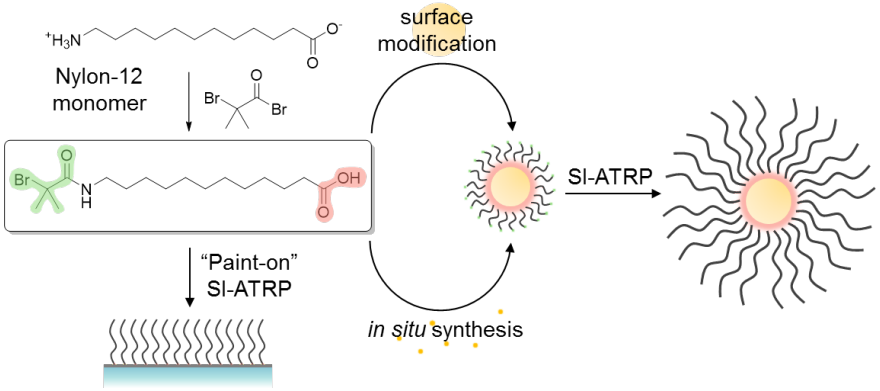

Fig. 5. Illustration of the use carboxylate-bearing tetherable initiator for surface functionalization of inorganic NPs, synthesis of NPs with *in-situ* surface functionalities, or functionalization of macroscopic surfaces. [71], Copyright 2017. Reproduced with permission from Ref. American Chemical Society.

Derivatives of carboxylic acid, *i.e.* activated acyl groups, such as acid halide or *N*-hydroxysuccinimide (NHS) esters, can directly react with some hydroxy/amino-functionalized surfaces.[72, 73, 97]

Phosphonates and phosphates are alternatives for metal oxide surface anchoring; they form stronger bonds with metal oxide surfaces than carboxylic acids.[98] Functional phosphonates were used as tethering agents for grafting polymer from/onto metal oxides and salts.[75, 99] However, phosphonate with phosphorus linked to less than three carbons are strictly regulated in the Chemical Weapon Convention, Annex of Chemicals, Schedule 2B(4), which limits the availability of such precursors as functional phosphonates. In addition to phosphate, phosphine oxides have been shown to attach to the surface of certain quantum dots, such as CdSe or ZnS, etc. [81, 82]

Radical species can be generated by heating, photo-irradiation, or redox reactions from their precursors or from the surface. For example, conventional thermal initiators were found to attach to carbon surfaces upon heating;[100] aryl radicals can be generated from electrochemical

reduction of diazonium salts;[77, 101, 102] and photochemically active surfaces undergo radical coupling with alkenes.[103, 104] These radical species can produce covalent carbon-carbon/metal bonds on the surface and introduce functionalities. Similar to the radical process, hydrosilylation can occur between hydrogen-treated silicon surfaces and allyl-based coupling agent via either a radical process (thermal or photo-induced) or a organometallic catalytic process.[66]

Organosulfur compounds form strong bonds with a variety of metals, such as Au, Ag, Hg, Fe, Cu, etc. For these systems, thiols and disulfides can be readily attached to the metal surface and hence provide suitable coupling groups. For example, thiols are widely used to modulate the size of gold nanocrystals.[105] Disulfides tend to split into thiolates upon chemisorption on metal surfaces.[106, 107] However, the nature of the sulfur-metal interaction is still being studied.[107, 108] Nevertheless, initiating groups or polymer chains were introduced to gold surfaces by reaction with functional thiols or thiol-terminated polymer chains. [54, 79, 80]

3.1.2 Adsorption of Block Copolymers

Surface adsorption of polymers was observed and theoretically discussed decades ago.[109] As early as the 1960s, hydrogen-bond accepting units, such as *N*-vinyl-2-pyrrolidone were rationally incorporated in a polymer backbone to promote adsorption on a silica surface.[110] In fact, poly(*N*-vinyl-2-pyrrolidone) (PVP) is still one of the most robust polymeric stabilizers for NPs to date.[111]

Block copolymers (BCPs) bearing anchoring groups in the repeating units of one block can possess strong affinity towards suitable inorganic surfaces. Direct adsorption of surfaces with BCPs is often categorized as a 'grafting-onto' approach, *vide infra*. The surface activity of a BCP with two blocks of different affinity to the surface was first reported in 1974.[112] Soon the

observation was applied to enable the stabilization of polymer particles in incompatible media.[113] The same concept was applied by the coating industry for the use of BCPs as pigment dispersants.[114] Immobilization of BCPs on inorganic surfaces was initially employed to study the surface anchoring force.[115] In this report, poly(2-vinylpyridine)-*b*-polystyrene (P2VP-*b*-PS) BCP was absorbed onto a mica surface via the hydrogen-bond between pyridine moieties and the surface while the PS brushes served as the surface for force measurement. A triblock copolymer, poly(methacrylic acid)-*b*-PMMA-*b*-poly(styrene sulfonate) (PMAA-*b*-PMMA-*b*-PSS), was attached to the surface of nanoscale zerovalent iron and created a highly negative zeta potential.[116]

Other hydrogen-bonding polymer blocks, such as poly(2-(dimethylamino)ethyl methacrylate) (PDMAEMA),[117] PSS,[116, 118] poly(meth)acrylic acid/poly(meth)acrylate (P[M]AA),[116, 119, 120] and PEG,[121, 122] were used for anchoring on inorganic surfaces, including metal or metal oxide surfaces, to determine how the contribution of coordination may further reinforce the binding. Therefore, direct attachment of BCPs provides opportunities of surface grafting without a strong covalent bond or stepwise surface modification. However, due to the often weak interaction within each repeating unit, the adsorption of BCP on surfaces is typically reversible and highly dependent on the thermodynamic parameters, especially temperature, concentration, and nature of the dispersant.[123-125]

Overall, three different types of surface anchoring of polymer brushes have been used, as illustrated in **Fig. 6**.

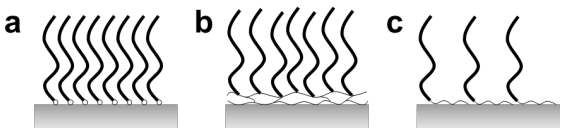

Fig. 6. Anchoring mechanisms for polymer brushes on surface (a) by an end-group; (b) by association with a crosslinked polymer network; or (c) by adsorption of a polymer block with affinity to surface.

Polymer brushes can be anchored by a single end-group, either a functional group to initiate the growth of polymer brushes or to join existing functional polymer chains with the surface. The first case (often referred to as 'grafting-from') usually allows higher density of polymer brushes. In both procedures a strong interaction between the end-group and the surface must be employed to establish sufficiently stable grafting of polymer brushes. In the second approach, multifunctional anchoring groups, such as triethoxysilane or dopamine, can polymerize on surfaces and create a robust crosslinked network (multilayer) which encloses the surface. Polymer brushes or functionalities can subsequently be introduced within the network. A side reaction that needs to be considered in this approach is the formation of nanogels via the polymerization of free precursor in solution.[126] Direct adsorption of BCPs is the third approach for surface anchoring of polymer brushes. Multiple noncovalent interactions along the anchoring block promote the formation of semi-stable polymer brush layer. This approach depends on the matching of the surface chemistry with suitable anchoring groups of the adsorbing block.

3.1.3 Functional Groups

Surface functionalities can be introduced by modification of surfaces with selected coupling agents. The functional surface can further undergo coupling with other reagents to create new functionalities or grafted polymer brushes. Typical surface functionalities and their reactivities are

listed in **Table 2**. Some of the reactions involve coupling between two functional groups, and thus do not restrict which side of the functionality is attached to the surface, *i.e.*, either moiety can serve as the surface functionality.

Table 2. Surface functionalities and their reactions for polymer grafting.

Surface functionality	Reactivity	Examples
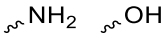 amino/hydroxyl	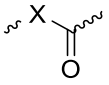 amidation/esterification[a]	[59, 78, 127, 128]
	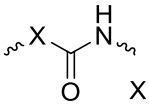 coupling with isocyanate into carbamate or urea	[129]
	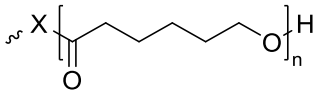 ROP	[130]
	 reductive amination	[131]
	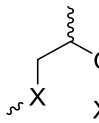 nucleophilic addition to epoxy	[132-134]

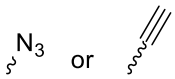 azide/alkyne	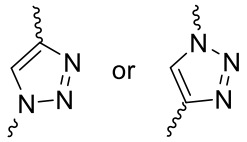 CuAAC click chemistry[a]	[131, 135-137]
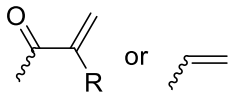 R = H or Me vinyl/(meth)acrylate or other (conjugated) unsaturated C-C bonds	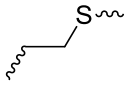 thiol-ene click chemistry[a]	[136, 138]
	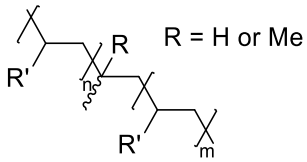 'grafting-through'	[5, 139, 140]
	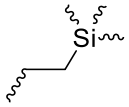 hydrosilylation[a]	[66, 141, 142]
	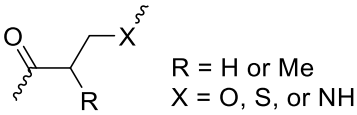 Michael addition[a]	[143-146]
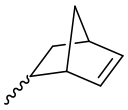 (strained) cyclic olefin	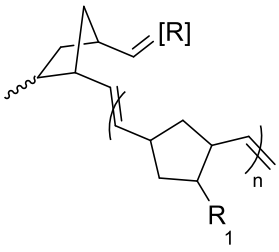 ROMP	[17, 147]
 (activated) alkyl halide	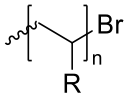 ATRP	[8, 15, 35]

	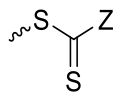 nucleophilic substitution by CTA	[19, 148]
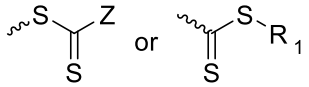 CTA	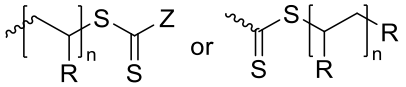 RAFT polymerization	[19, 54, 148, 149]
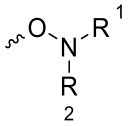 alkoxyamine	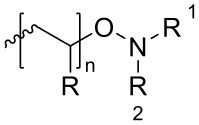 NMP	[16, 150]
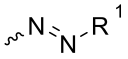 azo or other radical generating structures	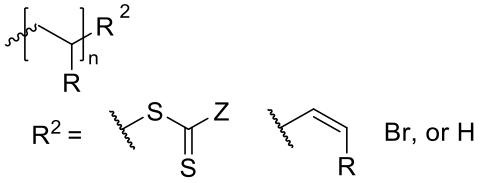 RAFT polymerization/FRP/Reverse ATRP	[5, 21, 151, 152]
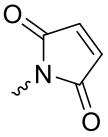 maleimide or other dienophiles	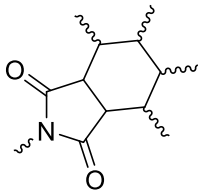 Diels-Alder reaction[a]	[137, 153-155]

[a] Reversed combination reported, see references.

Amino and hydroxyl groups are the two most commonly selected surface functional groups after surface modification. They can be introduced by a wide selection of commercially available coupling agents discussed in the previous section. As nucleophiles, they undergo coupling reaction with carboxylic acids and their derivatives to form stable ester or amides [59, 78, 127]. However, a recent report indicated swelling-induced mechanochemical cleavage of these groups on the

surface when tethered hydrophilic polymer brushes were immersed in water.[156] The same procedure can also be employed to introduce carboxylic acid and derivatives as the surface functionality. Similar to the process of esterification or amidation, both functional groups serve as initiating sites for the polymerization of lactones.[130] Two other typical reactions of such nucleophiles are Michael addition,[134-137] nucleophilic addition to epoxy groups to form β-hydroxyl ether/amine linkages[132-134] or to α,β-unsaturated carbonyl to form γ-carbonyl (thiol)ether/amine linkages. Another coupling reaction specific to amines is reductive amination to form an amine linkage.[131]

Unsaturated bonds, especially C-C bonds, are another important category of surface functionality. They undergo various (cyclo)addition reactions. For example, copper catalysts induce alkyne-azide cycloaddition reactions[131, 135-137] while thermally-induced Diels-Alder reactions also form cyclic linkages.[137, 153-155] Both reactions can proceed with either functionality on the surface. A platinum-catalyzed organometallic process or a radical addition allows H-Si to couple with unsaturated C-C bonds.[141, 142] Radical addition of thiol to C=C double bonds, *i.e.* thiol-ene click chemistry, creates a thioether linkage.[136, 138] Unsaturated bonds on the surface may also be incorporated as monomers for radical polymerization. This process is called 'grafting-through',[5, 139, 140] *vide infra*. Michael addition of α,β-unsaturated carbonyl mentioned above is another example of reactivity of unsaturated bonds.

Certain types of surface functionality allow polymerization directly from a surface, *i.e.* 'grafting-from', *vide infra*. For conventional radical polymerization, radical precursors, such as azo groups, are immobilized on the surface prior to activation.[5], [151] The same functional group can also initiate RAFT polymerization with free CTA in solution[21] or reverse ATRP.[152] Both SI-ATRP and SI-NMP require the dormant species to be immobilized on the surface.[8, 15, 16,

35, 150] However, in the case of surface-RAFT polymerization, the immobilized CTA, [19, 54, 148, 149] can be directly anchored or transformed from an ATRP dormant species.[19, 148] Detailed discussion of these techniques is included in the next section.

3.2 'Grafting-from' Approach

In the 'grafting-from' approach, polymer brushes grow directly from surfaces, allowing high/tunable grafting density, which is the most important advantage of this method. Grafting density is defined as the number of polymer chains per unit surface area and presents an important parameter governing the physicochemical properties of brush-based materials. Grafting density (σ) of polymer brushes grafted on NPs is typically determined by a combination of thermogravimetric analysis (TGA) and size-exclusion chromatography (SEC) using Eq. 1:

$$\sigma = \frac{(1 - f_{\mathrm{NP}})N_A \rho_{\mathrm{NP}} d}{6 f_{\mathrm{NP}} M_{\mathrm{n}}} \quad (1)$$

where f_{NP} is the weight fraction of NPs determined by TGA; N_{A} is the Avogadro number; ϱ_{NP} and d, are the bulk density and average diameter of the nanoparticles; and M_{n} is the number-averaged molecular weight of the cleaved polymer brushes determined by SEC. However, this equation could not be applied to polymer brushes grafted on macroscopic surfaces as the weight difference between the polymer brushes and the substrate is usually beyond the detection limit of TGA. Instead, the grafting density can be expressed by Eq. 2:

$$\sigma = \frac{\rho_{\mathrm{p}} h N_A}{M_{\mathrm{n}}} \quad (2)$$

where ϱ_{p} is the bulk density of the polymer, h is the thickness of the polymer brushes determined by AFM or ellipsometry; and M_{n} is the number-averaged molecular weight of the polymer brushes estimated from SEC of free polymers generated simultaneously from sacrificial initiators. This equation may also be used to determine grafting density of polymer brushes grafted on NPs, as

long as the brush thickness can be estimated by transmission electron microscopy (TEM) or dynamic light scattering (DLS). A recent review elaborated on the scope and limitation of current methods for experimental measurements of grafting density.[157] The grafting density in the 'grafting-from' approach can be tuned by diluting the concentration of the surface initiating sites. A well-established method is to employ non-reactive molecules with similar linkage structures as the tetherable initiators, *i.e.* a 'dummy' initiator, so as to partially cover the surface with the inert groups.[158] Alternatively, the surface density of functional groups, such as CTA, can be tuned directly, with less control, by the ratio between the coupling agent and the particles.[159] Both theoretical and experimental reports demonstrated that grafting density determines the conformation of polymer brushes.[160-164]

3.2.1 Reversible Deactivation Radical Polymerization

Conventional free radical polymerization (FRP) has been well studied, it remains a challenge to control multiple parameters of the targeted products at the same time, especially when the polymerization is performed on surfaces. Emergence of reversible deactivation radical polymerization (RDRP), also termed as controlled radical polymerization (CRP), enabled excellent simultaneous control of MW, MWD, and architecture while retaining the robustness and broad applicability of radical polymerization.

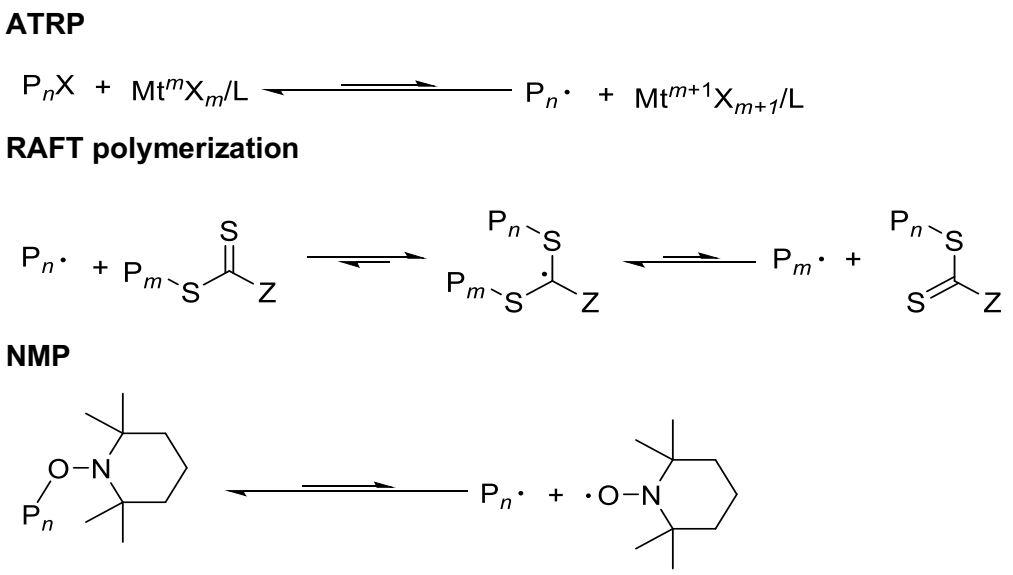

Fig. 7. Illustration of equilibrium of typical RDRP techniques.

ATRP is the most frequently employed RDRP method.[165] ATRP relies on the formation of a dynamic equilibrium between dormant alkyl halides and propagating radicals, typically modulated by a redox pair of transition metal complexes, **Fig. 7**.[165-169] ATRP employs transition metal catalysts, especially Cu complexes. The residual catalysts should be removed from the final product, especially for biomedical and electronic applications. Therefore, in the past decade, various new techniques were developed to permit a well-controlled polymerization with only ppm levels of Cu catalyst. They employ a reducing agent to regenerate the activator (Cu^{I} complexes) of highly reactive Cu complexes, such as Cu/Me_6TREN, Cu/TPMA, as well as even more reactive complexes based on TPMA derivatives.[170] For example, activator regenerated by electron transfer (ARGET) ATRP,[57, 58] supplemental activator and reducing agent (SARA) ATRP,[171, 172] and initiator for continuous activator regeneration (ICAR) ATRP[173] utilize chemical reducing agents. More recently, external stimuli,[174] such as electrochemical reduction,[175, 176] photoirradiation,[177, 178] and ultrasonication,[179-182] were introduced to generate reducing conditions. While allowing ppm levels of Cu catalyst, these techniques also

enabled spatial and/or temporal control of the polymerization. Other metal complexes, such as iron,[183-185] ruthenium,[186, 187] or iridium,[188] can also modulate an ATRP equilibrium. Recent development of metal-free ATRP eliminated the problem of metal residues in the product, but it remains a challenge to achieve a level of control of the polymerization and versatility that is comparable to Cu complexes, **Fig. 8**.[189-191] The ATRP procedure was recently automated using a DNA synthesizer, further promoting the efficiency and versatility of this procedure.[192]

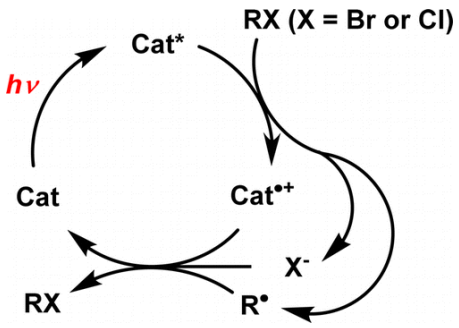

Fig. 8. Simplified activation/deactivation mechanism for photoinduced metal-free ATRP reactions. [191], Copyright 2016. Reproduced with permission from American Chemical Society.

RAFT polymerization is another well-studied RDRP technique. The equilibrium relies on the reversible addition of propagating radicals to and fragmentation from the CTA, typically a thiocarbonylthio species, **Fig. 7**.[193] The major feature of RAFT polymerization is that it relies primarily on the same conventional FRP reaction setup with the addition of a CTA. Conventional radical initiators are used to provide the radical species and initiate the polymerization while the CTA concentration determines the target MW. The degenerative transfer in the RAFT process ensures that all the polymer chains are grown at the same pace.[194] RAFT polymerization accommodates some reactive/functional monomers, such as acrylic acid.[195] However, the reactive RAFT chain ends often need to be cleaved to remove color and a potentially toxic residue

from the product. There is a small fraction of polymer formed from the conventional radical initiator preventing synthesis of pure hybrids and BCP.[196]

CTAs based on xanthates used in RAFT polymerization, also termed macromolecular design via interchange of xanthates (MADIX),[197] enabled the RDRP of vinyl acetate[198] and ethylene.[199] External controls were also implemented in RAFT polymerizations. The most important example is photoinduced electron/energy transfer (PET-)RAFT polymerization, **Fig. 9**.[200, 201] In contrast to the conventional RAFT process, the radical species in PET-RAFT is generated by the PET-excited photoredox catalyst from the CTA. Therefore, while no conventional radical initiator is needed, the process possesses an improved oxygen tolerance and capability of temporal/spatial controls.[200] The PET-RAFT polymerization can also be moderated by ruthenium complexes,[202] organic dyes,[203] or even chlorophylls.[204] Other external stimuli such as ultrasonication[205] and electrochemical reduction[206] were also successfully demonstrated for the RAFT polymerization. Recent research went even further beyond oxygen tolerance, allowing oxygen as external stimuli for RAFT polymerization.[207]

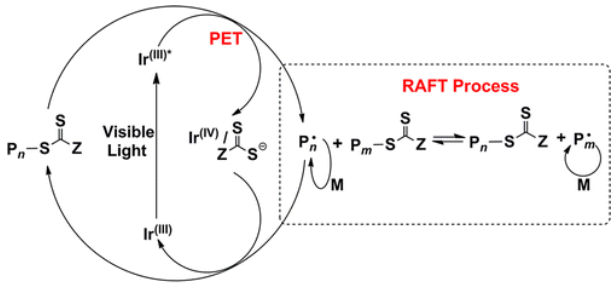

Fig. 9. Proposed mechanism of a photoinduced living polymerization using *fac*-[Ir(ppy)$_3$] as photoredox catalyst. [210], Copyright 2014. Reproduced with permission from American Chemical Society.

NMP, an example of stable free radical mediated polymerization (SFRP), is one of the first-reported RDRP techniques.[208, 209] In this technique, the dormant alkoxyamine undergoes

homolysis of the C-O bond at elevated temperatures to form an active radical species and a stable nitroxide radical, **Fig. 7**. The original TEMPO-based system requires a high temperature for the activation process. More recently, photosensitive alkoxyamines and more reactive alkoxyamines for low temperature activation were developed.[210-212] Although NMP was successful for styrenic monomers, it has been challenging for acrylic and methacrylic monomers, mainly due to slow homolysis and hydrogen abstraction, respectively.[213-215] When styrenic monomers are combined with the high reaction temperature, thermal self-initiation is an inevitable side-reaction.[216, 217]

Organometallic species such as cobalt complexes can also act as stable radicals and couple with radical species to form dormant species and mediate RDRP processes.[218, 219] These processes are termed organometallic-mediated radical polymerization (OMRP).

Some other RDRP techniques, including reversible iodine-transfer radical polymerization (RITP)[166, 220] and organotellurium-mediate radical polymerization (TERP)[221] can undergo a degenerative transfer process as in RAFT polymerization or can be homolytically cleaved like in NMP.

3.2.2 Surface-initiated RDRP

As mentioned in the previous section, three decades of development of RDRP techniques now allows for controlled polymerization of almost the entire spectrum of vinyl monomers under various conditions. This is the most important reason that RDRP is also the most often employed technique for the 'grafting-from' approach.[32, 55] Although there are reports of 'grafting-from' via all of the RDRP techniques, each technique has its advantages and limitations.

SI-ATRP counts for a large majority of all 'grafting-from' approaches due to the ready accessibility of alkyl halide functionalities on surfaces, its tolerance to different conditions and impurities, and the rich toolkit to meet specific process requirements. Advances in ATRP have overcome the main challenges for ATRP and all ATRP techniques discussed in the previous section were successfully applied to SI-ATRP. As one of the first ppm level Cu catalyst ATRP, ARGET ATRP permits the growth of polymer brushes in the presence of air, making it suitable for 'grafting from surfaces for 'everyone''.[23] Indeed, it is the most popular SI-ATRP technique, as demonstrated by a Google Scholar search (on 'surface-initiated *AND* ARGET') that generated 12,800 results on November 01, 2019. This technique was further developed into a direct brush-painting of polymer brushes on large-scale surfaces at a cost as low as \$2 m^{-2}, **Fig. 10**.[59] ATRP techniques with external stimuli have also attracted tremendous research attention, especially on macroscopic surfaces, due to the ability to pattern the surfaces with polymer brushes, **Fig. 4**.[24-26, 60, 64, 222]

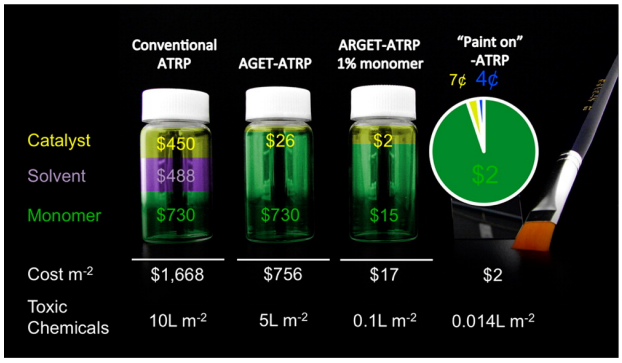

Fig. 10. Costs of polymer brushes created using conventional ATRP, AGET-ATRP, ARGET-ATRP and 'paint on'-ATRP. Green indicates cost of monomer, purple cost of organic solvent, yellow cost of catalyst, and blue cost of ascorbic acid. The total cost per square meter is shown at the bottom, along with the amount of toxic chemicals used. [59], Copyright 2014. Reproduced with permission from American Chemical Society.

Photoinduced ATRP from inorganic surfaces was further expanded to SI-ATRP mediated by organic photoredox catalysts, producing patterned/well-defined polymer-inorganic hybrid materials with no metal residues.[65, 223, 224]

However, SI-ATRP cannot be treated in the same way as polymerization in homogeneous solutions because of its multifunctional nature, **Fig. 11**. Assuming there are 1000 growing chains on a single NP, which is typical for silica NPs with a diameter of 20 nm and a grafting density of approximately 1 chain/nm^2, Flory-Stockmayer theory indicates that only ~0.2% of termination by combination between NPs could be sufficient for formation of a macroscopic gel.[225, 226] Conventionally, using a higher dilution of the reaction system with monomer helps suppress the unfavorable termination reactions. The rate of termination, $R_t = k_t[P_n^*]^2$, depends more on the radical concentration than the rate of propagation, $R_p = k_p[P_n^*][M]$. However, this approach is at the price of a slower reaction. Therefore, other approaches, such as SI-ATRP under a high pressure or in miniemulsion, were developed. Under a high pressure, k_t was suppressed due to limited diffusion of chain ends in a more viscous medium while k_p was boosted.[227] In miniemulsion polymerization, the trapping of particles within nanosized droplets prevents crosslinking (although dimer or trimer formation may still be observed if more than one particle is trapped within the droplet).[228]

Temporal control becomes especially important in SI-ATRP as it allows one to 'pause' the reaction and check the status.[63, 224] Intraparticle termination or termination on macroscopic surfaces only occurs between neighboring active chain ends. However, with the increase of copper catalyst concentration, migration of active chain ends is accelerated, thus promoting termination.[229, 230]

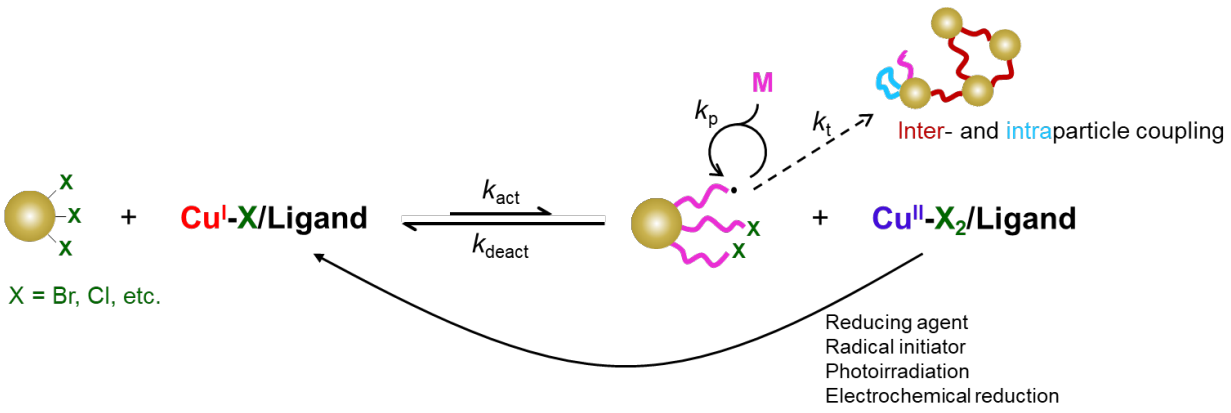

Fig. 11. Schematic illustration of SI-ATRP equilibrium including ppm level of Cu catalyst techniques and external stimuli.

RAFT polymerization can be performed on surfaces in three different ways, depending on how the CTA is anchored, **Fig. 12**. With conventional radical initiator anchored on surface and free CTA in solution, surface-initiated RAFT can be performed in the same manner as SI-FRP.[21] In other procedures, either the R-group[19, 231] or the Z-group[149, 232] of the CTA can be anchored to the surface, termed surface RAFT or S-RAFT polymerization as the initiation process takes place in solution.[55] In the case of R-group anchoring, the tetherable or tethered CTA is usually prepared by transformation from an ATRP initiator or chain end.[19, 231, 233] Application of functional CTAs, such as 4-(4-cyanopentanoic acid) dithiobenzoate (CPDB), provides an alternate choice, *i.e*. direct/indirect immobilization via the functionalities in the CTAs.[159] The reaction proceeds in a way similar to SI-ATRP but, as there is an equal number of active chain ends and free CTA, deactivation is usually inefficient causing broadened MWD. On the other hand, S-RAFT using Z-group anchored CTA suffers from the same challenge as the 'grafting-onto' approach, *vide infra*, the anchored surface CTA gradually becomes inaccessible to the growing radical chain ends. Regardless of the anchoring method, free polymer is usually inevitable in S(I)-RAFT polymerization. Nonetheless, S(I)-RAFT inherits the advantages of RAFT, such as

capability of polymerizing less reactive and/or functional monomers.[234] PET-RAFT from surfaces was also recently demonstrated.[235, 236]

Surface-initiated photoiniferter-mediated polymerization (SI-PIMP), though reported earlier,[7] takes the same strategy as R-group anchored S-RAFT polymerization. However, a substrate and monomers compatible with UV-irradiation are required for SI-PIMP while it also suffers from loss of deactivator.[237] Other RDRP techniques based on degenerative transfer, such as RITP and TERP, were also applied to grafting polymer brushes from surfaces.[238, 239]

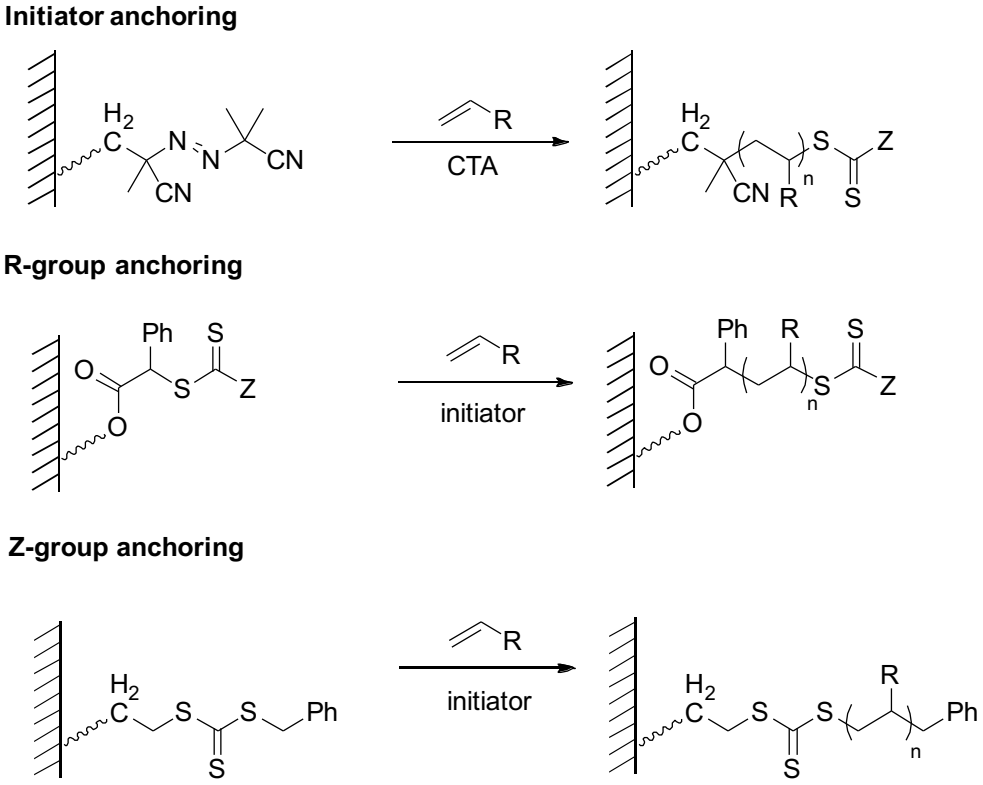

Fig. 12. Schematic illustration of three different anchoring methods for RAFT polymerization from surfaces.

SI-NMP is another facile method for grafting polymer brushes from surfaces. No reagents other than alkoxyamine-tethered surface and monomer is needed for this technique. Surface-anchored

alkoxyamine can be prepared either by synthesis of tetherable alkoxyamine[16, 150, 240] or by trapping surface radicals with nitroxide radicals.[241, 242] However, SI-NMP inherits the limitations of NMP. It is challenging for non-styrenic monomers, especially methacrylates. Tetherable derivatives of recently developed highly reactive alkoxyamines, such as SG-1 (also called DEPN), were employed in SI-NMP, enabling higher efficiency and/or polymerization of acrylic monomers.[150, 240-243]

3.2.3 Other Polymerization Techniques

In addition to SI-RDRP, other controlled polymerization techniques, including living anionic polymerization (LAP), living cationic polymerization (LCP), and ring-opening metathesis polymerization (ROMP) are viable approaches to polymer-inorganic hybrid materials.

LAP and LCP were demonstrated decades before the emergence of RDRP,[244, 245] but there are only sparse reports on the use of such techniques for surface-initiated polymerization.[11, 246, 247] Carbanions are usually introduced on to the surface via nucleophilic addition of BuLi to anchored 1,1-diphenylethylene.[247] Carbocations can be created through activation of alcohol or cleavage of ethers by Lewis acids.[40, 248] An alternate approach is to use the surface charge as the counterion in an ionic polymerization, while the polymer brushes grows in the same way as Z-group anchored RAFT polymerization, *vide supra*.[11] The major challenge of SI-LAP/LCP is the presence of the highly reactive carbanion/carbocation intermediates, making the reactions sensitive to even a trace amount of moisture/hydroxyl groups, which is difficult to eliminate from surfaces.

SI-Ring-Opening Polymerization (ROP) from amino/hydroxyl-functionalized surfaces was used for synthesis of polycaprolactone, polylactide, or poly(*N*-carboxyanhydride) brushes, **Fig. 13**.[12, 130, 249-252] SI-ROP can also be performed in a cationic manner, initiated from activated hydroxyl groups.[40]

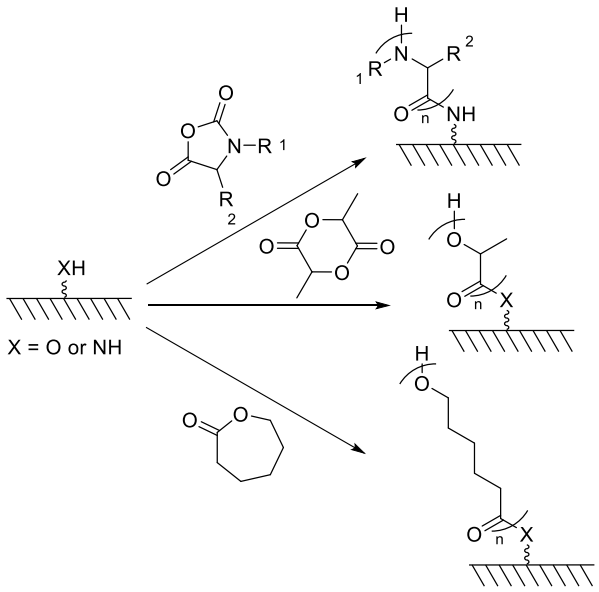

Fig. 13. Some examples of polymer brushes synthesized via SI-ROP from amino/hydroxyl-functionalized surfaces.

ROMP is an important polymerization technique since its first report in the 1970s.[253] Around 1990, mechanistic understanding of olefin metathesis and rational design of the organometallic catalysts allowed the approach to achieve livingness/control of polymerization.[254-256] The ROMP process is mediated by the metal-carbene catalyst, which also acts as the initiator for the polymerization, **Fig. 14**. Therefore, to perform SI-ROMP, surface immobilized metal-carbene catalyst was prepared *in-situ* through a one-step olefin metathesis from surface-immobilized cyclic olefin.[17, 147] The intrinsic challenges of SI-ROMP are similar to SI-ATRP, the metal catalyst, which becomes undesired residues in the final product. ROMP requires expensive catalysts based on Ru, Mo, or W. Although metal-free ROMP has been demonstrated recently,[257] there is no report on utilization of such a technique on surfaces. Another underlying problem is the presence of backbiting, *i.e.* olefin metathesis involving internal double bonds.[254] This side reaction can be mitigated by careful selection of the monomer and the catalyst.

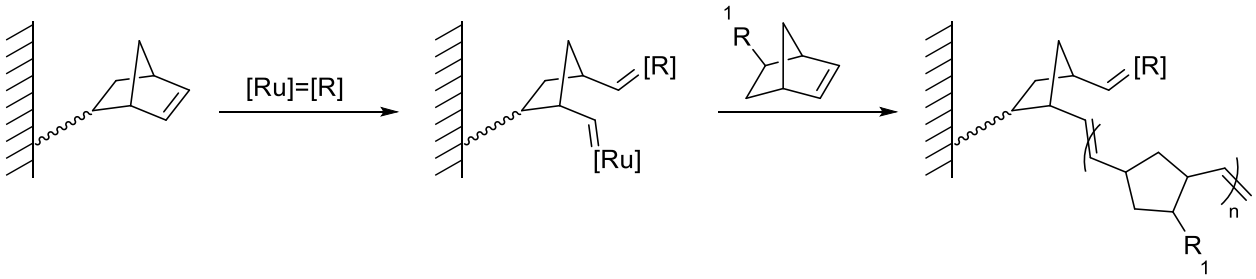

Fig. 14. Schematic illustrations of surface immobilization of metal-carbene catalyst and subsequent SI-ROMP.

3.3 'Grafting-onto' Approach

In comparison to the 'grafting-from', the 'grafting-onto' approach often considered to be more viable. Minimal surface functionalization is needed because an appropriate coupling end-group, **Table 1**, can often be found for the native surface functionalities. The major challenge for the 'grafting-onto' approach is that high grafting densities are difficult to achieve due to the steric hindrance exerted by grafted chains. Whereas in the 'grafting-from' approach the grafting density is limited primarily by the control of polymerization and thus can achieve high values,[258] the 'grafting-onto' typically results in more dilute graft layers with a grafting density of about 1 chain/(radius of gyration)^2 which corresponds to a more collapsed 'mushroom-type' morphology, **Fig. 15** [259].

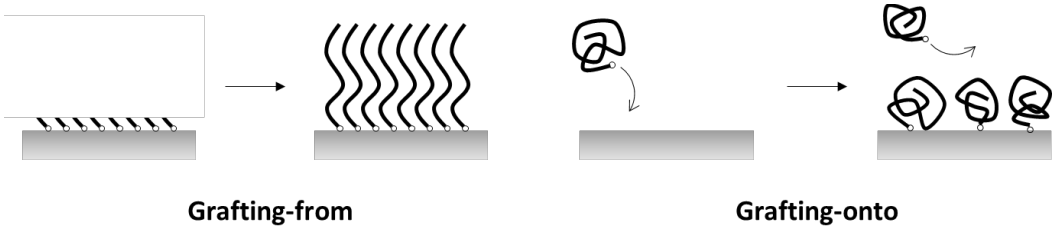

Fig. 15. Comparison of achievable grafting densities in the 'grafting-from' and 'grafting-onto' approaches.

3.3.1 Conventional 'Grafting-onto' Approach

Polymer chains can be grafted onto an inorganic surface if at least one functional end/side group or at least one functional block is present that can facilitate coupling to the surface, *cf*. Section 3.1.3. Conventionally, such functionality can be the reactive chain end of a polymer,[5, 260] comonomers introduced during polymerization, or an end-group attached by a transfer agent, **Fig. 16**.[128] However, strict conditions are required to trap living chain ends during the polymerization. If comonomers are introduced during the polymerization then control of the distribution of functional comonomers along the backbone is required to prevent the uncontrolled formation of loops on the surface. Some polymers, such as PEO, poly(propylene glycol) (PPG) and PDMS, have intrinsic chain-end functionalities, which can be used directly for grafting onto.[261, 262] This approach, however, only applies to a limited selection of polymers and many of these polymers are bifunctional, resulting in a mixture of polymer brushes and loops. When grafting-onto NPs, it may even cause interparticle crosslinking.

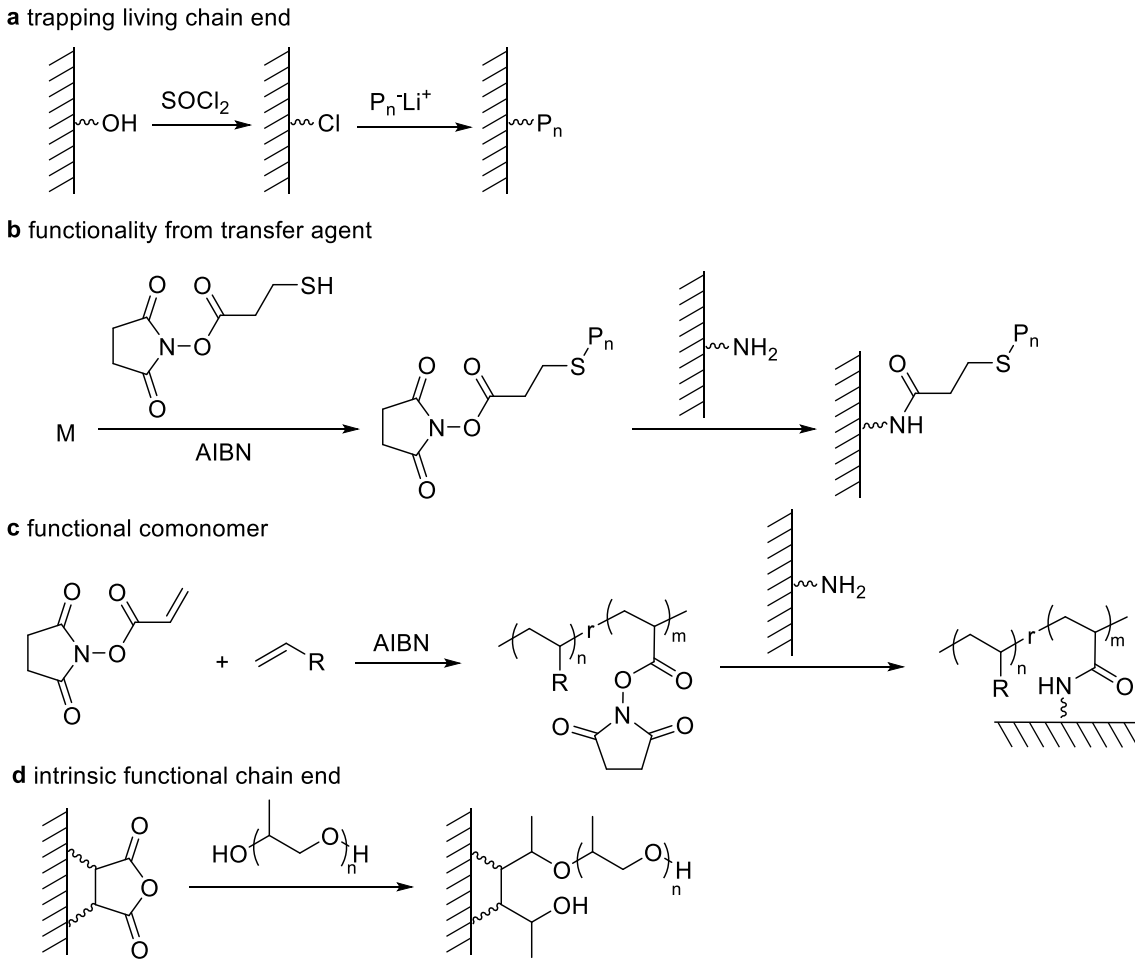

Fig. 16. Some examples of conventional approaches for grafting onto. (a) trapping a living chain end with the surface;[5] (b) capping polymer with a functional transfer agent;[128] (c) incorporating a functional comonomer;[128] (d) grafting of polymer with intrinsic functional chain ends.[261]

Controlled/living polymerization, especially RDRP enables the synthesis of polymers with precisely defined architecture, composition, and functionalities, in addition to allowing versatile control over grafting behavior of the polymer chains on surfaces. For example, the sulfur-containing chain end of RAFT polymerization is suitable for grafting polymer brushes onto noble metal surfaces, such as gold. An early example was to use $NaBH_4$ to reduce the dithioester chain

end to thiol, which was attached to gold NPs.[263, 264] Polymerizations mediated by functional CTAs can result in end-functional polymers for 'grafting-onto'. For example, esterification of propargyl alcohol with CPDB gives an alkyne-functional CTA leading to alkyne-functional polymer. The polymer can thus be anchored to a surface via copper-catalyzed azide-alkyne cycloaddition (CuAAC).[265] A similar procedure also applies to ATRP when propargyl 2-bromoisobutyrate is used as the initiator.[266] However, as the same Cu(I) species are shared among ATRP, CuAAC, and Glaser coupling, this procedure often leads to unfavorable side-reactions.[267] An alternative method is to form azide-functional chain-ends via nucleophilic substitution of the halide end group with an azide.[268-271] Other end functionalities, such as phosphonate or thiol (prepared via post-polymerization reduction from disulfide), **Fig. 17**, targeting iron oxide and gold surfaces, respectively, were also introduced into polymers via ATRP from functional initiators.[75, 272, 273] If the functional group is present in the middle of the polymer chain instead of a chain end, a Y-shaped polymer brush can be anchored to the surface, *cf*. Section 4.[46]

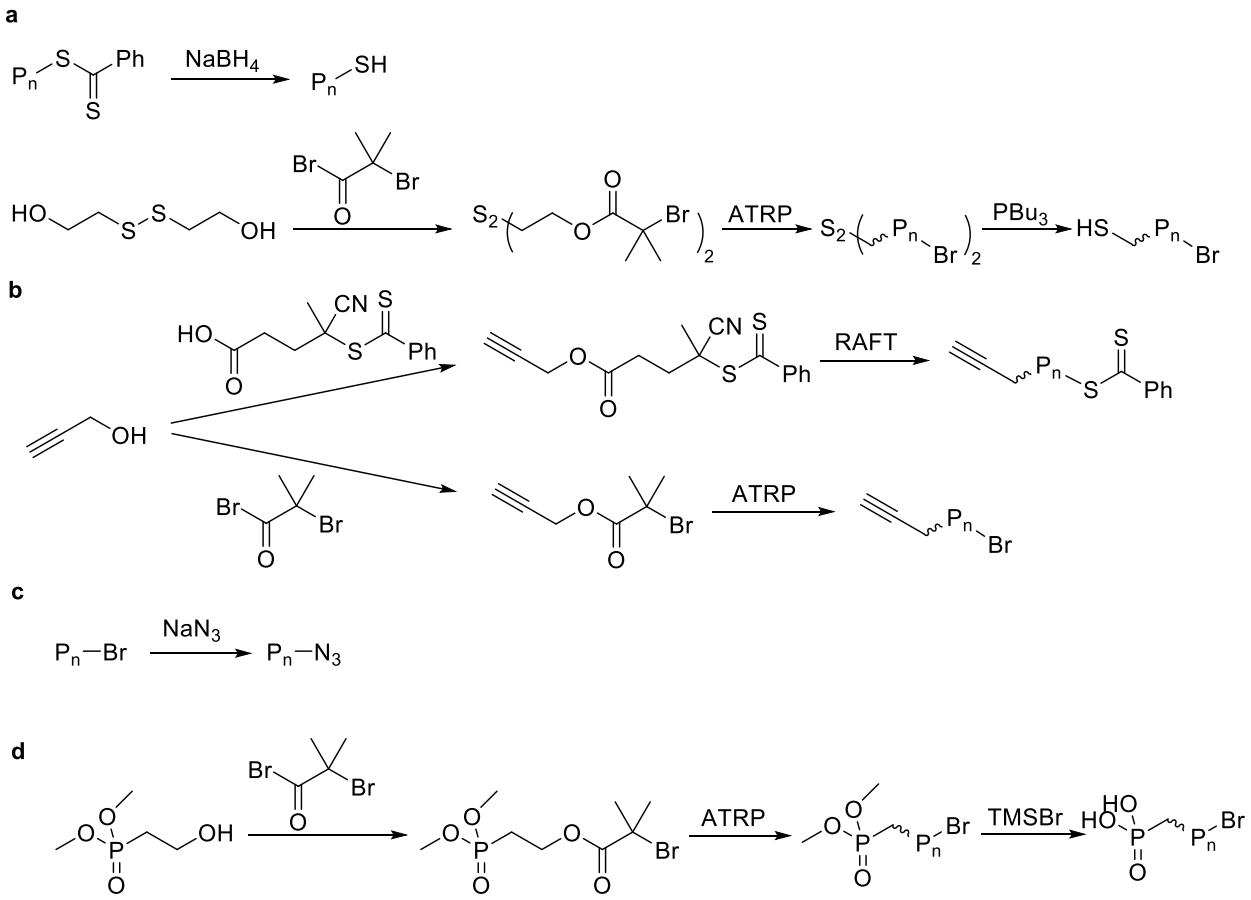

Fig. 17. Some examples of end-functionalities introduced by RDRP: (a) thiol; (b) alkyne; (c) azide; (d) phosphonate/phosphonic acid.

Another option provided by the 'grafting-onto' approach is the use of BCPs consisting of blocks with different surface affinities. Generally, only a weak interaction between the surface and each unit of the anchoring block is sufficient to tether the block to the surface, *cf*. Section 3.1.3; the other block without surface affinity takes the role of the polymer brush. When more than one anchoring group exists in the BCP, the non-affinity segments in between the anchoring groups will form loops.[274] For a diblock copolymer, the non-anchoring block does not always take the fully collapsed conformation since, as the chain length increases, it tends to be partially stretched.[117]

Grafting BCPs with different affinities onto surfaces is used to disperse and compatibilize inorganic NPs and pigments in organic media, such as solvents and polymer matrices, and organic pigments in aqueous media.[114, 120, 275] The difference in affinity between the two blocks was essential for prevention of aggregation. For example, PAA-*b*-PMMA was a better dispersant for ZnO NPs than PAA-*b*-PSAN because the more polar acrylonitrile units might have competed with the PAA block for the surface, causing bridging between ZnO particles, **Figure 18**.

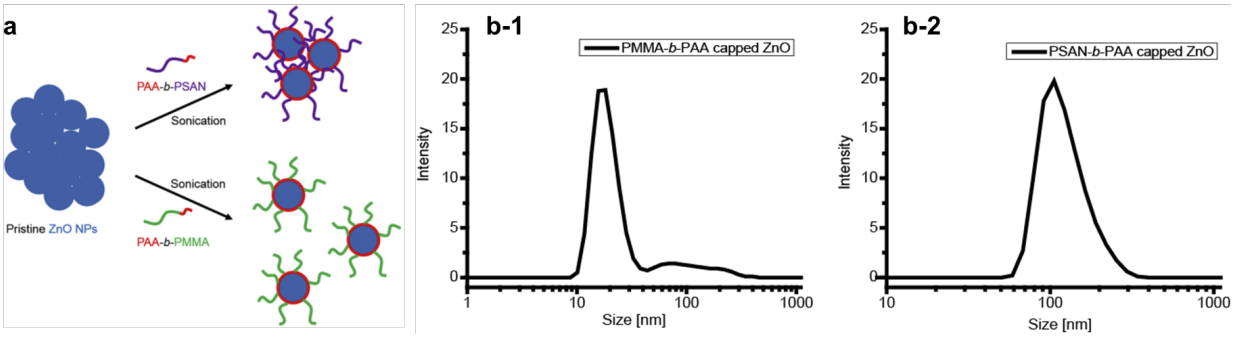

Figure 18. Comparison between ZnO stabilized by PAA_{12}-*b*-$PSAN_{62}$ and PAA_{12}-*b*-$PMMA_{59}$. Panel a illustrates the BCPs anchored to the particle surface. Panel b shows corresponding intensity-weighted hydrodynamic size distribution of the PAA-*b*-PMMA(b-1)/PSAN(b-2)-anchor ZnO particles in THF. [120], Copyright 2016. Adapted with permission from Elsevier Science Ltd.

3.3.2 Ligand Exchange

The ligand exchange approach is a special case of the 'grafting-onto' approach since removable small-molecule ligands, instead of corresponding functional groups, are present on the inorganic surface. This approach requires either a stronger affinity of the polymer ligands than that of the small-molecule ligands or removal of the small-molecule ligands from the reaction system.

The first example of ligand exchange was performed between the small phosphine oxide ligands as-synthesized on the CdSe/ZnS quantum dots (QDs) and multidentate PDMAEMA

ligands. The transfer provided stable coverage for the QDs in the organic medium.[276] However, the structure of polymer-wrapped QDs prepared in this technique has certain defined limitations as it is based on the dynamic equilibrium between the two ligands rather than formation of polymer brushes. Ligands with a single carbodithioate group replaced the pristine trioctylphosphine oxide ligands because of their overwhelmingly stronger affinity to QD surfaces.[277] Similarly, a single thiol group is usually strong enough to replace more labile ligands on noble metals.[278]

Polymer ligands with a single anchoring end-group without large difference in surface affinity, however, were insufficient for ligand exchange even with a large excess of the desired ligand.[279] This was resolved in a more complex approach which required adding a non-solvent for the polymer ligand and the NPs with small ligands. It was possible to drive the equilibrium by locally concentrating polymer ligand and NPs as aggregates thereby excluding the small-molecule ligand, which is perfectly soluble in the mixed solvents. The polymer-grafted NPs become non-dispersible in the reaction medium, pulling the equilibrium further forward. Unlike conventional 'grafting-onto' approach, gradual replacement of the high density small-molecule ligands in the vicinity of the NPs and the dynamic nature of the surface interaction promised a high grafting density. A grafting density up to 1.2 nm^{-2} was achieved by this ligand exchange approach. The ligand exchange approach was then simplified by selection of a removable ligand, octylamine, for NP synthesis.[70] Octylamine has a relatively low boiling point of 175 °C thus accelerating ligand exchange above this temperature (by continuous removal of the volatile ligand from the reaction mixture), **Fig. 19**. The advantage of high grafting density was retained with this simplified technique, achieving grafting densities 0.9-2.5 nm^{-2}. The polymeric ligand, PSAN-NH_2, synthesized via ATRP provided possibility of compatibilization of the ZnO nanoparticles in acrylic glasses[280] and acting as precursors for carbon-ZnO hybrid materials.[281, 282]

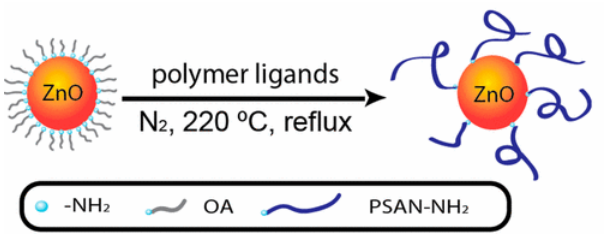

Fig. 19. PSAN-capped ZnO nanoparticles synthesized via ligand exchange with octylamine (OA). [280], Copyright 2017. Reproduced with permission from American Chemical Society.

3.3.3 'Grafting-through'

'Grafting-through' is a combination of 'grafting-onto' and 'grafting-from',[139] which resembles the 'in-out' method for miktoarm star polymer synthesis.[283] Tetherable monomers, such as 3-(trimethoxysilyl)propyl methacrylate, are first anchored to the inorganic surface and then growing polymer chain-ends react with the surface monomer in the 'grafting-onto' stage to form the polymer brushes. The polymerization may continue from the surface with monomers in solution in the 'grafting-from' stage to form polymer brushes. Thus, this approach shares the features of 'grafting-onto' and 'grafting-from'. When the surface is gradually occupied by polymer brushes, new growing chains with larger DP can no longer access the surface from the solution. However, the polymer brush layer still allows shorter chains to grow and monomers to diffuse through the polymer brush and consequently, 'grafting-onto' of these smaller chains and the 'grafting-from' process occurs even at the later stage of the reaction. Therefore, 'grafting-through' is not an ideal approach if high structural uniformity of the brush is required. Besides, free polymers are usually inevitable in this approach, as the free monomer in solution is always more accessible than the anchored ones for the growing chains. 'Grafting-through' via FRP emerged at the same time when 'grafting-from' and 'grafting-onto' was performed.[5] It was later demonstrated that polymer

brushes propagating in solution may again react with the surface monomers to form loops near the surface, *cf*. Section 4, as these chains are growing in a locally high surface-monomer concentration regime.[284]

The two-stage nature of 'grafting-through' allows preparation of miktoarm/binary/bimodal grafts on surface, *cf*. Section 4 and 5.1, if sufficient control of the process can be achieved.[140] In a typical procedure, a macroinitiator is reacted first with the surface monomers in the 'grafting-onto' stage, as the first type of polymer brushes, simultaneously generating initiation sites on the surface. Then, a second monomer was added to grow a type of brush in the 'grafting-from' stage, **Fig. 20**.

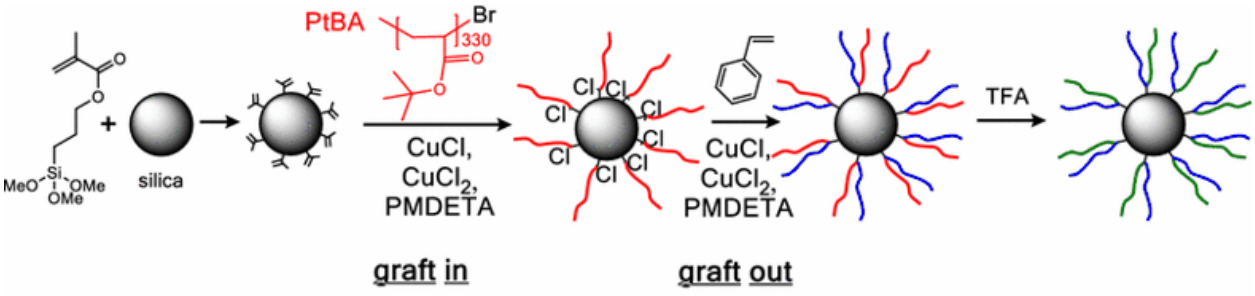

Fig. 20. Schematic illustration of preparation of binary polymer brushes via sequential 'grafting-onto and grafting-from' methods. PMDETA: *N*,*N*,*N*',*N*'',*N*''-pentamethyldiethylenetriamine; TFA: trifluoroacetic acid. [140], Copyright 2016. Reproduced with permission from Springer Nature.

A unique instance of grafting through was to treat 'nanoparticles' as macromonomers. Polyhedral oligomeric silsesquioxane (POSS) could be regarded as the smallest silica nanoparticles. POSS-derived methacrylates were polymerized via ATRP, resulting hybrid materials composed of POSS side groups along the polymer backbone instead of polymer brushes tethered to an inorganic core in conventional hybrid materials.[285-289]

3.4 Templated Synthesis

All the grafting approaches discussed in the previous section can be categorized as 'inorganic-first' approaches. In contrast, templated synthesis methods, *i.e.* synthesis of polymer-inorganic hybrid particles from a polymer template with complex architectures, can be considered as a 'polymer-first' approach. In the template approach, an inorganic NP is formed within the core of a template and the remaining polymer corona serves as the shell. As MW, MWD, and architecture of the polymer template can be precisely controlled, such control is passed over to the hybrid NPs.

3.4.1 Block Copolymer Templates

Organic surfactants play an important role in inorganic nanoparticle synthesis, defining size and shape, compatibilization with the medium, and prevention of aggregation.[290] In the presence of an organic surfactant, micelles are formed from a homogenous solution while the precursor decomposes into inorganic nanoparticles, which are no longer compatible with the medium. Organic-inorganic hybrid materials can also be prepared from pre-formed micelles in a heterogeneous mixture in the presence of surfactant as templates.

Before the application of BCP micelles as liquid-phase template was reported, microphase separated BCPs in the solid state were considered to be attractive templates for the synthesis of inorganic nanoparticles and microstructured polymer-inorganic films.[9, 291-293] PS-based BCP films, such as PS-*b*-P2VP, PS-*b*-PEO, or PS-*b*-PAA films containing metallic precursors were converted into inorganic semiconductor or metal nanoparticle-polymer hybrid films.[9, 293, 294] An alternative approach involves the incorporation of the metal precursor in one of the repeat units of the BCP.[291] In one example, the metal-carrying monomer was copolymerized with the inert monomer via ROMP into the BCP. Later, this strategy was simplified by incorporating a bidentate

ligand-bearing monomer instead of the metal complex, allowing post-polymerization introduction of metallic precursors, **Fig. 21**.[292]

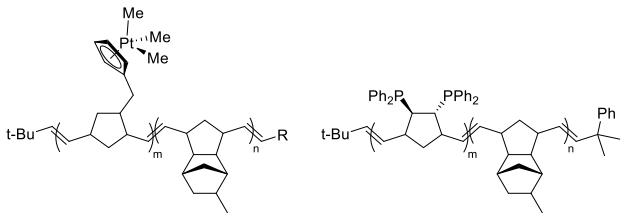

Fig. 21. Metal bearing and ligand bearing block copolymers synthesized via ROMP.[291, 292]

Use of copolymer micelles to induce formation of well-defined inorganic nanoparticles can be traced back to PMMA-PEA-PVP random copolymers used to guide decomposition of $Co_2(CO)_8$ into Co NPs.[295, 296] However, this initial technique provided limited rational design beyond adjustment of formulation. Early practice of templated synthesis of inorganic nanoparticles focused on the use of BCPs, or small-molecule ligands, to induce the formation of micelles.[49, 297] When the inorganic particles are generated inside the micelles, hybrid nanoparticles with organic surfaces are synthesized. Otherwise, if the continuous phase is converted to inorganic materials, it becomes a porous inorganic material with organic internal surfaces.

The template assisted preparation of metal and semiconductor nanoparticles [49, 298-304] was most widely researched with PS-*b*-P4VP or PS-*b*-P2VP as copolymer templates because of the strong coordination strength of pyridine nitrogen and the relative inertness of styrene. The amphiphilic nature of the BCPs furthermore facilitated the use of W/O emulsions. Au,[49, 298, 301, 303, 304] Pd,[299, 301] Pt,[301] Rh,[301] Co,[300] and CdS[302] colloidal NPs were prepared from $HAuCl_4$, $Pd(OAc)_2/Na_2PdCl_4$, $K[Pt(C_2H_4)Cl_3]\cdot H_2O$, $[Rh(CO)_2Cl]_2$, $Co_2(CO)_8/CoCl_2$, and $Cd(OAc)_2$, respectively, as precursors. The catalytic activity of the noble metal NPs,[303] magnetic properties of Co NPs,[300] and the optical properties of the CdS QDs were evaluated.[299, 301, 302]. The recently developed polymerization-induced self-assembly (PISA)

augments BCP template assisted synthesis by allowing more dynamic morphology control.[305-309] Such dynamic control can be leveraged to enable the synthesis of inorganic NPs of diverse shapes and sizes using PISA templates.[310, 311]

3.4.2 Star Polymer Templates

Due to the reversible and dynamic exchange of ligands, micellar templates cannot provide precise control of size (and even shape) of the resulting nanoparticles. Star block copolymers, on the other hand, can be considered more stable unimolecular templates.

Generally, there are two approaches to synthesize star polymers, the 'core-first' approach and the 'arm-first' approach. The 'core-first' approach requires polymerization directly from a multifunctional initiator core, derived from multifunctional molecules, such as cyclodextrin (CD),[312, 313] hexakis(bromomethyl)benzene,[314] silsesquioxane,[315] perylene diimide,[316] or even a molecular spoked wheel.[317] In this approach, there is a definite number of arms determined by the functionality of the core and there is no linear impurity in the product if the star is formed by ATRP. However, there is a limited number of arms and the only way to measure the DP of each arm is to calculate from the absolute MW of the star, for example, by static light scattering. An alternative way to synthesize the core is to polymerize crosslinkers at a high concentration giving a rigid polymeric core with high functionality.[318] However, linear polymer impurities are always inevitable and each star molecule can have a different number of arms. However, the MW of the linear polymers may indicate the length of the arms and with the absolute MW of the star, the average number of arms can be estimated.[319] On the other hand, the 'arm-first' approach gives an opportunity to synthesize narrowly distributed linear 'arms' before crosslinking them to form a polymeric core.[320] This approach also allowed easy synthesis of

miktoarm star polymers[283, 321] but the presence of unreacted linear polymer in the reaction solution requires additional purification. Besides, the average number of arms can only be calculated from the MW of the linear macroinitiators and the absolute MW of the star.

A similar technique demonstrated the preparation of hollow Au, SiO_2, and TiO_2 NPs.[322-324] PDMAEMA brushes were grafted from the surface of a crosslinked polystyrene nanosphere, which can be considered as star polymers with a large PS core and many PDMAEMA arms. Morphological control over the resulting NPs, which appeared as clusters of smaller NPs, was limited. The size of the PS core and the length of the PDMAEMA brushes determined the void size and thickness of the hollow NPs. Besides, no polymeric brushes remained after the sacrificial template was removed.

A recent publication demonstrated a universal approach for the synthesis of polymer-inorganic hybrid NPs using star polymers with BCP arms as nanoreactors, **Fig. 22**.[52] PS (as outer block) was chosen to be the inert polymer brush shell while P*t*BA (as inner block) was the precursor to the anchoring PAA block. The *β*-CD-*g*-PAA-*b*-PS star polymer was used as a nanoreactor to convert inorganic precursors into a large library of uniform hybrid NPs. To prepare the core-shell nanoparticles, a P4VP block was introduced first as the reactive coordinating block in the *β*-CD-*g*-P4VP-*b*-P*t*BA-*b*-PS star and the P*t*BA block was hydrolyzed after conversion of the core NP. Furthermore, hollow NPs could be synthesized from a *β*-CD-*g*-PS-*b*-PAA-*b*-PS star. A large variety of nanoparticles, such as Au, Ag, $PbTiO_3$, $BaTiO_3$, Fe_3O_4, ZnO, TiO_2, CdSe, Cu_2O, Fe_3O_4@$PbTiO_3$, and hollow Au NPs were prepared. This approach was further expanded to the synthesis of silica-based hybrid NPs by introduction of a triethoxysilyl group bearing polymers.[325]

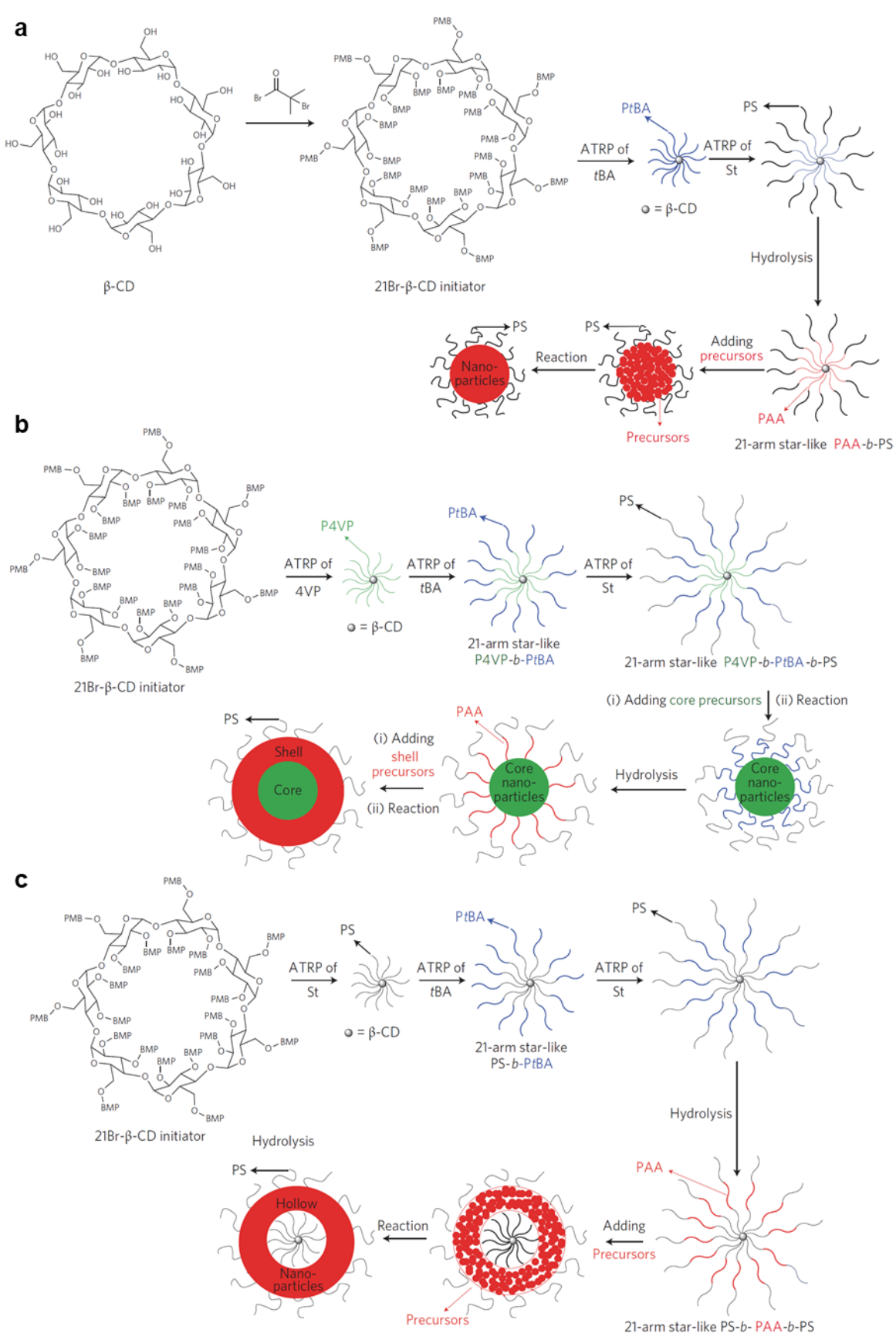
a
β-CD
21Br-β-CD initiator
ATRP of tBA
PtBA
ATRP of St
PS
= β-CD
Hydrolysis
21-arm star-like PAA-b-PS
Adding precursors
PAA
Precursors
Reaction
Nano-particles
b
21Br-β-CD initiator
ATRP of 4VP
P4VP
ATRP of tBA
21-arm star-like P4VP-b-PtBA
ATRP of St
21-arm star-like P4VP-b-PtBA-b-PS
(i) Adding core precursors
(ii) Reaction
Core nano-particles
Hydrolysis
(i) Adding shell precursors
(ii) Reaction
Shell
Core
c
21Br-β-CD initiator
ATRP of St
ATRP of tBA
21-arm star-like PS-b-PtBA
ATRP of St
Hydrolysis
21-arm star-like PS-b- PAA-b-PS
Adding Precursors
Reaction
Hollow Nano-particles
Precursors
Hydrolysis

Fig. 22. Schematic representation of synthetic strategies for preparation of nanoparticles with different architectures (plain, core–shell and hollow) using amphiphilic star-like block co-polymers as nanoreactors. (a–c) Formation of plain nanoparticles (a), core–shell nanoparticles (b) and hollow nanoparticles (c). CD: cyclodextrin; BMP: 2-bromo-2-methylpropionate; St: styrene. [52], Copyright 2013. Adapted with permission from Springer Nature.

Later, it was demonstrated that 'arm-first' star polymers with a much higher number of arms can also act as nanoreactors for the synthesis of hybrid NPs.[120] It was also shown that nanoparticle size could be controlled by control of the precursor loading.

3.4.3 Molecular Bottlebrush Template

Molecular bottlebrushes are macromolecules with a one-dimensional chain-extended structure.[326-328] It is a special type of well-defined graft copolymer with high grafting densities and narrow MWDs. They can be considered as unimolecular cylindrical micelles. There are three major approaches for the synthesis of bottlebrush macromolecules, 'grafting-from', 'grafting-onto', and 'grafting-through'. Similar to the 'grafting-from' and 'grafting-onto' approaches for polymer-grafting onto inorganic nanoparticles discussed in Section 3.2 and Section 3.3, 'grafting-from' is polymerization from an initiator-functionalized backbone while 'grafting-onto' requires anchoring of pre-synthesized end-functional polymers to the backbone. The 'grafting-through' approach is, however, different from the same term for hybrid particles as it describes polymerization of macromonomers to form the backbone.

Polymer-inorganic hybrid NPs synthesized from molecular bottlebrushes inherit the morphology of the template and thus in most cases are one-dimensional. Molecular bottlebrush

templates were reported before the star polymer templates because anisotropic nanoparticles were more challenging to prepare by conventional methods.[22] Similar to the early contributions of BCP templates, molecular bottlebrushes with P2VP-*b*-PS sidechains were used as templates to immobilize $HAuCl_4$ precursors which were then reduced to Au. Other one-dimensional objects, such as DNA and carbon nanotubes were employed as templates for nanorods even before molecular bottlebrushes.[329, 330] However, merely one-dimensional clusters of smaller NPs were prepared in most of the early works while the nanorod morphologies were not uniform.

Later, more systematic approaches to prepare well-defined one-dimensional hybrid materials were demonstrated by Müller et al.[50, 51, 331-336] SiO_2/silsesquioxane, CdSe, and TiO_2 nanowires, nanorods, and nanotubes were prepared utilizing molecular bottlebrush templates. A generic synthetic route starts with poly(2-hydroxyethyl methacrylate) (PHEMA) or its precursor poly(2-trimethylsiloxyethyl methacrylate) (PHEMA-TMS). Then it was converted to the ATRP initiator-bearing backbone poly(2-(2-bromoisobutyryloxy)ethyl methacrylate) (PBiBEM). If a hollow space was needed, an inert or convertible polymer block, e.g. P*t*BA, was first grown from the backbone. An inert poly(*ε*-caprolactone) block could also graft directly from the PHEMA backbone prior to initiator functionalization. Subsequently, the precursor block, e.g. poly(3-(tri(m)ethoxysilyl)propyl acrylate) (convertible to SiO_2/silsesquioxane) or P*t*BA, or the coordinating block, e.g. PDMAEMA, was grafted. Finally, a block such as poly(oligo(ethylene glycol) methacrylate) (POEGMA) or PDMAEMA, was extended from the previous block to enable compatibility or responsiveness. The one-dimensional hybrid NPs were obtained by conversion of either the precursor block or precursors loaded in the coordinating block, **Fig. 23**.

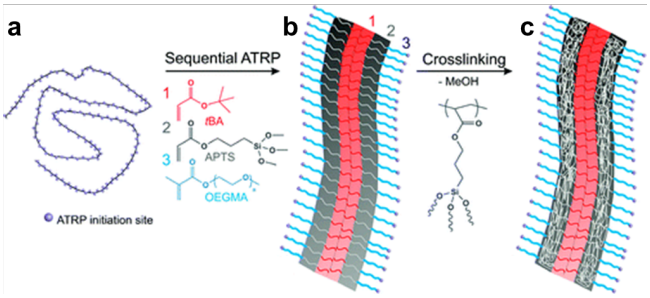

Fig. 23. Synthetic route to obtain water-soluble organo-silica hybrid nanotubes templated by core–shell–corona structured molecular bottlebrushes: (a) ATRP macro/polyinitiator backbone (PBiBEM); (b) core–shell–corona structured molecular bottlebrush; and (c) water-soluble organo-silica hybrid nanotubes. [51], Copyright 2010. Reproduced with permission from American Chemical Society.

Recently, hybrid NPs with tunable anisotropy and more complex topologies were prepared via precise control over molecular bottlebrush structures and synthesis of branched molecular bottlebrushes.[337]

A series of procedures has been developed to prepare polymer brush-grafted inorganic materials. The next section will discuss how these methodologies were employed in regulation of polymer brush architectures.

4. Controlling the Architecture of Grafted Polymers

The properties of polymer brushes – and similar of polymer-tethered particles – are sensitive to the molecular characteristics or architecture of tethered polymer canopies (where in the following the term ‘architecture’ will be used to describe characteristics such as the MW, MWD, composition, topology, density and functionality of grafted polymer chains). The development of synthetic methods to fine tune the architecture of polymer brushes thus presents an important

objective of research in the field. In this section, we discuss recent advances in controlled/living polymerization techniques that hold particular promise to advance the ability to tailor the architecture of brush materials.

MW and MWD are the two fundamental parameters of polymers. Ultrahigh molecular weight PMMA brushes, up to 27 million, on inorganic nanoparticles were achieved by SI-AGET ATRP of MMA from 120 nm silica particles under a pressure of 6 kbar.[227] The target DP ($[Monomer]_0/[Initiator]_0$) was as high as 100,000 while the reaction only proceeded for 4 h. A low dispersity of 1.17 indicated a good control of polymerization. However, at ambient pressure, the same molecular weight of PMMA is difficult to achieve due to the high radical concentration during the polymerization. Eventually, PMMA brushes with MW over 1 million and a moderate MWD was obtained.[338] As for short chains, DP as low as 17 was achieved by quenching the reaction at a low conversion.[339] MWD distribution, however, is more challenging to manipulate while multiple theoretical works have put emphasis on the MWD.[340-342] A narrow MWD is usually accessible via controlled polymerization techniques but there are limited means to broaden MWD in a controlled manner. For linear polymer or the 'grafting-onto' approach, simply blending polymers with different MW may lead to the desired MWD. Kent *et al*. studied polymer brushes with a bimodal MWD by adsorbing PDMS-*b*-PS diblock BCP with two different MWs onto an air-ethyl benzoate interface.[13] A similar approach was also applied to solid surfaces.[343-346] Several different strategies employing the 'grafting-from' approach have been demonstrated, including repeated surface functionalization, partial deactivation of growing chains, chain-extension from chain ends with differentiated reactivities, partial chain-end functionalization with a mixture of initiator and 'dummy' initiator, and partial attachment of polymer to chain ends, **Fig. 24**.[43, 44, 347] Most of these strategies can be expanded to more complex MWD beyond bimodal

by repetition of these steps. In the case of ATRP, as the polymerization is generally governed by the copper coordination compounds, a facile method was developed to broaden the MWD by lowering the copper concentrations.[348, 349] Remarkably, the grafting density was observed to drop simultaneously with decrease of the catalyst concentration. Further investigations differentiated the behavior of styrene and MMA, two most common monomers for radical polymerization, in SI-ATRP with extremely low initiator (particle) concentration. SI-ATRP of MMA with less than 100 ppm of initiator showed a rapid drop in resulting grafting density. On the of hand, grafting density of PS decreased significantly accompanied by broadening of MWD with the decrease of the initiator concentration because of the competing reaction of thermal self-initiation (TSI). Therefore, methacrylate-based monomers were more conducive to the synthesis of well-defined ultrahigh MW polymer brushes than styrenic monomers.[350]

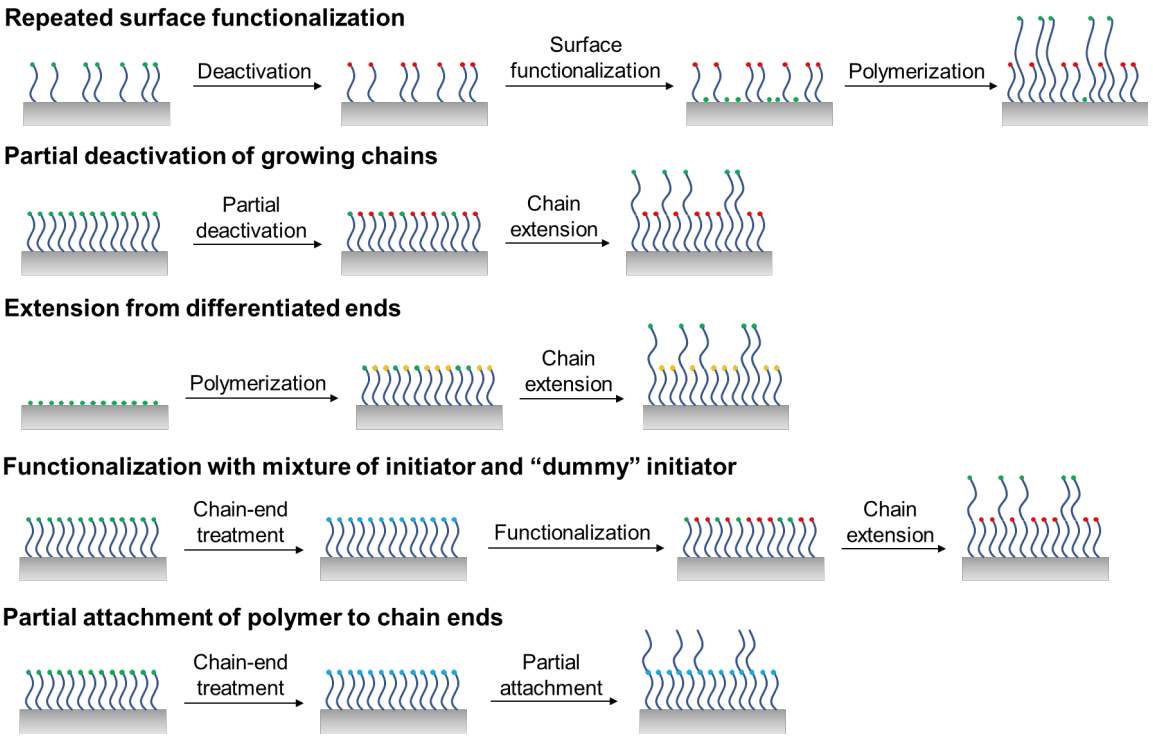

Fig. 24. Exemplified strategies for synthesis of polymer brushes with bimodal MWD by grafting from surfaces. Red: dead chain end; green: living chain end; yellow: chain end with lower reactivity; blue: other reactive functionality, *e.g.* alkyne, azide, etc.

Another relevant aspect of polymer brush architecture is binary/miktoarm brushes, *i.e.* two different types of polymer brushes grafted onto the same surface. Methodologies for binary brushes can also be used to prepare polymer brushes with bimodal MWD, if narrow MWD is achieved in both types of polymer brushes. The first work utilized the slow initiation nature of FRP[18] where azo-based thermal initiators decomposed over a period of time. Therefore, surface-grafted azo groups can be activated in two separate sequential steps. In each step, one monomer was polymerized via FRP. The same strategy can also be applied to reverse ATRP while Cu^{II} catalysts provided deactivation and some level of control of polymerization.[45, 140] Another approach is to graft a mixture of end-functionalized polymers to the surface. Similarly, a mixture

of two orthogonal initiators, such as alkyl halide and alkoxyamine, could also lead to binary brushes.[47] However, none of the aforementioned strategies provided precise control over the ratio and distribution of the two types of polymer brushes. A more sophisticated strategy was to construct a diblock copolymer with an anchoring group in the middle.[46] In this way, precisely 1:1 ratio of uniformly distributed binary brushes could be anchored on the surface. Two different initiators were able to combine different polymers in one molecule.[48, 351] Another strategy is via the 'in-out' approach,[283] *i.e*. the switching to another monomer when macroinitiators were grafted through the surface (similar to the preparation of miktoarm star polymers).[140] This approach does not result in equimolar distribution of the two polymers as some of the chain end functionality is inevitably lost during propagation on the surface. Indeed, the 'surface monomer' does not have to be on the surface during polymerization.[140] Instead, a tetherable monomer can consist of an anchoring block with functional chain end. In this way, chain-end fidelity may be better preserved but the anchoring block can limit the accessible grafting density.

The synthesis of BCP brushes using RDRP techniques is generally straightforward if the chain-end fidelity can be well-preserved. Good temporal control can improve the control over block length and help design material properties.[63, 352] The preparation of functional random copolymers, on the other hand requires less the control of chain-end functionalities but rather the consideration of the feeding ratio and the reactivity ratio. These brushes provide tunable properties based on the composition.[353]

Gradient polymer brushes may refer to several distinct concepts, including the composition change along the polymer chain, i.e. in a conventional gradient copolymer, composition change along the substrate, MW change along the substrate, or grafting density change along the substrate, **Fig. 25**.[354] Other more complex forms of gradients are generally a combination of these four

types. It is possible to prepare gradient copolymer brushes from comonomers with a large difference in reactivity ratios or using slow feeding of the second monomer.[355, 356] Both composition gradient and MW gradient of polymer brushes along a substrate were achieved by lifting the substrate from the polymerization medium.[357, 358] Composition gradient could also be achieved through application of a temperature gradient, *i.e.* due to the difference in reaction kinetics, during a 'grafting-onto' process.[359] The kinetic approach has also been applied to achieve MW gradients via a gradual change of catalyst concentration or the strength of an external stimulus. [26, 64, 360, 361] For example, the controlled variation of the distance of between an electrode and substrate was shown to facilitate gradients of catalyst concentration.[64] The use of SARA ATRP mediated by a copper plate significantly simplifies this procedure as the distance between the copper plate and the substrate dominates the catalyst concentration.[360] Gradients of each block composition in a multiblock copolymer-grafted surface were achieved by simple adjustments to the slope of the copper plate during the polymerization of each block, **Fig. 26**.[361] Tailored variation of the grafting density change along substrate can be achieved by tuning the initiator density on the surface, for example, by allowing the tetherable initiator solution to flow while evaporating.[160] Alternatively, the initiator can be transferred to the substrate from a surface-patterned PDMS stamp. Concave regions across the stamp surface created reduced initiator density which led to a gradient in the brush density.[362]

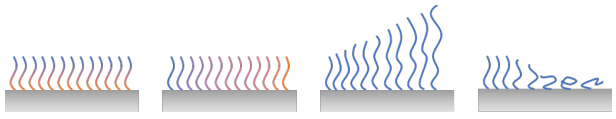

Fig. 25. Illustration of typical gradient structures of polymer brushes on surfaces. From left to right: composition change along the polymer chain, composition change along the substrate, MW change along the substrate, and grafting density change along the substrate.

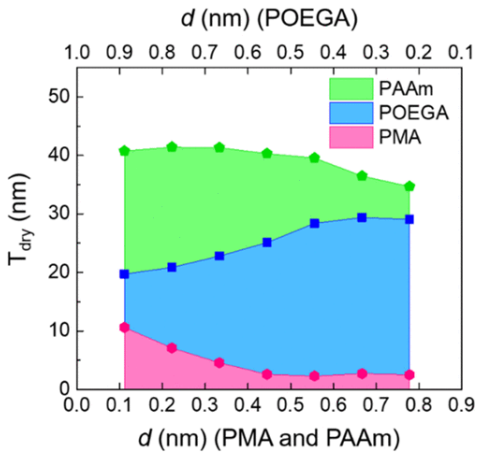

Fig. 26. Thickness (T_{dry}) of structured PMA-*b*-POEGA-*b*-PAAm triblock copolymer brush gradient as a function of the distance between copper plate and the substrate (*d*). The thickness of each brush component along the gradient is highlighted. Polymerization times applied were 20 min for MA, 1 h for OEGA, and 1.5 h for AAm. [361], Copyright 2018. Reproduced with permission from American Chemical Society.

Control of the connectivity (*i.e.* topology) of tethered chains also presents an important objective for polymer chemistry. Polymer brushes with various topologies including loops, (hyper)branches, molecular bottlebrushes, and crosslinked networks were grafted from surfaces. Early reports of polymer loops usually presented unintentional observations during the grafting of multidentate polymer ligands or grafting through surface monomers.[128, 276, 284] Therefore, there was always a mixture of linear tails and loops instead of well-defined loops. To improve the selectivity for polymer loops, RAFT polymerization with chemically modifiable CTA was utilized.[363] Either a bifunctional polymer chain grew from two surface anchored CTAs (Z-group anchoring) or two surface anchored polymer brushes mediated by a bifunctional CTA may lead to formation of loops on surfaces. However, neither approach can prevent formation of linear brushes due to exchange of CTA. A more straightforward approach was to directly attach both ends of a

telechelic polymer to the surface,[364] but it did not exclude the possibility that only one end of the polymer was attached, resulting in a linear polymer brush. Recently, a robust method for preparation of well-defined polymer loops via intramolecular cyclization of narrowly distributed linear polymers followed by 'grafting-onto' was developed.[365, 366] A major difference is that the substrate is no longer part of the loop in these tethered polymer loops. Derived topologies, such as loops as side chains of polymer brushes,[367] were also demonstrated. A recent review provided an extensive discussion of the preparation, properties, and applications of polymer loops on surfaces.[368] (Hyper)branched polymer were synthesized from solid surfaces via a stepwise approach similar to dendrimer synthesis or more efficiently via surface-initiated self-condensing vinyl polymerization (SI-SCVP).[20, 369, 370] SI-SCVP is a process of SI-ATRP of halide-bearing inimers. Thus, each inimer added to the polymer chain end leads to a new branch. Similar, ROP of cyclic ethers bearing a hydroxy group also gives rise to two propagating sites.[371]

Molecular bottlebrushes can also be grafted onto or from surfaces. Using the 'grafting-from' approach, a polymer backbone is usually polymerized from the surface first followed by growth of the side chains.[53] Otherwise, macromonomers can also polymerize directly from the surface.[372] In the case of the 'grafting-onto' approach, pre-synthesized molecular bottlebrushes may anchor to the surface via functional side-groups or end-groups on the backbone, leading to a 'lying-down' or a 'standing-up' conformation.[373] In addition to isolated polymer brushes, crosslinked polymer network were grafted from surface initiators or through surface monomers via (co)polymerization of multifunctional crosslinkers.[374, 375] Crosslinking of linear polymer induced *in situ* or after growth of brushes can also produce grafted polymer networks.[376] The resulting polymer network behaves as a single macromolecule attached to the surface. The combination of conventional linear brushes and polymer networks in various ways was

demonstrated by photoinduced stepwise polymerization of monomers and/or crosslinkers.[80, 377]

The functionalities discussed in **Table 2** can be introduced to polymer brushes at the chain-end or at the side groups. The halide chain-end of SI-ATRP, being an excellent site for nucleophilic substitution, makes post-polymerization modification, such as CuAAC, facile.[44, 378] Several protected monomers, such as *t*BA or HEMA-TMS, and non-coordinating/non-nucleophilic functional monomers, such pentaflurobenzyl methacrylate, were polymerized via SI-ATRP.[140, 379, 380] A broad range functional polymer brushes bearing, e.g. amide, azide, or vinyl groups, were prepared by S-RAFT polymerization.[381-383] They can either carry the R-group or the Z-group depending on how the CTA is immobilized. Besides, the CTA chain-end itself as a functional group may also serve as the precursor to thiol group or undergo heterocycloaddition.[155, 384] Most functionalities available for incorporation into linear polymers are also available for distribution in grafted polymer brushes.[385]

Preparation of polymer brush-based hybrid materials often begins with surface functionalization. Various methodologies were developed for subsequent polymer grafting. Almost any known polymer architecture has been successfully applied to surface-grafted polymer brushes via either the 'grafting-from' or the 'grafting-onto' approach. Advancement of the synthetic strategies is the basis of tunable properties of the polymer-brush-based hybrid materials and the diversity of applications.

Architectures of the grafted polymer brushes were tuned by carefully selected reaction conditions. The architectures in turn dominated the conformation of the polymer brushes and the interactions among particle brushes and between particle brushes and matrices. The next section will explain the physical aspect of the architecture of particle brushes.

5. Architecture, Interaction, and Assembly of Polymer-Grafted Particles

This section summarizes recent progress in the understanding of the effect of particle brush architecture on molecular characteristics (such as conformation) of polymeric tethers as well as the interaction and assembly formation of particle brushes in solution and the solid state. In this physicochemical context, the term 'architecture' is used to describe structural characteristics such as the particle radius, the degree of polymerization, molecular weight dispersity and density of tethered chains. We will focus on particle brush systems in which the 'core' can be considered to be an impenetrable volume to polymer chains. A typical example are inorganic nanoparticles; however, crosslinked microgels, globular proteins, or micellar cores could also fall into this category and often show related behavior. It will further be assumed that the ligands are permanently and strongly bonded to the core. A typical example are covalently bound ligands. Hence, the consequences of dynamic ligand exchange (as it has been observed in gold nanoparticles modified with thiol ligands) will not be considered.[386] Finally, the emphasis of the following discussion will be on spherical particle shapes which have been at the center of research in this field. The constant surface curvature of spherical particles simplifies the categorization of distinct conformational states of tethered chains and hence simplifies the interpretation of structure-property relationships. However, conclusions should extend also to non-spherical shapes (such as nanorods, or nanoplatelets) since the latter could be analyzed in terms of a combination of distinct surface curvatures.

5.1 Conformation of Polymer Brushes

Understanding the structure of particle brush coronas is important because of its impact on the interactions and dynamical properties of brush particles both in solution and the melt state. The first and currently most widely used description of the structure of brush particle coronas takes advantage of the topological similarity between polymer-tethered particles and star polymers. For a star polymer comprised of f chains with uniform degree of polymerization N that is immersed in a solvent, Daoud and Cotton (DC) developed a mean field model that predicts three conformational regimes to exist (**Fig. 27a**): (I) In the proximity of the junction, a core of constant density and radius $r_{core} = N_{core}\, l$ is predicted, where N_{core} is the number of segments of each chain in the core region (the DC model predicts $N_{core} \sim f^{1/2}$) and l is the segment length. Note that the scaling of unity indicates that chains are stretched in the proximity of the junction. (II) A 'swollen regime' in which the segments adopt expanded conformations is predicted at intermediate distances. (III) At distances $r > f^{1/2}\, v\, l$ from the junction (where $v = ½ - \chi$ is the excluded volume parameter and χ denotes the Flory-Huggins interaction parameter), the 'unswollen regime' is predicted in which the star radius scales with $N^{3/5}$. Ohno and Fukuda extended the DC model to the case of polymer-tethered (spherical) particles.[387] The authors postulated a critical distance $r_c = r_0(\sigma^*)^{1/2}(\nu^*)^{-1}$ to separate polymer coronas into two regimes: First, for a total particle size $r_0 + h < r_c$ (where h denotes the brush height and r_0 the particle core radius) particle brushes are assumed to be in the concentrated particle brush (CPB) regime. Here, $\sigma^* = \sigma a^2$ is the reduced grafting density, a denotes the length of a repeat, and $\nu^* = \nu/(4\pi)^{1/2}$ is the effective excluded volume parameter. In the CPB regime the brush height scales with $h \sim N^x$ ($1 > x > 3/5$). This regime thus corresponds to the 'swollen regime' in the original DC model. For a total particle size $r_0 + h > r_c$ the semi-dilute particle brush (SDPB) regime is predicted in which ideal scaling $h \sim N^y$ ($y = 3/5$ in good solvents)

is expected (**Fig. 27b**). Light scattering studies of PS-tethered silica particles in good solvents by Ohno *et al*. and Dukes *et al*. confirmed a scaling of the brush height in the CPB regime of approximately 0.8 (**Fig. 27c**).[388, 389] It is noted that the DC model was originally derived for star polymers in the presence of a solvent (or matrix) and thus is not directly applicable to solvent- or matrix-free systems. This limitation is expected to apply also for the case of brush particles and the extended DC model.

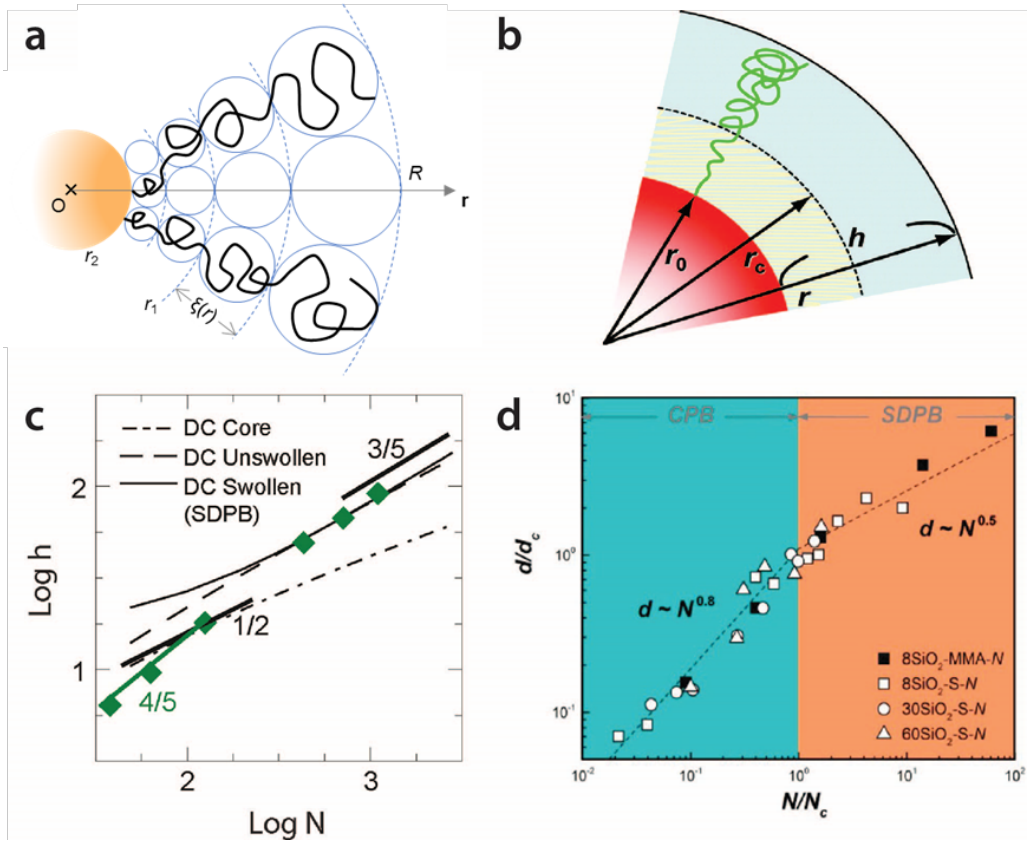

Fig. 27. Panel a shows illustration of star polymer according to Daoud-Cotton (DC). The parameters r_1 and r_2 refer to the radius of the swollen and the inner dense regime, $\xi(r)$ refers to the size of a thermal blob. Redrawn based on Ref. [390]. Panel b depicts the chain conformational transitions in the extended DC model. [387], Copyright 2007. Adapted with permission from American Chemical Society. The parameters r_0 and r_c refer to the particle core radius and the

critical brush height, respectively (see text for more detail). Panel c shows dependence of hydrodynamic radius of brush particles (grafting density $\sigma \sim 0.4$ nm^{-2}) in solution as determined by dynamic light scattering. [389], Copyright 2010. Adapted with permission from American Chemical Society. Panel d shows dependence of the reduced brush height d/d_c (equal to $h/(r_c - r_0)$ using the terminology used in the text) on the reduced degree of polymerization of surface-grafted chains (N/N_c) as determined from analysis of electron micrographs of particle monolayers for PS- and PMMA tethered silica particles of different size (grafting density $\sigma \sim 0.5$ nm^{-2}). [56], Copyright 2014. Adapted with permission from American Chemical Society. Different colored regions correspond to the predicted CPB and SDPB regimes (extended DC model).[390]

The most extensive analysis of brush architecture in matrix- and solvent-free brush particle systems is due to Choi *et al*. and Schmitt *et al*. who applied electron imaging to evaluate the scaling of brush height in particle brush monolayers. The evaluation of extensive libraries of PS- and PMMA-tethered silica particles with diameters ranging between 15-120 nm revealed the existence of two distinct regimes that are characterized by brush height scaling exponents 0.8 and 0.5, respectively.[391] Furthermore, the scaling of brush height for all particle systems as well as the transition between the regimes was shown to conform (within the experimental uncertainty) with the predictions of the extended DC model (**Fig. 27d**). The self-consistent field theory (SCFT) model originally developed by Millner, Witten, and Cates (MWC) to describe chain conformations in planar polymer brushes provides an alternative starting point to describe the structure of polymer canopies on curved surfaces.[392] Wijmans and Zhulina (WZ) extended the MWC model to predict chain conformations in particle brushes. The model recovers the fundamental trend predicted by the DC model but provides further insight into the scaling exponent within each

regime. In particular, it renders the conformation of tethered chains a function of the chain length, a feature that is not accounted for by the extended DC model. Computer simulation as well as dynamic light scattering studies suggest that the WZ model adequately describes the structure of brush particles in solution.[393-395]

Despite this progress in the theory and simulation of brush materials, open questions remain, for example, with regard to the role of molecular weight dispersity on the microstructure of polymer coronas. While most theoretical and simulation studies have focused on brush coronas comprised of chains with uniform molecular weight, synthetic methods – even those based on SI-RDRP – often yield grafted chains with appreciable dispersity ($Đ > 1.3$). In one example, Dodd and Jayaranan used Monte Carlo simulations to investigate the effect of molecular weight dispersity on the conformation and distribution of end groups in polymer coronas.[396] The authors reported increasing dispersity to result in more compressed conformations of short chains while long chains adopted more relaxed conformations. Better understanding of the role of molecular weight dispersity as well as chain connectivity (such as linear vs. comb or bottlebrush) on the structure of brush particle coronas could not only advance the interpretation of experimental results but also inspire new approaches to tailor properties of particle brush materials. In this context it is important to note that in real systems, structural inhomogeneity can have a variety of origins that are not considered in the models. Examples are particle size dispersity or statistical fluctuations in the number of grafts among tethered brush particles. Hakem *et al*. reported a statistical model to describe the compositional heterogeneity associated with surface modification reactions that was shown to apply for a wide range of particle-like systems such as inorganic nanocrystals, proteins or dendrimers.[397] Recent findings by Kumar and coworkers highlight the subtle effects of heterogeneity on the assembly of brush particles in solution[398] and thus

highlight the need for future research to better understand the role of structural and compositional inhomogeneity on the assembly behavior of particle brush materials. Open questions also exist with respect to the effect of brush confinement on the structure of brushes that are comprised of polymer tethers that form associative bonds. For example, dense tethering of poly(N-isopropylacrylamide) (PNIPAM) to gold nanoparticles was reported to result in the splitting of the lower critical solution temperatures (LCST) of brush particle systems.[399] Monte Carlo simulations suggested that the lower transition temperature was to be attributed to the collapse of the dense brush region in which associative solvent-polymer bonds are destabilized due to chain crowding.[400] It is conceivable that better understanding of the interplay of brush architecture and chemistry will enable novel innovative approaches, for example, for the design of drug delivery systems.

5.2 Interactions and Assembly Behavior of Brush Particles

As elaborated above, a common conclusion of the DC and WZ models is that – depending on the architecture of the brush particles – polymer coronas can display chain conformational transitions across the brush layer. Because the physical properties of polymers are sensitive to chain conformation and orientation, this feature of brush systems has motivated research into the effect of brush architecture on the interactions and assembly behavior of brush particle materials as will be described below. It should be noted that this research has occurred in the broader context of 'polymer-functionalized particle-like systems', that is, systems that bear similarity to 'brush particles'. Examples are block copolymer micelles or polymer-protein conjugate systems in solution and the solid state (both represent 'soft particle' systems)[401-403] or tadpole-type nanoparticles in which an inorganic particle is tethered with (ideally) one polymer chain that have

been pursued because of their resemblance to 'giant surfactants'.[404-406] For the sake of brevity, the following discussion will focus on research performed on brush particle systems in which an inorganic core carries a sufficient number of tethers to render the application of the 'brush picture' meaningful. However, in the limit of low grafting density, the boundaries may be blurred and thus, where appropriate, a reference to alternate material systems will be made to point out 'generalizable' aspects of behavior. Finally, for the purpose of the ensuing discussion, it is helpful to categorize brush particles into distinct grafting regimes. Thus, the high, medium, and low grafting regimes are defined on the basis of the DC model as those corresponding to $r_0 < r_c$ (high), $r_0 \sim r_c$ (medium) and $r_0 > r_c$ (low), respectively. Note that only particle brushes with high grafting density may display a transition between the CPB and SDPB regime depending on the degree of polymerization of tethered chains.

In a first approximation, insights into the effect of polymer coronas on the interactions between particles may be drawn from studies on star polymer analogs. For the case of multi-arm star polymers, Likos and coworkers developed an expression for the effective pair interaction potential $V(r)$ by considering excluded volume constraints.[407, 408] The potential reduces to the hard sphere potential in the limit of large number of arms ($f \rightarrow \infty$). For finite numbers of f, the potential predicts stars to interact via a Yukawa-type potential at large distance while short-range interactions are predicted to follow a more logarithmic trend. The normalized interaction potential for various star architectures is illustrated in **Fig. 28a**. Matsen and Kim developed a numerical scheme based on self-consistent field theory to evaluate the interaction between polymer-tethered particles in solution.[409] The simulated interaction potential (**Fig. 28b**) revealed qualitative similarity to those of star polymer systems and confirmed that interactions are purely repulsive for all particle spacing. Light scattering experiments on PS tethered silica particles with systematically

varied degree of polymerization and grafting density by Fytas and coworkers confirmed the principal trends predicted by theory and simulations.[410] The analysis of the static and dynamic structure factor of brush particle solutions (in good solvents) across the dilute and semidilute concentration range revealed a transition from hard-sphere-type interactions for brush particles in the CPB regime to soft star-like interactions for brush particles in the SDPB regime.[410] Goel et al. evaluated the interaction between brush particles in the solid state using small angle X-ray scattering. The authors reported a repulsive potential $U(r) = r^{-12.5\pm2}$ which indicates stronger repulsive interactions as suggested by Likos et al. for star polymers. This difference was attributed to the contribution of the hard inner core of brush particles.[411] Jayaraman and coworkers applied Langevin molecular dynamics and Polymer Reference Interaction Site Model (PRISM) calculations to evaluate the effect of comb-like polymeric tethers on the interactions between brush particles in solvents and athermal polymer matrix.[412] Interestingly, their simulations predicted attractive interactions to exist due to the increased crowding of coronas comprised of comb polymer tethers (**Fig. 28c**). This prediction, yet to be validated by experiments, suggests a wide range of tunability of brush particle interactions that is enabled through variation of the chain architecture of polymeric tethers.

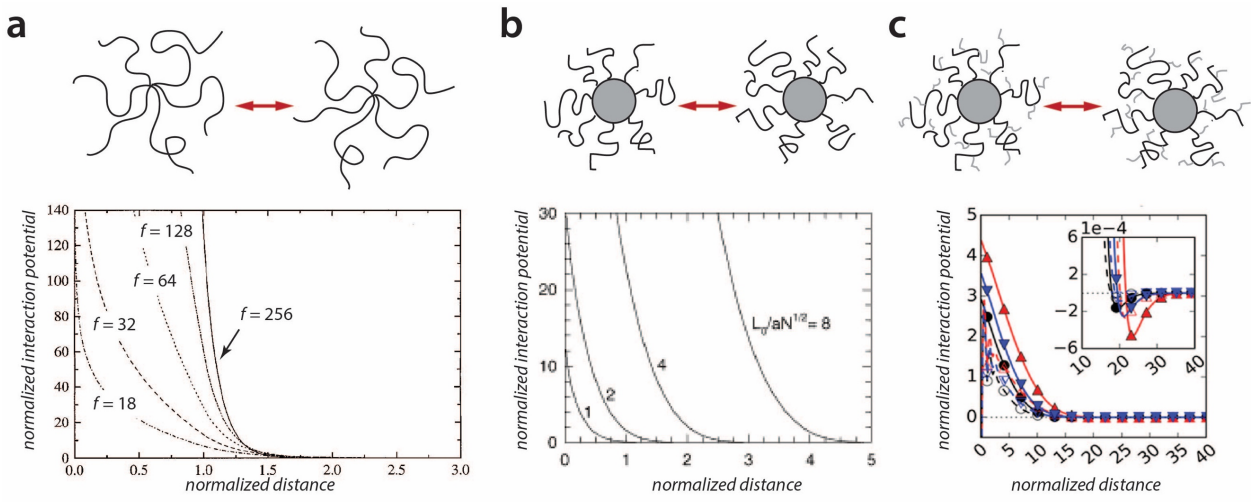

Fig. 28. Panel a: Pair potential between two star polymers as a function of the distance of the junction points (normalized with respect to the star radius). Interactions are purely repulsive. [407], Copyright 1998. Adapted with permission from American Physical Society. Panel b shows corresponding normalized pair potential for brush particles with constant grafting density. Numbers indicate various brush thicknesses (L_0 denotes the brush height). Interactions are purely repulsive. [409], Copyright 2008. Adapted with permission from American Chemical Society. Panel c shows pair potential simulated for comb-brush particles. Attractive interactions are observed for certain densities of side chains. [412], Copyright 2017. Adapted with permission from American Chemical Society.

Analysis of the interaction potential between brush particles in solution is important because it enables the prediction of the assembly behavior of brush particles in a solvent environment. For example, Likos and coworkers applied their potential of mean force in conjunction with Monte Carlo simulations to predict a hierarchy of crystal structures (such as face-centered cubic (fcc), hexagonal close packed (hcp), body-centered cubic (bcc), or diamond cubic (dc)) to form with increasing softness of the potential.[413] Albeit their predictions were derived

specifically for star polymers, the results may provide a guideline for the expected structure formation in brush particle systems with high and medium grafting density. Indeed, recent experiments have provided evidence for the existence of fcc, hcp, and bcc superlattice structures in films of assembled PS-tethered silica brush particles (110 nm particle diameter) in the high grafting regime (**Fig. 29a** and **Fig. 29b**). However, given the unknown role of mechanical stresses on structure formation during the solvent casting and thermal annealing process, no final conclusions could be reached on the basis of these experiments.

Most studies on brush particle materials have focused on the high and medium grafting regime. In these regimes, the grafting density is high enough so that interactions between particle cores are effectively 'shielded' and thus the formation of uniformly dispersed structures is observed. Insights into the role of grafting density on the interaction and assembly behavior of brush particles comes from simulations and experiments on particle systems that are tethered with few polymer chains. These studies were originally designed to advance understanding of the governing parameters that control organization in surfactant and colloidal systems rather than the design of hybrid materials; however, some significant insights of these studies will be presented in this section as they provide a basis for the interpretation of the assembly behavior in the low grafting regime. For example, Glotzer and coworkers analyzed the organization of mono- and di-tethered particles using computer simulations and reported the formation of a hierarchy of microstructures that bear similarity to mesophases found in surfactant solutions (**Fig. 29c**).[414] Schweizer and coworkers applied the polymer reference interaction site model (PRISM) theory to evaluate the effect (as well as placement) of polymer tethers on the structure formation in systems with low grafting density. The authors found that microphase separation was increasingly hindered as the number of tethered chains on nanoparticles increased from one to four.[415] Experimental

results by Kumacheva and coworkers supported this prediction and demonstrated the formation of 'patchy' colloids in the limit of low grafting densities (**Fig. 29d**).[416] While the material systems in these previous studies are quite different from low density brush particles (which will generally feature a non-uniform distribution of particle size and number of grafts), the results illustrate that in the low grafting limit, polar interactions can drive the formation of non-isotropic mesophases. This has indeed been observed in the case of low grafting density silica particle systems that were found to spontaneously organize into string-like aggregate structures.[395] The symmetry breaking of interactions was attributed to the partitioning of polymer tethers into the galley regions between the particle strings (**Fig. 29e**).[417] The resulting increase of core-core interactions was argued to give rise to an increase of the Young's modulus of hybrid materials assembled from low grafting density brush particles. Recent computational investigations by Midya et al suggest that the partitioning of polymer chains can occur even in the case of medium chain grafting densities in which anisotropic superstructures are typically not observed.[418]

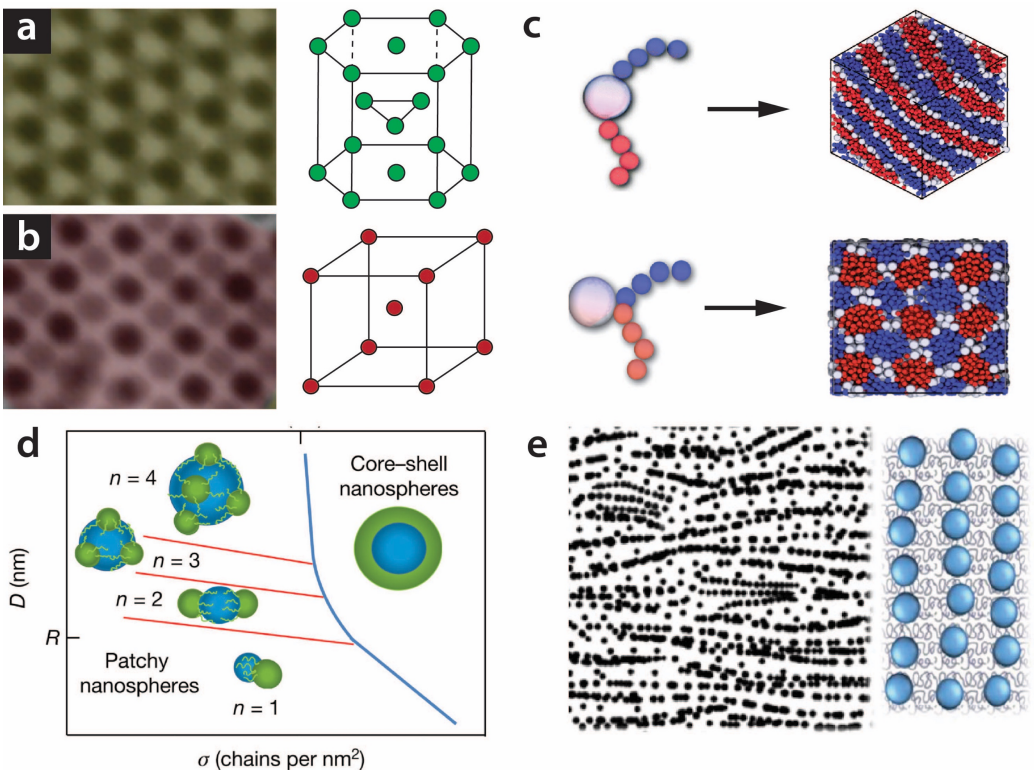

Fig. 29. Panel a shows transmission electron micrograph (TEM) of particle brush (SiO_2-PS, r_0 = 60 nm, N = 530, σ = 0.7 nm^{-2}) multilayer film displaying hcp order. Panel b shows TEM of particle brush (SiO_2-PS, r_0 = 60 nm, N = 530, σ = 0.7 nm^{-2}) multilayer film displaying bcc order. Panel c depicts simulated microstructures of di-tethered nanoparticles comprised of two distinct chains of equal length. [414], Copyright 2009. Adapted with permission from American Chemical Society. A transition from layered to cubic microstructures is observed depending on the position of chains on particle surface. Panel d shows the partitioning of surface-tethered chains as a function of the grafting density. Partitioning is observed in the very low grafting limit. [416], Copyright 2016. Adapted with permission from Springer Nature. Panel e displays string formation in a particle brush composite materials in the low grafting density limit. The figure is deduced by analysis of X-ray spectra of the corresponding material (not shown). [417], Copyright 2013. Adapted with permission from American Chemical Society.

Exciting new opportunities to control structure formation in brush particle systems are provided by designing systems in which multiple organization processes relating to core- and ligand-interactions are concurrently active during the self-assembly process. Examples are semicrystalline polymers in which the crystallization of ligands occurs under the constraints of the framework that is defined by the particle cores or block copolymer ligands that – in pristine form – self-organize into a given microdomain morphology.[419] In these systems, the competition of energetic contributions of the respective competing processes, that are also subject to the constraints of the brush architecture, can be expected to result in rich structural variety. An indication of how the competition between hard-sphere type interactions of particle cores and the microphase separation of copolymer ligands can drive the formation of novel microdomain morphologies was provided by Zhang and coworkers who combined SCFT and density functional theory (DFT) to simulate structure formation in mono-tethered block copolymer-brush particles.[405] Only few synthetic studies of block copolymer tethered particles have been reported, and those only concerned brush particles with high grafting density.[38] Interestingly, no 'special' microstructures were observed in these cases, indicating that the constraints of steric confinement that are imposed in dense polymer canopies constrain the self-assembly process and thus structure formation.

Complementary insights into the role of architecture on the interactions between brush particles have been gained through the analysis of the mechanical properties of particle brush materials in the bulk state. These investigations have been motivated by the potential application of brush particles as platform for 'one-component hybrid materials'. The latter term refers to a composite materials that is fabricated via the assembly of brush particles rather than the dispersion of particles within a matrix polymer. The one-component nature of this type of hybrid material

results in inherently better control of the materials' microstructure and thus potentially enhanced functionality. Mechanical analysis refers to the characterization of the various mechanical quantities such as the elastic (or Young) modulus, yield strength, strain-to-fracture, toughness as well as the various viscoelastic response functions. Because the focus of this section is on structure and interactions rather than the dynamical characteristics of particle brush assemblies, the following discussion will be limited to polymeric tethers that exhibit a high glass transition temperature. In this case, viscoelastic contributions at room temperature can be neglected and the material behavior can be described in terms of time-independent quantities such as modulus or toughness. Bulk materials that are assembled from brush particles satisfying this condition will in the following be denoted as 'particle brush solids'. Readers interested in the dynamical and viscoelastic properties of brush particle materials are referred to the literature.[420-423]

Research into the mechanical properties of particle brush solids has focused on two primary mechanical parameters, *i.e.* the bulk elastic modulus as well as the fracture toughness. The elastic or Young modulus (also known as 'stiffness') describes the resistance of a material to uniaxial elastic deformation. Besides its obvious importance in describing the response of a material to the application of a load, Young's modulus is of interest because it is measured in the limit of small deformations and thus its value is a direct measure for the strengths of chemical bonds between the constituents of the material. In contrast, fracture toughness is a measure for the energy absorption of a material until fracture and thus depends on large-strain response characteristics that are influenced by microscopic flows and chain entanglement.

Various methods have been used to determine the elastic modulus of particle brush solids, including nano- or microindentation, tensile stress-strain measurements, film buckling analysis, or Brilluoin scattering.[395, 424] The most extensive characterization of the elastic properties of

brush particle solids is due to Choi *et al*, Schmitt *et al*, and Lee *et al* who applied nanoindentation to evaluate extensive libraries of PMMA- and PS-tethered silica particles of various particle size, grafting density and degree of polymerization of tethered chains.[391, 425, 426] PMMA and PS are particularly suitable for this purpose since both polymers are amorphous and exhibit high glass transition temperatures. This simplified the interpretation of results since crystallization or viscoelastic phenomena could be neglected. Interestingly, the response of particle brush solids was found to sensitively depend on the grafting density of brush particles. In the high and medium grafting density regime, the elastic modulus increased with the degree of polymerization of grafted chains and subsequently leveled off at intermediate chain lengths ($N \sim 50$) at values close to the corresponding bulk polymer (**Fig. 30a**). This trend was interpreted as being indicative of particle brush interactions being dominated by dispersion interactions between polymeric tethers with little contribution of particle cores (which were argued to be screened by sufficiently dense ligand layers). A similar conclusion was reached before by Shevchenko and coworkers who evaluated the elastic properties of (low molecular) surfactant coated nanocrystal superlattice structures.[427] Normalization of the Young's modulus with respect to the organic fraction revealed that medium grafting densities were more effective in raising the Young's modulus of brush assembly structures (*i.e.* a lesser amount of organic phase was required to achieve a given increase in modulus). This was rationalized as a consequence of more efficient brush interdigitation in the case of medium grafting densities and the associated increase of dispersion interactions *between* adjacent brush particles.

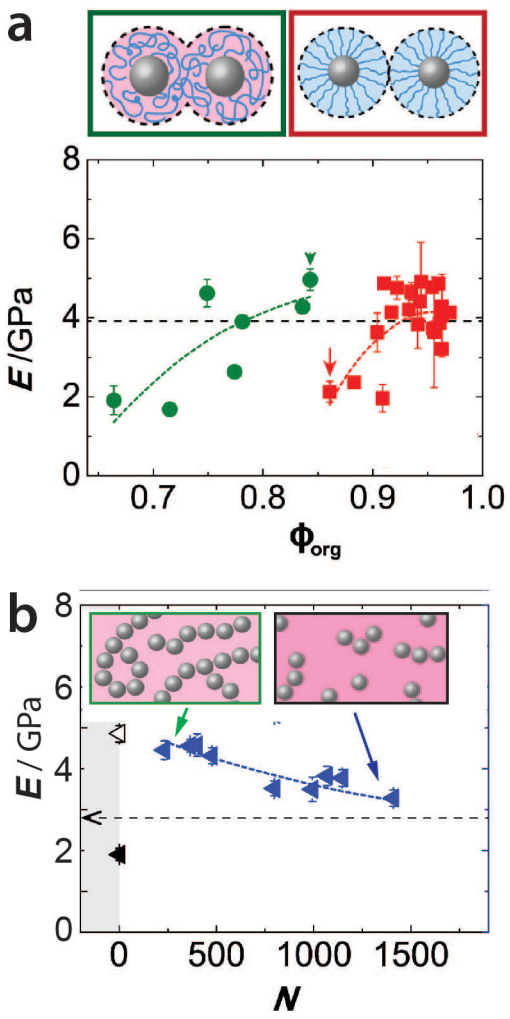

Fig. 30. Elastic (Young) modulus of SiO_2-PS particle brush solids (particle radius r_0 = 7.7 nm) determined by nanoindentation. Panel a depicts high (red squares) and medium (green circles) grafting density corresponding to $\sigma \sim 0.8$ nm^{-2} and 0.1 nm^{-2}, respectively, as a function of organic content. The dotted line indicates bulk PS (M_w = 300,000). The increase of Young's modulus at lower organic content implies that repeat units are more effective in raising interactions. Schemes contrast distinct interdigitation depending on grafting density. Panel b shows Young's modulus of particle brush solids with low grafting density. The decrease of modulus is rationalized with decreasing string formation as indicated in the inset. For all measurements, the film thickness was

500 μm, approximate indentation depth was 10 μm. Experiments followed the process described in Ref. [425]

Interestingly, low grafting density brush particle systems displayed an opposing behavior, *i.e.* the Young's modulus was found to continuously decrease with increasing *N* of tethered chains, ultimately leveling off at bulk values of the corresponding homopolymer (**Fig. 30b**). This contrasting behavior to medium or high grafting density systems was attributed to the string-like microstructure formed by low density brush particles in the thin film state.[417] The partitioning of chains into the galley regions between particle strings was argued to increase the contribution of core-core interactions to the total cohesive energy density and hence the elastic modulus. With increasing degree of polymerization of tethered chains, the string-length decreased thus recovering regular bulk characteristics in the limit of long tethered chains. Fytas and coworkers pioneered the application of Brillouin scattering to analyze the elastic properties of particle brush solids. One advantage of this method is that it provides insight into mechanical anisotropy by judicious selection of the scattering vector parallel or normal to the film surface. Results obtained on individual brush particles in the high grafting regime indicated a higher modulus of the polymer brush in transverse direction (*i.e.* normal to the particle surface).[428] This splitting of the elastic modulus into transverse (stiff) and tangential (soft) components is, in fact, consistent with the orientation of densely tethered chains normal to the surface that is predicted, for example, by the DC model. Chain orientation of bulk polymers is known to induce mechanical anisotropy and to alter a wide range of physical properties. The deliberate engineering of the orientation of polymer canopies has thus far been utilized to realize low-resistance thermal interface materials as well as new phononic crystal materials. The further development of this concept presents an intriguing direction in the field of brush-based materials.

As elaborated above, the elastic modulus of a material is measured in the limit of small deformation. It is an important parameter because it yields insight into the cohesive energy density (*i.e.* the density and strength of bonds) of materials. In contrast, 'toughness' (or 'fracture toughness') relates to the total energy absorption of a material during the entire deformation process. 'Tough' materials will resist fracture and crack formation; for this reason, toughness is a relevant parameter from an application perspective. In glassy polymers, toughness is related to 'craze formation', that is microscopic flow processes that occur within an entangled polymer matrix.[429, 430] Toughness is typically determined by integration of tensile stress strain curves or – in indentation analysis – by evaluation of the length of cracks that emanate from the tips of indent regions.

Vaia and coworkers were the first to demonstrate large-strain extensibility in one-component hybrid materials (**Fig. 31a**).[431] For the example of PS-tethered titania brush particle solids (cylinders with $d \sim 18$ nm and $h \sim 40$ nm) with medium graft density ($\sigma \sim 0.5$ nm^{-2}) the authors reported extensibilities of up to 100% for inorganic content of 80% (w/v). The authors rationalized the ability of the materials to undergo large strain plastic deformation as indication of entanglement formation. Choi *et al* and Schmitt *et al* used indentation analysis to systematically evaluate the fracture toughness of particle brush solids for a library of PS- and PMMA-tethered SiO_2 ($r_0 = 7.7$ nm) in the high grafting density regime. The results are summarized in **Fig. 31b** that depicts the fracture toughness of brush particle solids K_{Ic} (also called the stress intensity factor for mode I fracture) normalized by the respective value K^0_{Ic} for the reference homopolymer (M_w = 300,000) as a function of the degree of polymerization of tethered chains. The figure reveals a step function increase of K_{Ic} at a critical degree of polymerization approximately equal to the CPB-SDPB transition. The authors concluded that entanglement formation in particle brush assemblies

required relaxed chain conformations which are only expected to occur in the SDPB regime. By stipulating that, for entanglements to occur, the segment length of tethered chains in the SDPB regime ought to exceed twice the critical segment length for entanglement formation N_e, the authors derived the minimum degree of polymerization of tethered chains as $N_{min} = 2N_e + [a^{-1}(r_c - r_0)]^{1/x}$ where r_c depends on the grafting density, a is the length of a repeat, and x is the scaling exponent of brush height in the CPB regime (**Fig. 31c**). This result may be used as design guideline for the synthesis of tough particle brush solids.

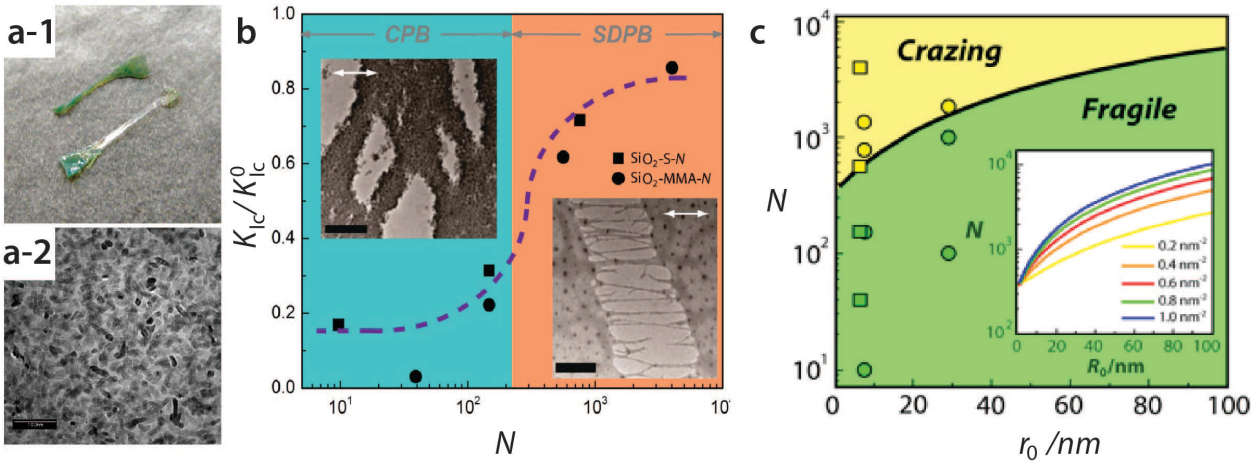

Fig. 31. Panel a shows picture of strained dogbone-shaped sample of TiO_2-PS particle solid (a-1) as well as TEM of thin film (a-2). The scale bar is 100 nm. [431], Copyright 2010. Adapted with permission from American Chemical Society. Panel b depicts normalized stress intensity factor of SiO_2-PS and SiO_2-PMMA (r_0 = 7.7 nm, σ ~ 0.6 nm^{-2}) as function of degree of polymerization of tethered chains. Highlighted areas correspond to the CPB (green) and SDPB (orange) regime. Insets show TEMs of crack formation in monolayer films. Sharp cracks in CPB regime indicate brittle fracture, consistent with low fracture toughness. Craze formation is seen in SDPB regime. Scale bars are 50 nm. [56], Copyright 2014. Adapted with permission from American Chemical Society. Panel c shows minimum degree of chain length to facilitate crazing in brush particle solids

calculated for various brush architectures. Points indicate measured responses of materials in respective regime. [391], Copyright 2012. Adapted with permission from Royal Chemical Society.

The (rather high) threshold degree of polymerization for effective interparticle entanglement implies that the maximum attainable inorganic fraction for processable particle brush hybrid materials is generally constrained by the particle brush architecture and polymer composition.[432] In a particular case, for PS grafted from silica NPs with radius r_0 ~7.7 nm, a N of 770 is necessary for a sufficient interparticle entanglement. Therefore, the maximum inorganic fraction was only about 10 wt%. Hence, an underlying dilemma hindering the application of brush particle solids is that short polymer brushes cannot provide entanglement for a tough processable material while long polymer brushes diminish the inorganic fraction as well as the desired properties/enhancements provided by the inorganic particles. If one circumvents the dilemma by using loosely grafted long polymer brushes, the exposed inorganic surfaces can lead to aggregation which is generally detrimental to the properties of the material.[344]

A possible solution to this dilemma was demonstrated by polymer brushes with bimodal MWD, *vide supra*.[44] In an ideal case, densely grafted short polymer brushes shields the inorganic surfaces as particle brushes with high grafting densities without compromising the inorganic fraction. Meanwhile, sparsely grafted long polymer brushes provide entanglement as particle brush with low grafting densities because the CPB to SDPB transition takes places at the chain end of the short brushes, **Fig. 32** and

Table 3.

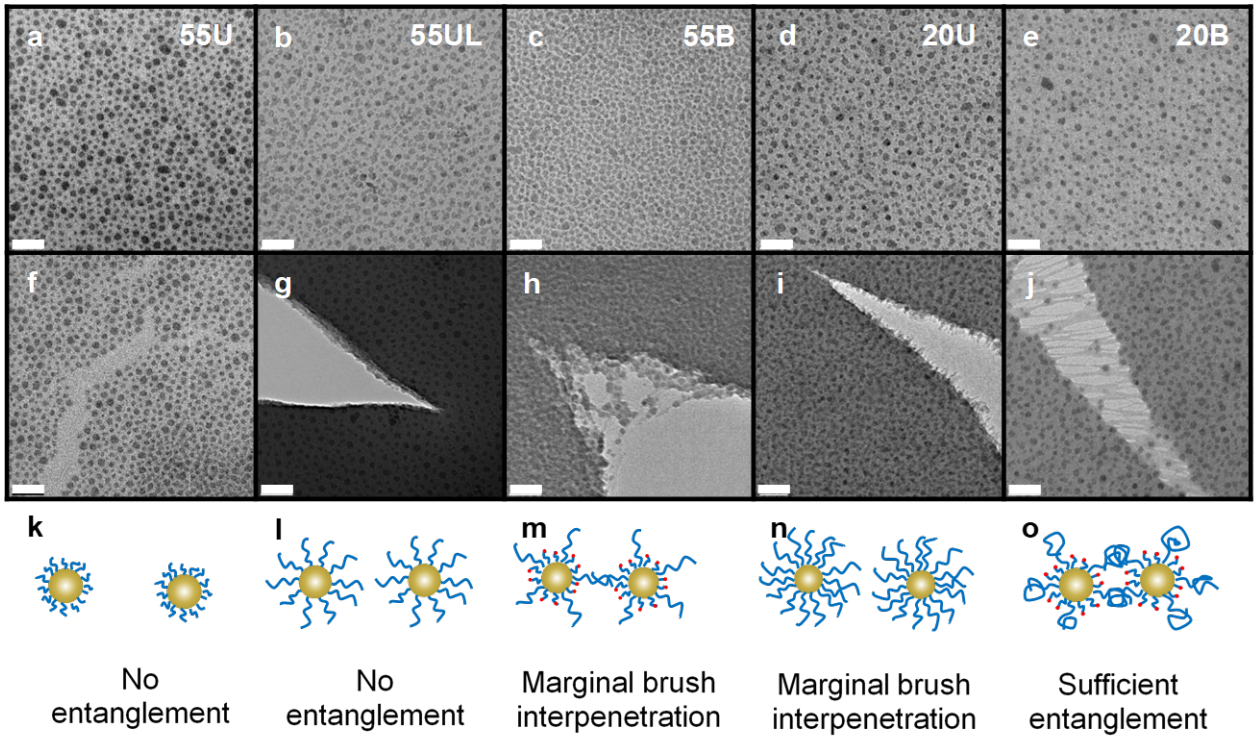

Fig. 32. Panel a-j show bright field TEM images of approximate monolayers (a–e) and crack formation (f–j). Panel k-o illustrate interparticle interactions of the five samples. All scale bars: 100 nm. Sample specifications are listed in

Table 3. Unimodal sample 55U (SiO_2-*g*-PS_{80}, a, f, k): $N < N_e \sim 160$, extensive crack propagation. Unimodal sample 55UL (SiO2-g-PS170, b, g, l): above entanglement limit but in CPB regime ($N < 250$), sharp crack formation. Bimodal sample 55B (SiO_2-*g*-*bi*-$PS_{13,170}$, c, h, m): long brushes above N_e and slightly beyond CPB-SDPB transition ($\sigma_1 \sim 0.11$ nm^{-2}), plastic deformation. Unimodal sample 20U (SiO_2-*g*-PS_{250}, d, i, n): $N > N_e$ and slightly beyond CPB-SDPB transition, stent-like undulation formation. Bimodal sample 20B (SiO_2-*g*-*bi*-$PS_{69,790}$, e, j, o): long brushes in SDPB regime and far above N_e, craze formation. Scale bars = 100 nm. [44], Copyright 2015. Adapted with permission from American Chemical Society.

Indeed, plastic deformation of particle brushes induced by marginal entanglement among the N = 170 PS was observed on silica NPs with similar radius and polymer brushes with bimodal MWD. Moreover, well-defined craze formation was observed for N = 790 long brushes coexisted with 72 mol% of DP69 short brushes. The CPB to SDPB transition for the long brush happened essentially at N = 69 while the effective grafting density for the long brushes was only 0.11 nm^{-2} thus resulting in a low threshold degree of polymerization. The toughness was measured by nanoindentation and AFM to be 23% higher than comparable linear PS with similar N to the unimodal particle brushes, *i.e.* N = 250. Eventually, a matrix-free silica-PS hybrid material with 21 wt% of inorganics was obtained while the similar silica NPs and the same polymer was employed as the unimodal system. Similarly, ZrO_2-grafted PDMS with multimodal MWD displayed higher inorganic loading and better structure integrity than the unimodal counterpart. Therefore, the materials were more resistant to crack formation and performed better as a high refractive-index encapsulant for LED.

Table 3. Degree of polymerization (N), dispersity ($Đ$), short chain number fraction (f_s), graft density (σ), inorganic content (f_{ino}) and interparticle distances (d_{ip}) of the two bimodal hybrid samples (**55B** and **20B**) and the corresponding unimodal samples (**55U**, **55UL**, and **20U**) shown in **Fig. 32**.

Sample	N_s[a]	$Đ_s$[a]	N_l[a]	$Đ_l$[a]	$f_{s,theo}$	$f_{s,exp}$[a]	σ(nm^{-2})[b]	σ_s (nm^{-2})	σ_l (nm^{-2})	f_{ino}	d_{ip} (nm)[c]	T_g (ºC)
55B	13	1.06	170	1.46	0.80	0.69	0.37	0.26	0.11	0.57	19.3±0.6	98.1
55U	-	-	80	1.04	1	-	0.34	-	0.34	0.51	24.5±0.5	103.8
55UL	-	-	170	1.07	1	-	0.15	-	0.15	0.53	29.8±1.1	100.7
20B	69	1.05	790	1.10	0.80	0.72	0.43	0.31	0.11	0.21	30.9±0.8	106.4
20U	-	-	250	1.05	1	-	0.45	-	0.45	0.20	34.4±1.2	105.9

[a] Calculated from the deconvoluted SEC peaks; [b] calculated from the TGA plot of purified sample following equation (1); [c] measured from TEM image of monolayer. All samples were PS grafted from initiator modified silica nanoparticles ($R_0 \approx 7.9$ nm). [44], Copyright 2015. Adapted with permission from American Chemical Society.

Beyond its effect on the mechanical properties and microstructure of brush particle assembly structures, the interaction between polymeric ligands has also shown to enable the dynamic alteration of the structure of particle brush solids. For example, ligand interactions in blends of brush particles that are tethered with distinct polymeric chains (such as PMMA or PS) were shown to drive phase separation in brush particle blends similar to phase separation in polymer blends.[433] This could enable the future design of particulate materials that can be reversibly organized into different microstructures with tailored functionality.

5.3 Brush-Matrix Interactions

Polymer-grafted NPs are not always standalone materials. In fact, use of polymer-grafted NPs as fillers in polymer matrices composes a majority of nanocomposites. In most cases, the polymer matrices dominate the properties of the nanocomposites while a small amount of NP fillers influence them.[280] However, polymer matrices play an important role even if only a small fraction of the material is the matrix or the free polymers are introduced unintentionally. It is known that styrenic monomers undergo a thermal self-initiation (TSI) side reaction at an elevated temperature.[434] If the polymerization of styrene is performed from a NP surface, the homopolymers generated from TSI are carried over to the final material and become the polymer matrix.[216] Although the homopolymers from this typical side reaction make the nanocomposite harder to precisely describe,[435] they may improve the overall fracture strength of the material. The small amount of homopolymer essentially filled up the interstitial space among the particle

brush assembly, providing additional entanglement for the immobilized polymer brushes. Further studies revealed the two-step process of particle brush-homopolymer interaction by addition of homopolymers.[436] In the limit of low filling fractions, homopolymers were found to reside in the interstitial spaces and improve the fracture toughness of the material. After all interstitial spaces are occupied, additional homopolymers take two different distributions depending on the respective degree of polymerization. If the homopolymer is shorter than the polymer brushes, the homopolymer tends to swell the ordered particle brush assembly, leading to further improvement in fracture toughness. However, if the homopolymers are longer than the brushes, the material undergoes phase separation due to entropic preference for interparticle attraction and eventually a cost to the structural integrity.[437, 438]

Due to the ubiquitous incompatibility among different polymers, the polymer matrix usually has to share the exact composition of the polymer brushes or the outer layer of BCP grafts. However, there are a few exceptions, among which the most well-known combination is PMMA and PSAN with a ratio of S:AN ~ 3:1.[439, 440] The origin of the miscibility was ascribed to the strong repulsion between S and AN being screened by PMMA, resulting in a negative enthalpic change enhancing mixing. The enthalpic preference between the two polymers can even overwhelm the aforementioned entropic tendency.[339] PSAN-grafted 16 nm silica nanoparticles with a low brush $N = 17$ was miscible with a $N = 9588$ PMMA matrix with a high inorganic loading of 52 vol% or a particle brush filling of 72 vol%, **Figure 33**. Remarkably, the filling ratio is only slightly lower than that of an fcc packed sphere, *i.e.* 74 vol%. As no chemical crosslinking was present, although the material was rather rigid at room temperature, it could be extended to 200% at 70 °C. The favorable interaction between the two polymers could also be used for preparation of materials with high transparency.[70, 441]

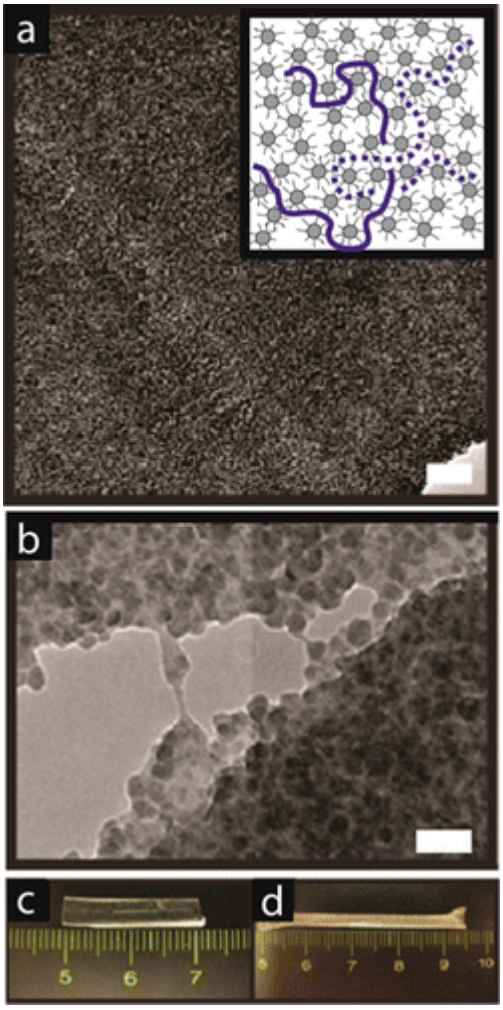

Figure 33. (a) TEM image of PMMA/8SiO_2-SAN_{17} composite film with a particle brush volume fraction of 72% (corresponding to inorganic volume filling fraction $\phi_{SiO2} \approx 0.52$) and $N_{M,PMMA}$ = 9588. The micrograph reveals uniform particle distribution. Scale bar is 100 nm. Inset shows illustration of entangled network structure of high molecular chains in particulate matrix. (b) Micrograph of crack formed during early state of fracture upon deformation at 23 °C. The formation of 'particulate fibrils' that connect the fracture surface is observed. The formation of fibrils indicates the formation of entanglements between the high molecular weight matrix chains. Scale bar is 50 nm. (c) Image of $\phi_{SiO2} \approx 0.52$ nanocomposite sample before tensile deformation. (d) Picture of sample after strain application of 200% at 70 °C. Whitening occurs due to scattering

of surface cracks that form during deformation. [339], Copyright 2013. Reproduced with permission from American Chemical Society.

Turbidity originates from scattering of visible lights on the filler matrix interface and scattering of electromagnetic waves only occurs when there is a difference in permittivity between the filler and the matrix. More specifically for the visible range, if the filler and the matrix have close enough refractive indices, scattering can be minimized.[442] The refractive index of PMMA coincidentally lies between those of PSAN and silica. Therefore, it was possible to match the refractive index of SiO_2-*g*-PSAN particle brushes with the PMMA matrix based on the Maxwell Garnett theory, *cf*. Section 5.2.[443] Meanwhile, the scattering cross-section is proportional to the sixth power of particle size. Enthalpically favorable mixing of the PSAN-grafted silica nanoparticles in the PMMA matrix significantly suppresses aggregation, ensuring a small average filler size.

Anisotropic self-assembly of polymer-grafted NPs was observed in solutions and was simulated in a parametric phase diagram model.[444-446] While no 'matrix' MW was taken into account, as the solvent molecules are far smaller than the polymer brushes, three important parameters were considered: number of brushes on each particle, n_p, particle radius, r, and radius of gyration of the polymer brushes, R_g. Phase diagrams were plotted based on n_p vs. r/R_g. Good dispersion could only be achieved with a small r/R_g and a large n_p, which can be translated to high-density long polymer brushes grafted on small NPs. The simulation was extended to polymer-grafted NPs in matrices by introduction of a fourth parameter, P, the degree of polymerization of the matrix.[343] In general, a larger P leads to shrinkage of the dispersion phase and expansion of the agglomeration phase on the phase diagram, which is consistent with the previous studies.

Remarkably, the influence of P is more profound for a large r/R_g, i.e. short brushes grafted on large particles. Experimental observations on unimodal PDMS-grafted TiO_2 NPs in PDMS matrices agreed well with the theoretical prediction. The theoretical model was further developed to envision the dispersion of particle brushes with bimodal MWD, *vide infra*. Particle brushes with bimodal MWD generally dispersed better than their unimodal counterpart, **Fig. 34**. This is because the presence of the densely grafted short polymer brushes screened off the enthalpic gain from particle-particle attraction. Consequently, the dispersion-agglomeration boundary moved toward the agglomeration phase, *i.e.* a smaller n_p is required to disperse the bimodal PDMS-grafted TiO_2 NPs in the PDMS matrices.

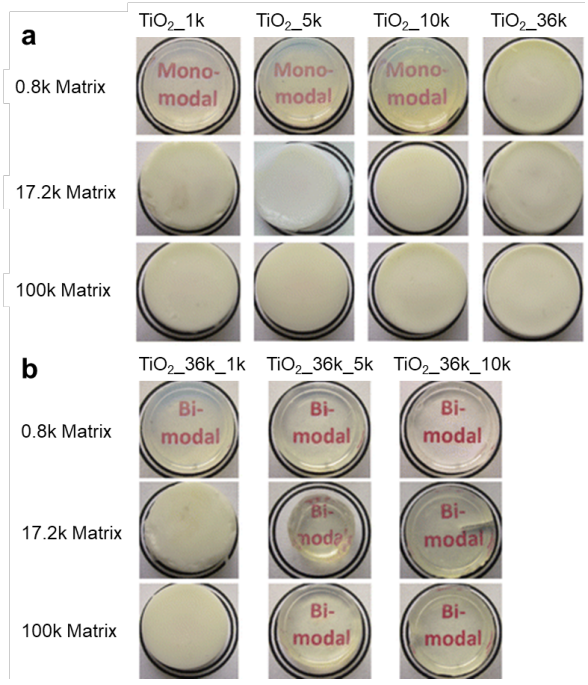

Fig. 34. Digital photographs of 5 mm thick silicone nanocomposites filled with 5 wt % (a) monomodal-brush-grafted and (b) bimodal-brush-grafted TiO2 NPs. [343], Copyright 2013. Adapted with permission from American Chemical Society.

6. From Properties to Applications

The ability to concurrently augment physical properties of polymer materials while retaining the benefits of their processability has driven the interest in using inorganic nanoparticles as additives to polymer matrix materials. While this is an established field of research with myriads of commercial applications, the recent progress in controlling the architecture of polymer-tethered particle fillers has further advanced the ability to control microstructure and properties of nanoparticle-in-polymer dispersions. Furthermore, advances in the control of brush architecture on the interactions and assembly behavior has driven the emergence of a new direction of research, *i.e.* 'one-component hybrid materials' that are formed via the assembly of brush particles in the absence of an additional matrix polymer. This field is driven by the potential to synergistically combine the enhanced control of microstructure (both in terms of particle dispersion as well as polymer chain conformation) with the properties of inorganic nanoparticles to realize novel functionalities in hybrid materials. This section summarizes recent advances and trends in the field of functional particle brush-based hybrids and delineate opportunities for future research.

6.1 Mechanical Properties

The very first motivation of introducing inorganic materials into polymers, including natural rubbers and synthetic resins, was to increase strength.[2, 3, 447] For example, ZrO_2-*g*-PMMA hybrid NPs containing ~74 wt% 40 nm ZrO_2 and PMMA brushes with N = 556 displayed over twice higher elastic modulus and ten times higher hardness compared to linear PMMA of similar MW. Meanwhile, the hybrid NPs retained solvent-processability and long-term stability in organic solvents.[71] Moreover, fragile inorganic materials reinforced by the polymer component became more processable.[27, 391, 425, 448]

Enhancement of mechanical properties by polymer-grafted NPs can occur for a molten polymer matrix ($T > T_g$) and for a glassy polymer matrix ($T < T_g$). In a molten matrix, strengthening can be achieved by percolation of nanoparticle fillers, thus resulting in particle (aggregate) network structures that can support stress. [449, 450] The entanglement of grafted polymer chains allows percolation to occur at a lower particle loading and more efficient stress propagation across network structures. [451] Grafting of polymer brushes with bimodal MWD further promoted the brush-matrix and brush-brush entanglement. Therefore, a higher elastic modulus (along with increased glass transition temperature, T_g) were observed for such systems.[44, 344] A proper selection of the filler may also help improve the toughness of polymer matrix in some case.[452, 453] Overall, the combination of polymer brushes and inorganic particles improves the processability of the resulting nanocomposites.[425]

A related field of research that only recently emerged concerns the study of phonon propagation in polymer hybrid materials. In its basic definition, the term 'phonon' refers to coherent lattice oscillations that occur in crystalline materials. Phonons play a fundamental role in the transport of heat and sound but have also been linked to a number of functional material attributes (such as thermal rectification behavior) that hold the promise of innovative material technologies.[454] For the specific case of particle brush based materials, measurements of phonon dispersion relations in the gigahertz regime (using Brillouin scattering) were used to evaluate the elastic properties of individual brush particles as well as ordered particle brush assembly structures. For individual densely tethered brush particles, the results revealed the splitting of elastic moduli parallel and normal to the particle surface, indicating a higher modulus in normal direction to the interface. These results were the first to confirm that the orientation of chains in dense brush layers induces the increase in modulus – in analogy to the increase in Young modulus

that is observed in oriented polymers.[428] Interestingly, the splitting of elastic moduli in normal and tangential direction gives rise to a symmetry reduction that was found to fundamentally alter the phonon propagation characteristics in brush particle assembly structures. In particular, a new class of phononic band gap – called a 'hybridization gap' – was demonstrated to exist in face-centered cubic particle brush assemblies.[455] Because hybridization gaps are resistant to defect formation, this finding might inspire the design of novel functional materials with tailored phononic behavior. Further research revealed the distinct dependence of local and global relaxation of polymer segments on grafting densities and on the grafting densities between individual and isolated particle brushes, implying the difference in phononic properties of polymer-brush-based hybrid materials according to the processing method.[423]

Polymer-grafting of inorganic nanoparticles not only impacts the material properties in the solid state. Applications have also been found utilizing the unique mechanical properties of particle brush solutions, as a lubricant, for example. Lubrication by surfactant-anchoring on surfaces is a long-known phenomenon.[456] Later, this approach was extended to polymer brushes immobilized on surfaces, especially in the CPB regime.[457] Polymer brushes with long aliphatic sidechains compatible with mechanical oils were developed to accommodate several applications.[458] Surface-immobilized molecular bottlebrushes and cyclic polymers further improved the lubricating performances and resistance to wear due to reduced entanglement.[367, 459, 460] Lubricants taking the architecture of particle brushes started from sulfonate-bearing polymethacrylate brushes grafted from PNIPAM-based nanogels.[461] Recently, poly(alkyl methacrylate)-grafted inorganic NPs were applied as an additive in poly(α-olefin) lubricating base oil.[462] The particle brush-based additive was stable in the base oil at a temperature of 100 °C over a period of 55 days while the friction of the oil was significantly reduced. Better lubrication

efficiency was observed with lower degree of polymerization of the grafted polymer, which is consistent with the expectation that stretched chain conformations (*i.e.* brush particles in the CPB regime) are required to reduce friction. Further studies revealed that long or branched aliphatic sidechains improved dispersibility of the particle brushes in the oil as well the stability and lubrication properties.[463]

Moreover, functionalities incorporated into the polymer brushes, such as dynamic bonding, provides inorganic NPs with the capability of self-healing. Entanglement of polymer brushes is not yet as strong as non-chemical dynamic interactions. Therefore, a physical gel with intrinsic self-healing capability was created by adding liquid crystal (LC) molecules with a low nematic to isotropic transition temperature in PMMA-grafted SiO_2 NPs.[464] Adding a photoswitchable azobenzene derivative, with a similar structure to the LC, allows disturbance of the phase transition upon UV-irradiation. The gel could therefore be turned into a sol upon irradiation, acquiring the capability of photo-repair. Stronger dynamic interactions between polymer brushes, such as hydrogen-bonding, ensures better mechanical performance without compromising the self-healing capability, **Figure 35**.[465] Poly(5-(acetamido)pentyl acrylate) was grafted from 170 nm SiO_2 particles. The hydrogen bonding provided by the amide moiety not only enabled self-healing but also promoted interparticle interaction even in the CPB regime, *i.e.* no polymer brush entanglement was needed. This allows small interparticle distance in the solid film. Along with the highly defined spatial order enabled by SI-ATRP, uniform spacing of particles lying within the half-wavelength of the visible range was formed, *cf.* Section 5.2, resulting in a mechanochromic elastomer with color change upon stretching.

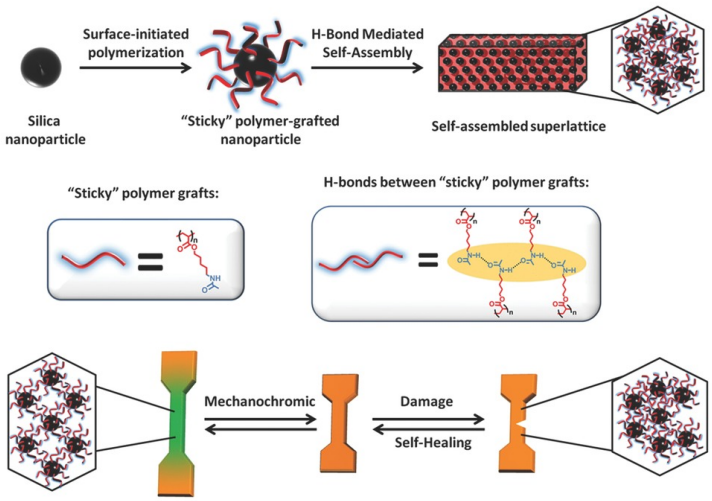

Figure 35. Preparation of dynamic superlattice nanocomposite materials from 'sticky' polymer-grafted nanoparticles. Surface-initiated polymerization was used to graft polyacrylate amide chains from the surface of monodisperse silica nanoparticles. Hydrogen bonding interactions between the amide functionalities on neighboring chains results in the ordered self-assembly of the polymer-grafted nanoparticles into a superlattice nanocomposite structure, which yields mechanochromic and self-healing materials. [465], Copyright 2015. Reproduced with permission from John Wiley & Sons Inc.

6.2 Optical Properties and Applications

The addition of inorganic nanoparticles may alter the manner in which the polymer matrix interacts with electromagnetic waves. In this section, the recent results concerning the optical properties of particle brush-based hybrid materials in the visible range as well as their potential applications are discussed. Properties and applications related to other electromagnetic waves will be discussed in Section 5.3 and Section 5.5.

Optical transparency is a critical characteristic for many optical applications. As discussed in Section 4.2, the scattering of inorganic fillers often results in turbidity of nanocomposites and hybrid NP dispersions.[466, 467] For non-agglomerated small hybrid NPs, the scattering cross-section takes the Rayleigh approximation, *i.e.* $C_{sca} \sim V_p^2(\Delta\alpha)^2$ where V_p is the volume of the particle, and $|\Delta\alpha| \sim |(\varepsilon_p - \varepsilon_m)/(\varepsilon_p + 2\varepsilon_m)|$ denotes the polarizability of the particle within the host medium. The parameters ε_p and ε_m represent the permittivity of the particle and the medium, which is equal to the square of their corresponding refractive indices in the visible range, i.e. $\varepsilon = n^2$ (assuming no absorption). Therefore, there are two ways to reduce the scattering: first, by reducing particle size, which implies avoiding particle agglomeration. Second, by matching the refractive indices of the particle and the medium ($\varepsilon_p = \varepsilon_m$) which amounts to vanishing of the polarizability $\Delta\alpha$.[443] Because inorganic particles often differ in their refractive index from the corresponding polymer matrix, optical scattering presents a problem to the design of transparent hybrid materials. Bockstaller and coworkers demonstrated that the scattering cross-section (which is a measure for the scattering strength) of particle fillers can be reduced by several orders of magnitude by means of suitable polymer modification of particle fillers. Specifically, grafted polymer chains were chosen such that the effective refractive index of the particle brush is equal to the refractive index of the host medium. [442] **Fig. 36** illustrates this idea by displaying the scattering cross section for PSAN-modified silica particles embedded within a PMMA matrix calculated using Mie theory. 'Star' symbols indicate the minimum scattering compositions.

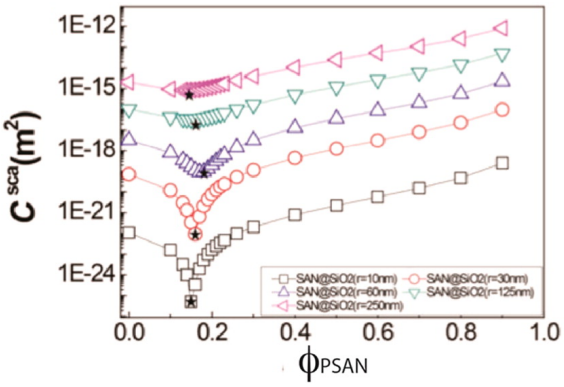

Fig. 36. Scattering characteristics of PSAN–SiO_2/PMMA composites as a function of particle core size calculated using core–shell Mie theory [where, for example, 1E-12 represents 1×10^{-12}]. Calculated scattering cross-section (C_{sca}) as a function of particle core radius (r_0) and composition (ϕ_{PSAN}) at λ = 532 nm. Compositions corresponding to the minimum scattering cross-section are highlighted with star symbols. [441], Copyright 2014. Reproduced with permission from American Chemical Society.

Fillers can also adjust the refractive index of the matrix if the fillers are small enough to mitigate scattering that arises from the particle size. The effective medium approximation applies to the entire nanocomposite and the refractive index of the bulk materials changes with the filling ratio. 5 nm ZnO NPs grafted with dense PSAN (M_n = 2300) brushes managed to boost the refractive index of the PMMA-based nanocomposite from 1.49 to 1.64 at λ = 632.8 nm while the overall transparency was mostly retained. Meanwhile, the elastic modulus of the material increased from 1.12 GPa to >1.7 GPa. This is a result of synergic contributions from the small ZnO NPs and enthalpically favorable interaction between PMMA and PSAN, *cf*. Section 4.2.

Densely grafted polymer brushes with uniform degree of polymerization became accessible via SI-RDRP. Therefore, it was possible to prepare nanoparticle assemblies with highly ordered structure that acted like photonic crystals, **Fig. 37**. When the spacing lies near the half

wavelength of the visible range, the diffracted light from such colloidal crystals exhibits as color change. Such crystals are often called photonic crystals. Polymer-grafted NPs with narrow core size and shell thickness distributions tend to assemble into these photonic crystals when the concentration is beyond the dispersion to assembly boundary, *cf*. Section 4.1. Before complete conversion into a stable heterogeneously iridescent crystal state at a higher concentration (crystal phase), N = 1580 PMMA-grafted 130 nm SiO_2 NPs were found to spontaneously assemble into tiny iridescent flecks in mixture of 1,2-dichloroethane/chlorobenzene/*o*-dichlorobenzene = 53/20/27 (v/v/v), indicating formation of Bragg-reflecting crystallites (coexisting phase).[388] The solvent mixture formulation was selected to match the density and the refractive index of SiO_2-*g*-PMMA so as to mitigate the influence of gravity and scattering. The iridescent flecks vanished upon mechanical agitation but reform after standing. Below the certain concentration range, which depends on the polymer brush length,[387] the dispersion appeared to be slightly turbid due to scattering (fluid phase). Such phenomena was also observable in glassy and elastomeric assemblies of well-defined polymer-grafted nanoparticles.[425, 465, 468]

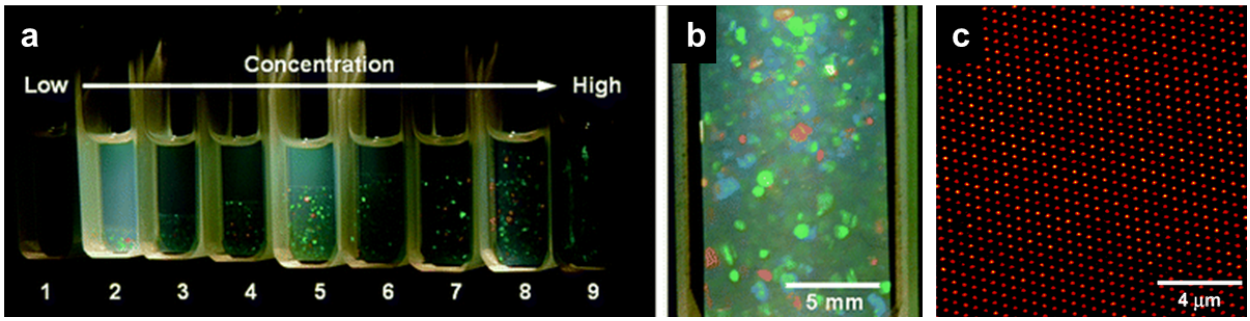

Fig. 37. Panel a is a digital photograph of SiO_2-*g*-PMMA suspensions in the mixed solvent (1,2-dichloroethane/chlorobenzene/*o*-dichlorobenzene = 53/20/27 volume ratio) illuminated from behind by white light, 7 days after sample preparation. The number-average molecular weight of the PMMA grafts is 158,000, and the diameter of the SiO_2 core is 130 nm. Samples with different SiO_2-*g*-PMMA volume fractions (ϕ). The ϕ value increases from 0.0785 (leftmost) to 0.111

(rightmost). In samples 2–8, Bragg-diffracting crystalline and (random) fluid phases coexist, with the volume fraction of crystalline phase increasing with increasing ϕ. Sample 9 (ϕ = 0.111) crystallizes heterogeneously and sample 1 (ϕ = 0.0785) remained unchanged (fluid phase). Panel b shows close-up of sample 8. The crystals are 0.1-1 mm in size, and show different colors depending on their orientation. Panel c displays a confocal laser scanning microscopic image of SiO_2-*g*-PMMA crystals. Observations were performed with an Ar laser of 488 nm wavelength and ×63 objective in reflection mode. The distance of the focal plane from the inside of the coverslip was 100 μm. The diameter of SiO_2 core is 130 nm. The number-average molecular weight of PMMA grafts is 158,000 and the mean nearest-neighbor interparticle distance was 560 nm. [388], Copyright 2006. Adapted with permission from American Chemical Society.

Light-absorbing capability of nanoparticles, *vide supra*, were also introduced to nanocomposites to filter certain wavelengths of light. TiO_2 and ZnO are two widely employed inorganic NPs for sun screening in cosmetic products. However, the photocatalytic activity of these particles may lead to the release of reactive oxygen species causing skin damage. One solution was to cover the surface of the NPs with a blend of antioxidant and surface-anchoring polymers. For example, a mixture of oligomeric proanthocyanidins, poly(methyl vinyl ether-maleic acid) copolymer, and triethoxysilylethyl-bearing PDMS were used to cover TiO_2 NPs and block the ability for radical generation from the surface.[469] Recently, PEO-*b*-PDMAEMA-*b*-PS triblock copolymers were used as template to generate polymer-TiO_2 hybrid UV-screening vesicles.[470, 471] The triblock copolymer self-assembled into a core-shell-corona structure in a mixture of THF/methanol (1/3, v/v). The particle precursor, tetrabutyl titanate, was loaded into the PDMAEMA shell and converted into TiO_2 NPs. Meanwhile, an antioxidant, ferulic acid was loaded in the PS core to

consume the radical species generated by photoinduced charge separation in TiO_2. The water-soluble PEO corona acted as an additional shield layer as well as the compatibilizer.

Certain inorganic nanoparticles, for example QDs, were grafted with polymer brushes to produce light-emitting hybrid NPs. The pioneering reports of polymer brushes grafted on QDs included coating the GDs with silica followed by surface-initiated polymerization and direct ligand exchange with PDMAEMA.[276, 472] Although the quantum efficiency was slightly compromised , the processability was improved while the photoluminescence was mostly retained. An improved BCP ligand with a structure of poly(4,4'-methyl-4''-vinyltriphenylamine-*b*-cysteamine acrylamide) synthesized via RAFT polymerization significantly improved the quantum efficiency in the QD LED (QLED) device despite a slightly lower photoluminescence intensity after coating.[473] This was attributed to the HOMO of the poly(4,4'-methyl-4''-vinyltriphenylamine) lying between those of PEDOT:PSS and CdSe@ZnS QDs, lowering the energy barrier for hole injection from PEDOT:PSS into the QDs. Meanwhile, the hybrid QDs were solvent-processable. A recent report revealed the transparency of QD-PDMS nanocomposites was significantly improved by grafting PDMS brushes with bimodal MWD on QDs.[474] These discoveries may find applications in future QLED displays. Besides, phase separation of polymer brushes may be used to guide bottom-up fabrication of QLED devices.[433]

Exfoliated clay-polymer nanocomposites were one of the first-studied polymer-brushed based hybrid materials. Since the thickness of the clay nanoplatelets is on the atomic level while the other two dimensions are magnitudes larger this class of hybrid particles has shown good performance in applications as barrier materials, flame retardants or in corrosion protection.[475, 476] Uniform dispersions of exfoliated clay nanofillers that were obtained after polymer

modification exhibited high optical transparency which should further their application.[94, 477-479]

6.3 Biomedical Applications

Polymer-brush-based hybrid NPs find various applications in biomedicine, including imaging enhancement, drug delivery, controlled release, antimicrobial/antifouling, etc., depending on the compositions.

X-ray computed tomography (CT) imaging can usually be enhanced by heavy elements such as, heavy metal (oxide) nanoparticles including Au, TaO_x, or Bi_2S_3. However, those NPs are not readily compatible with the physiological environment. Polymer brushes such as PEG or PVP can help to disperse those NPs and allow extended circulation in blood streams.[480-482] More complex polymer architectures, such as AuNPs synthesized in dendrimeric templates provided long circulation times.[483]

Magnetic resonance imaging (MRI) is another non-invasive diagnosis technique. In addition, the magnetic field and radio-frequency irradiation used in MRI is non-ionizing, thus exerting a minor negative impact on patients compared to CT. Generally, MRI can be enhanced by paramagnetic Gd^{3+} chelates (T_1-weighted) or superparamagnetic iron oxide (SPIO) NPs (T_2-weighted). Due to the lower cost and lower toxicity, SPIO NPs grafted with polymer brushes, including polysaccharides, PEG, PEG derivatives, and the polymeric analogue of DMSO were applied as T_2-weighted MRI contrast agents.[71, 75, 484-486] More hydrophilic polymer brushes promoted NP-water interactions, and hence, achieved better contrast enhancement. Functionalities were introduced to polymer brushes. Folate-terminated PEG-grafted SPIO NPs targeted folate receptors populated on various cancer cells, leading to an increased uptake.[487, 488] On the other

hand, polyPEGMA brushes significantly lowered the uptake of SPIO due to their antifouling capability. The MRI contrast agent could, therefore, circulate for longer time without being recognized by the macrophage system.[75, 376] Moreover, multimodal hybrid contrast agents for orthogonal enhancement of several different imaging techniques were developed. For instance, a copolymer of PEGMA and Gd(III)-DOTA-bearing acrylamide was prepared via RAFT polymerization and grafted onto AuNPs, **Fig. 38**.[489] The longitudinal relaxation behavior was found to be improved 8 times compared to free Gd^{3+} chelates while the hybrid NPs could act as a bimodal MRI/CT contrast agent. Similarly, bimodality can be introduced to SPIO NPs by coating with a TaO_x shell followed by PEGylation.[490]

Recent applications of nanophosphors in near infrared (NIR) upconversion luminescence (UCL) imaging as a novel non-invasive diagnosis technique led to the development of UCL/CT/MRI trimodal hybrid NPs.[491] A paramagnetic $NaGdF_4$ layer was first grown on the upconversion $NaYF_4$:Yb^{3+}/Er^{3+}/Tm^{3+} nanocrystal. Then, the core-shell NP was encapsulated in a PEG-based W/O micelle, which acted as a nanoreactor for TaO_x deposition. The TaO_x surface was readily PEGylated via silane chemistry.

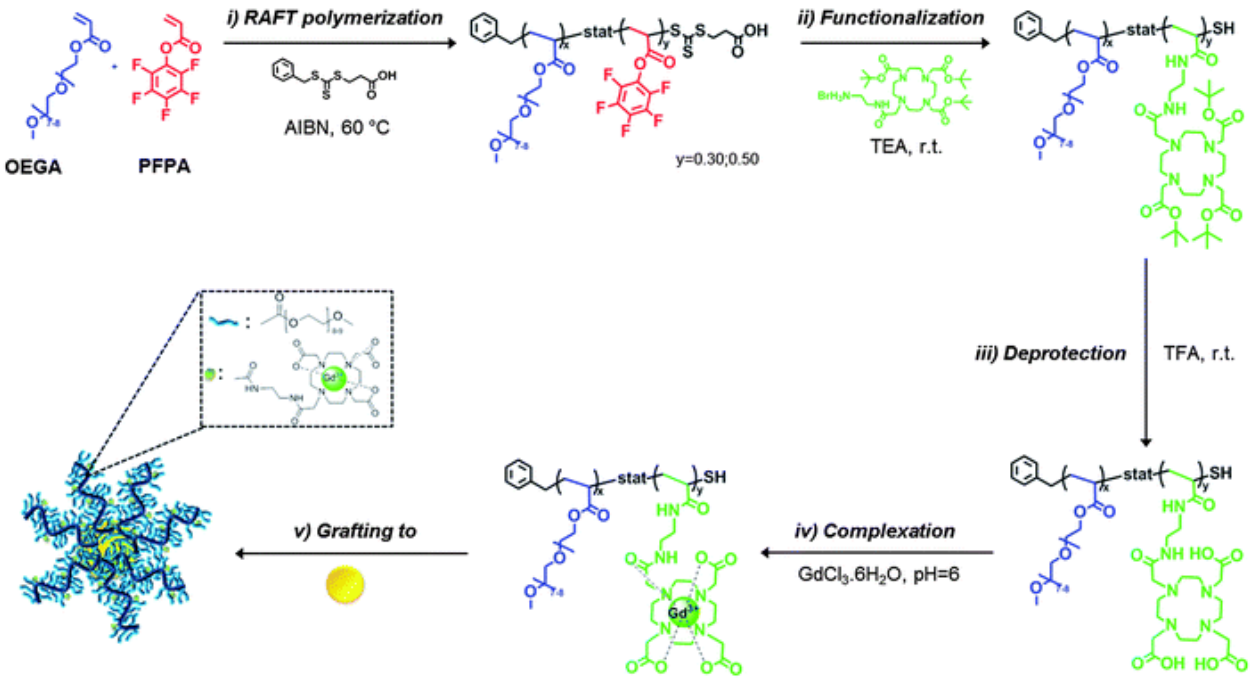

Fig. 38. General procedure for the preparation of Gd(III)-chelate-modified polymer-grafted AuNPs. [489], Copyright 2012. Reproduced with permission from Royal Society of Chemistry.

Drug delivery using polymer-brush-based hybrid materials was not initially a straightforward concept. Early reports focused on using inorganic nanoparticles as templates for preparation of polymeric nanocapsules rather than using the entire hybrid NP as a carrier.[492, 493] To use polymer-grafted hybrid NPs as carriers, drugs are generally loaded in three different locations, among/on polymer brushes, inside NPs, or between polymer brushes and the NP. One of the pioneering works took advantage of the carboxylic acid end-group of PEG-grafted AuNPs. The carboxylates acted in place of oxalate ligand of oxaliplatin.[494] The immobilized oxaliplatin displayed similar or better cytotoxicity compared to free oxaliplatin in various cancer cell lines. In addition, it showed an ability to penetrate the nucleus of lung cancer cells. Another way to incorporate the drug molecules was to encapsulate both the drug molecules and inorganic NPs within a BCP micelle.[495, 496] It is especially feasible for SPIO due to their small particle sizes.

The presence of SPIO enabled targeted delivery of drugs using an external magnetic field as well as real time monitoring via MRI. This versatile strategy also facilitates incorporation of additional functionalities. For example, introduction of upconversion NPs within the micelles enabled in *vivo* UCL[495] imaging and attachment of a peptide to the chain-end of the polymer brushes enhanced recognition and uptake of tumor cells.[496] In the case when the passenger moieties are nucleic acids, for example, in gene delivery, they could be grafted directly on the surface of inorganic NPs[497] or electrostatically adsorbed onto positively charged polymer brushes.[498, 499]

Biomacromolecules can also be delivered via direct polymer brush modification into bioconjugates.[500] In order to load drugs inside NPs, a porous structure is typically needed. For example, mesoporous silica NPs were employed as carriers. Thermo- or pH-responsive polymer brushes were grafted on the surface of the NPs as 'gates', whose status depended on the conformations.[501, 502] More complex NP structures, such as gold nanocages may function in a similar way; copolymers of polyacrylamides with precisely adjusted LCST were grafted onto the gold surfaces, **Fig. 39**.[273, 503] Either NIR or high-intensity focused ultrasound triggered the collapse of the polymer brushes and a release of the drugs within the nanocages. There are only sparse reports on incorporating drugs between polymer brushes and the NP. One examples was to load the hydrophobic drug molecules among the oleic acid surface ligands on iron oxide NPs.[504] The surface was further modified with a PEO-*b*-PPO-*b*-PEO so that the PEO brushes could compatibilize the NPs in the physiological environment. Another approach was to coat SPIO with poly(3-(trimethoxysilyl)propyl methacrylate)-*r*-PPEGMA-*r*-poly(*N*-acrylosuccinimide) random copolymer.[505] Therefore, a layer of crosslinked silsesquioxane/polymethacrylate with a high (activated) carboxylic acid concentration was formed between the PEG brushes and the SPIO NPs, which acted as loading site for amine-bearing or positively charged drugs.

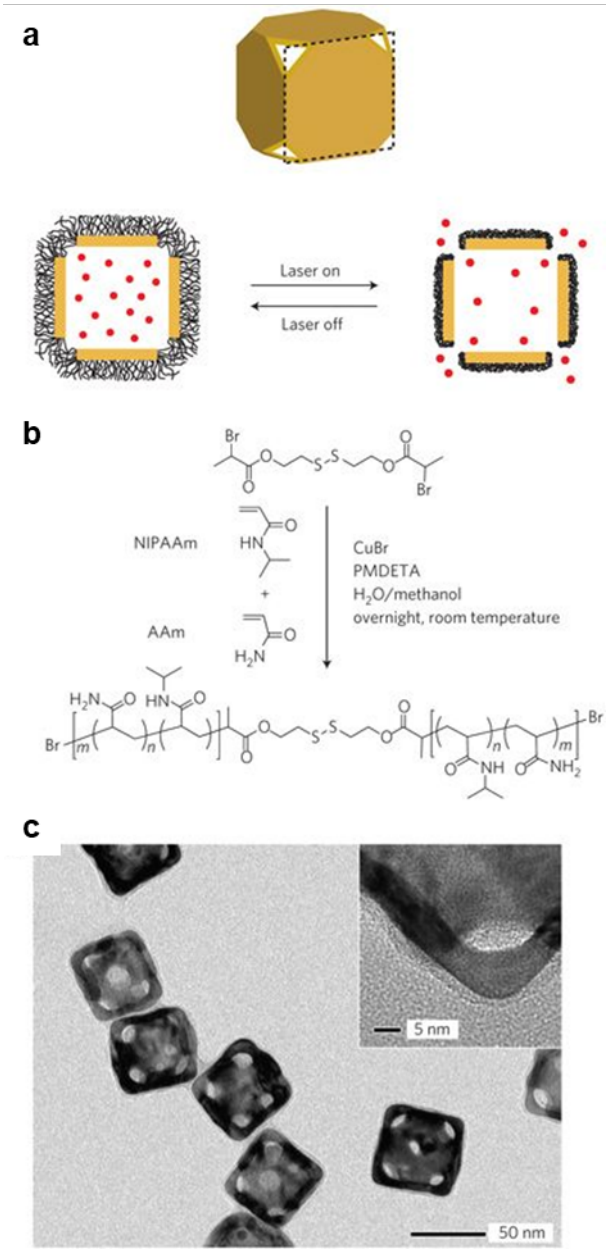

Fig. 39. Panel a illustrates the temperature responsive release system. A side view of the Au nanocage is used for the illustration. On exposure to a near-infrared laser, the light is absorbed by the nanocage and converted into heat, triggering the smart polymer to collapse and thus release the pre-loaded effector. When the laser is turned off, the polymer chains will relax back to the extended conformation and terminate the release. Panel b depicts ATRP of NIPAAm and AAm monomers (at a molar ratio of *m*/*n*) as initiated by a disulfide initiator and in the presence of a Cu(I) catalyst.

Panel c shows TEM images of Au nanocages for which the surface was covered by a pNIPAAm-*co*-pAAm copolymer with an LSCT at 39 °C. The inset shows a magnified TEM image of the corner of such a nanocage. NIPAAm: *N*-isopropylacrylamide; AAm: acrylamide. [273], Copyright 2009. Adapted with permission from Springer Nature.

Next to drug delivery and antibiotic applications, photothermal or magnetothermal hybrid particles were used as targeted therapy for cancer. Polymer-grafted graphene oxide, plasmonic particles, or metal-organic particles were demonstrated to generate localized high temperature and eliminate cancer cell at the lesion.[506-508] Similar, high-frequency alternating magnetic field may induce a significant temperature increase in magnetic NPs, termed magnetothermal therapy or magnetic hyperthermia,[509] and the two responsiveness could be combined in one hybrid material.[510, 511] Such strategies were used as well in induction of drug release via thermal-responsive polymers.[512, 513]

Either the polymer brushes or the nanoparticle core of polymer-brush-based hybrid nanoparticles can display antibacterial properties. Silver and copper NPs are the two typical choices for antibacterial NPs due to their ability to release cytotoxic metal ions. However, most reports were on direct incorporation inside polymer matrices without surface modification. There were only limited reports on polymer brush grafted silver or copper NPs.[514, 515] Hydrophobic acrylic or styrenic polymers were grafted through or onto copper or silver NPs for preparation of antibacterial coatings. Quaternary ammonium compounds are a type of antimicrobial known for over a century.[516] Therefore, early research on antimicrobial surfaces focused on polymer brushes bearing quaternary ammonium moieties.[517, 518] Polymeric quaternary ammonium moieties led to locally high concentration of these antimicrobial moieties, significantly boosting

the efficiency of the bactericide. Additional functionalities can be introduced when these polymers are grafted on inorganic nanoparticles. For example, when poly(quaternized-DMAEMA) was grafted on iron oxide NPs, the antibacterial particles became recyclable.[76] poly(quaternized-DMAEMA) were grafted on macroscopic surfaces to create non-leaching antibacterial surfaces.[274, 519-521] The hybrid NPs were recovered by magnetic precipitation after each use. There was full elimination of a 10^5 to 10^6 *E. Coli*/mL solution by 1 mg/mL poly(quaternized-DMAEMA)-grafted iron oxide after 8 cycles. In addition to direct annihilation of bacteria by polymer brushes, the polymer brushes could be used as loading sites for small-molecule antibacterial agents. Penicillin-G was found to bind with PMAA via hydrogen-bonding between carboxylic acids.[522] Due to the high local concentration of the antibacterial agents, both carboxylic-acid-functionalized silica NPs and PMAA-grafted silica NPs were demonstrated to kill various bacterial pathogens, including methicillin-resistant *Staphylococcus aureus* strains, with significantly improved efficiencies, as shown by cell viability images before and after treatments in **Figure 40**.

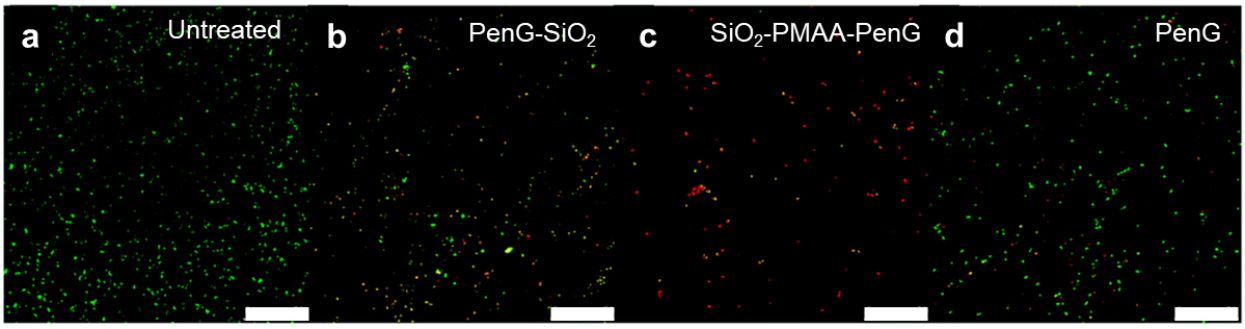

Figure 40. Confocal scanning laser microscopy images of bacterial cells (a) *S. aureus*; (b) *S. aureus* exposed to complexed penicillin-G on monolayer carboxylic acid coated silica NPs; (c) *S. aureus* exposed to complexed penicillin-G on PMAA-grafted silica NPs; (d) *S. aureus* exposed to free penicillin-G (Scale bars: 50 μm). The penicillin-nanoparticles complexes (B and C) have equal

doses of penicillin-G as the free penicillin-G group (D). Scale bars: 50 μm. [522], Copyright 2014. Adapted with permission from Royal Society of Chemistry.

This concept was further improved by replacing the PMAA brushes with positively charged cobaltocenium-containing polymethacrylate brushes.[523] The negatively charged penicillin-G was loaded in a simple ion-exchange process. The stronger electrostatic interaction allowed a higher loading ratio of the antibacterial. Therefore, the bacteria lysis effect was again amplified by the locally high concentration. Remarkability, neither *S. aureus* nor *E. coli* displayed a detectable drop of lysis after 15 consecutive passages of exposure to the complex of penicillin-G and cobaltocenium-bearing particle brushes, indicating a considerable barrier for the bacteria to develop the drug resistance.

Antifouling surfaces are usually achievable via grafting (super)hydrophilic polymer brushes on flat surfaces. In this way, the surfaces become less wettable by less polar molecules, including many fouling proteins present in water.[87, 524] These polymer brushes can be PEG-based, zwitterions, quaternary ammonium-bearing, or hydroxy-bearing, polymers.[86, 525] Antifouling polymer-inorganic hybrid NPs could also be introduced as additives in ultrafiltration membranes. The PHEMA-grafted TiO_2 NPs embedded in the polysulfone membrane noticeably reduced adhesion of bovine serum albumin (BSA) and extracellular polymeric substance on the membrane, resulting in an extended membrane lifetime as well as a larger water flux.[526]

Another biomedical application for polymer brush-based hybrid materials is detection of biomolecules, which typically involved surface plasmon resonance (SPR) due to specific interactions of noble metals being close to each other. A color change can usually be visually or colorimetrically detected in this process. It is especially useful for rapid (semi)quantitative analysis

of biomolecules, such as antigens, proteins, or nucleic acid due to the presence of specific bindings. To detect antigens or antibodies, their corresponding antibodies or antigens, respectively, are usually required. For example, IgG-AuNP conjugates and ATRP initiator coupled IgG were prepared and coupled by anti-IgG. SI-ATRP of HEMA from the immobilized initiators resulted in PHEMA-grafted AuNPs.[527] In the presence of free competing IgG in the solution, the anti-IgG linking the polymer and AuNPs was removed, resulting in aggregation and color change of the AuNPs colloidal dispersion. Therefore, the IgG concentration could be quantitatively determined by the change in optical intensity. Similarly, PEG-grafted AuNPs with saccharide moieties in the chain-ends could be used to detect lectins.[528]

Nucleic acid detection on the other hand usually does not require quantitative analysis. Instead, a Boolean response of the exact sequence is desired. Therefore, in order to capture a nucleic acid the complementary sequence of the targeting sequence needs to be immobilized.[529] Since only qualitative responses are needed, methods were developed to amplify the response. For instance, polyadenine was grafted from the end of the targeting RNA after it coupled with the captured nucleic acid immobilized on a gold chip.[530] Subsequently, the chips were treated with polythymine$_{30}$-grafted AuNPs. As no polyadenine was present if no targeting RNA was detected, the AuNPs selectively amplified the positive SPR imaging signals by accumulation along the polyadenine connected to the targeting RNA. Since specific interactions ensured selective detection of certain (type of) biomolecules, non-specific interaction is not always unfavorable. The non-specific interaction between proteins and ammoniums were creatively utilized in the detection of a library of different proteins.[531] On AuNPs, PEG with ammonium chain ends were grafted and electrostatically coupled with highly fluorescent carboxylate-substituted poly(phenylene ethynylene) (PPE), which was quenched by surface attachment. Six different ammonium chain

ends were prepared. As each protein has different affinity to each of the ammonium entities, their characteristics were barcoded by their competing power with PPE and read out as fluorescence intensities, **Fig. 41**.

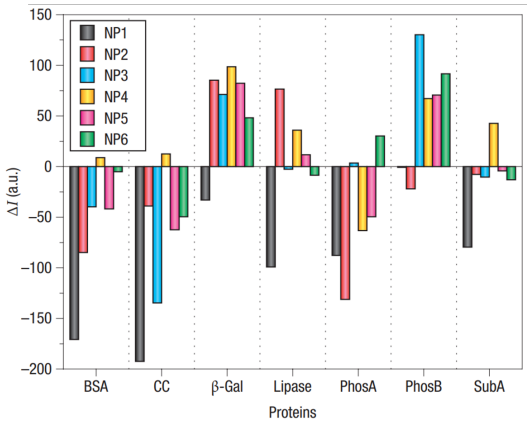

Fig. 41. Array-based sensing of protein analytes with identical absorbance of 0.005 at 280 nm and corresponding fluorescence response patterns of the AuNP-PPE sensor array. NP1: PEG-trimethylammonium; NP2: PEG-ethyl(dimethyl)ammonium; NP3: PEG-hexyl(dimethyl)ammonium; NP4: PEG-cyclohexyl(dimethyl)ammonium; NP5: PEG-benzyl(dimethyl)ammonium; NP6: PEG-3-hydropropyl(dimethyl)ammonium. [BSA] = 110 nM; [cytochrome c (CC)] = 215 nM; [β-galactosidase (β-gal)] = 4 nM; [lipase] = 90 nM; [acid phosphatase (PhosA)] = 20 nM; [alkaline phosphatase (PhosB)] = 80 nM; [Subtilisin A (SubA)] = 190 nM. [531], Copyright 2007. Reproduced with permission from Springer Nature.

6.4 Catalysis

Typically, reactions catalyzed by noble metals are heterogeneous with the reaction taking place at the interface. Therefore, efficiency is largely regulated by the effective interfacial area. Conventional deposition of the noble metal on activated carbons increases the chance of reactant adsorption on metal surfaces but it does not change the overall heterogeneous nature of the

reaction. To overcome this obstacle, Pd colloidal NPs were modified with polymer brushes to create dispersed, homogeneous reaction media. Hence, the catalysis efficiency and even selectivity were boosted in comparison to conventional Pd/C catalysts.[299, 301, 532] Polymer grafts are also able to modulate the catalysis efficiency by providing control of the surface coverage. PNIPAM-grafted AuNPs were extensively studied.[533] The apparent rate constant of reduction of *p*-nitrophenol to *p*-aminophenol by $NaBH_4$ catalyzed by $PNIPAM_{126}$-*b*-$P4VP_{34}$-grafted on 3.3(±0.2) nm AuNPs were found to increased steadily at a temperature <30 °C following the Arrhenius equation. It dropped significantly above that temperature because the PNIPAM brushes (T > LCST) collapsed on the Au surface preventing *p*-nitrophenol from reaching the surface, **Fig. 42**. Similarly, Au NPs were loaded in polymer networks to achieve a superior catalytic activity.[534]

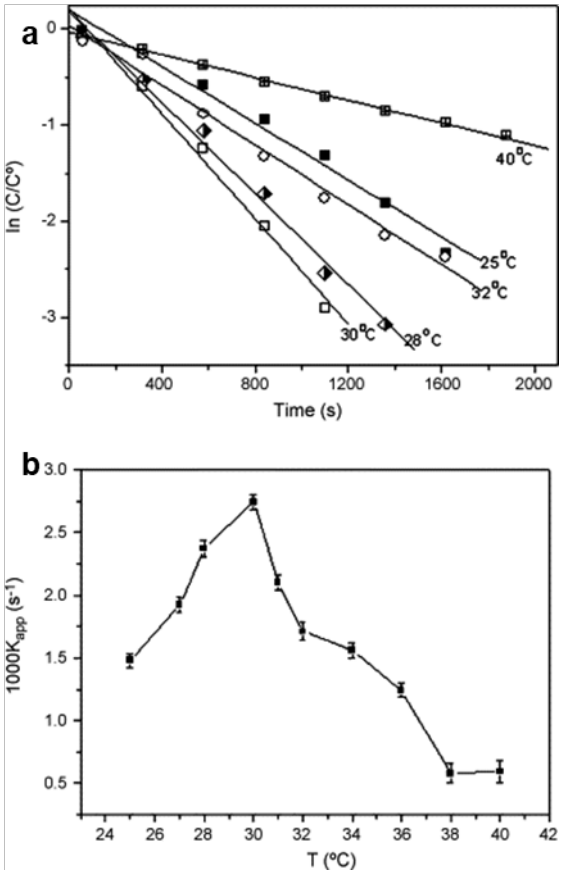

Fig. 42. Panel a shows plots of concentration ratios C/C_0 of *p*-nitrophenol vs. times at different temperatures and Panel b shows plots of the apparent rate constant K_{app} of the reduction catalyzed with the PNIPAM-grafted AuNPs. The concentrations of 4-nitrophenol, $NaBH_4$ and gold were 0.107, 3.57 and 0.0214 mmol/L, respectively. [533], Copyright 2007. Adapted with permission from Elsevier Science Ltd.

Further studies showed crosslinks of the PNIPAM brushes further reduced the efficiency of the catalyst, especially at $T <$ LCST. In another study, three types of polymer brushes of MW 10,000 were grafted on AuNPs, PNIPAM, PAA, and poly(3-(acrylamido)propyl(trimethyl)ammonium chloride) (PAPTAC).[535] Catalytic reduction efficiency of *p*-nitrophenol was compared across the three polymer-grafted AuNP catalysts. While reduced efficiency and an induction period

comparing to bare AuNP colloidal dispersions were observed in all three cases, PAA severely inhibited the reaction probably because of repulsion between the same negative charges on the polymer brushes and the substrate. On the other hand, the positively charged PAPTAC caused the least drop in efficiency and shortest induction period. Temperature-dependent catalytic activity was only seen for the PNIPAM-grafted AuNPs. While a prolonged induction period of 900 sec. was observed at 35 °C, there was no conversion at 40 °C. Metallic nanoparticles could also be loaded with polymer brushes immobilized on an inorganic surface, such as graphene oxide.[536] In this way, the catalytic reaction still occurred on the metal surface but the graphene oxide core helps electron transfer.

Photoexcitation from valence band (VB) to conduction band (CB) often occurs in semiconducting NPs when appropriate photon energy is applied, which may be accompanied by electron transfer reactions. This is the basis of their photocatalytic properties. Similar to noble metal NPs, polymer brush modification improves homogeneity of these NPs in the reaction medium. To achieve enhanced antibacterial/antifouling performance, *cf.* Section 5.3, antibacterial 2-(tert-butylamino)ethyl methacrylate and antifouling ethylene glycol dimethacrylate were grafted from photocatalytic TiO_2 NPs.[537] The TiO_2 NPs acted as a photoinitiator when irradiated with UV light and induced polymerization of the two monomers on the surface. The resulting hybrid material was able to kill bacteria, not only by the cytotoxicity of the ammonium moieties but also by the radical species generated by photoexcitation of TiO_2. The TiO_2 NPs also catalyzed photolysis of organic dyes. A similar technique was employed to conduct FRP 'grafting-through' reactions.[538] Methacrylate-functionalized ZnO NPs were utilized as a photocatalyst and monomers in preparation of PMMA-ZnO nanocomposites. The rates of polymerization were observed to increase in the early stage as the PMMA brush growth stabilized the ZnO NPs in the

dispersion. However, they dropped significantly after the first 200-400 sec, when the growth of PMMA started to hinder access to surface.

A combination of semiconducting NPs, noble metal surface, and polymer brushes was demonstrated with ZnO NPs immobilized on the chain ends of PNIPAM grafted on a gold substrate.[539] PNIPAM was first grafted from an initiator-modified gold surface via SI-ATRP. The bromide chain-end was switched to primary amines in a nucleophilic substitution followed by a CuAAC. The amine group allowed the polymer brushes to 'graft-onto' ZnO NPs. The photocatalytic activity of ZnO-catalyzed photolysis of *p*-nitrophenol was enhanced when ZnO NPs and the Au substrate were connected by short dense PNIPAM brushes above LCST. Such enhancement was attributed to PET from the CB of ZnO NPs to Fermi level of Au when irradiated by UV and surface plasmon-induced hot electron transfer from Au to the CB of ZnO NPs. Both processes required the polymer brushes to bring the two parties to a close vicinity so that recombination could be inhibited. Polymer brush-based hybrid materials may also serve as precursors for photocatalysts. PS_{22}-*b*-$PSAN_{20}$-grafted 5 nm ZnO NPs were pyrolyzed into ZnO/C hybrid materials with a high surface area of 170 m^2/g as the sacrificial PS corona prevented aggregation of ZnO/C core-shell NPs during the pyrolysis.[281] The apparent rate of methylene blue photolysis under 100 mW/cm^2 visible light irradiation (420-1200 nm) catalyze by this catalyst were determined to be 0.021 min^{-1}, which was 840 times faster than the pristine 5 nm ZnO NPs and 7000 times faster than commercially available 18 nm ZnO NPs, **Fig. 43**.

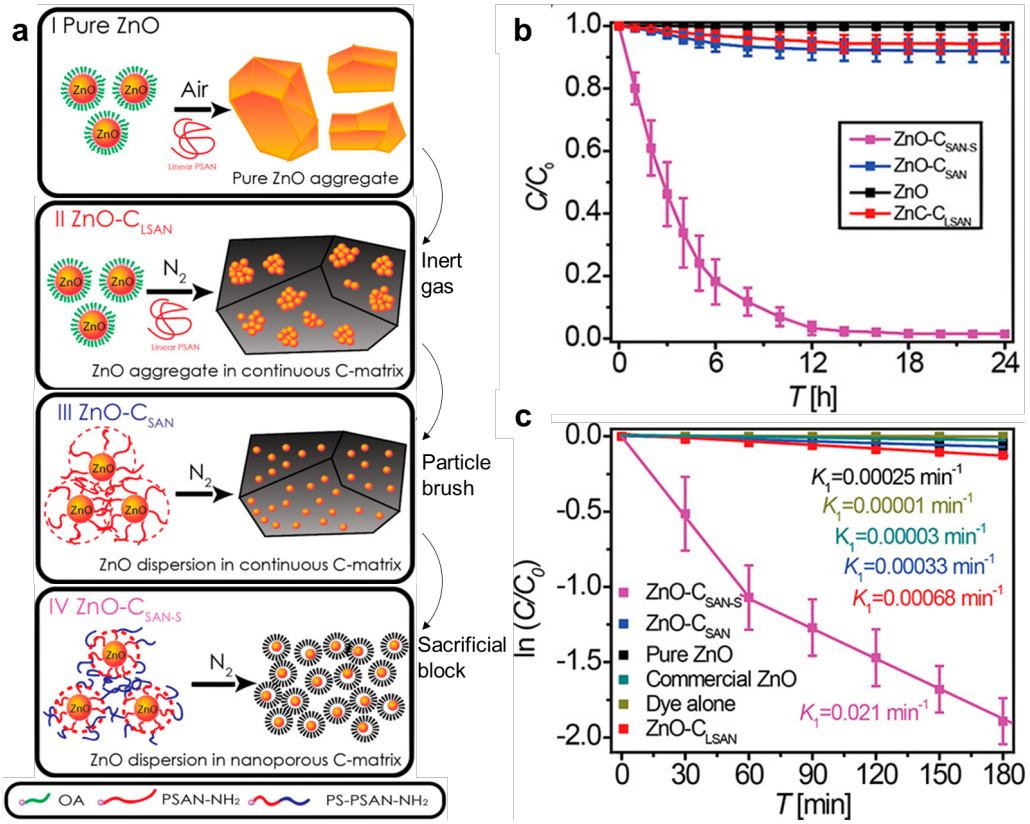

Fig. 43. Panel a compares the synthetic routes I–IV towards ZnO/C hybrid materials and resulting morphology of ZnO/C hybrid materials. Panel b depicts effect of contacting time on methylene blue adsorption for pure ZnO (system I, black), ZnO-C_{LSAN} (system II, red), ZnO-C_{SAN} (system III, blue), and ZnO-C_{SAN-S} (system IV, magenta) in dark. Panel c shows methylene blue degradation catalyzed by different ZnO catalysts. Black: pristine 5 nm ZnO (system I); red: ZnO-C_{LSAN} (system II); blue: ZnO-C_{SAN} (system III); magenta: ZnO-C_{SAN-S} (system IV); dark cyan: commercial 18 nm ZnO; and dark yellow: no catalyst. 100 mW/cm^2 irradiation @ λ = 420-1200 nm. [281], Copyright 2017. Adapted with permission from American Chemical Society.

In addition to photoirradiation, mechanical force can also cause charge separation in certain inorganic materials, this is property is called piezoelectricity. Macroscopic shape change in

piezoelectric materials leads to distortion of the crystalline structure, which becomes polarized. Electron transfer can be induced if there is electron donor or acceptor in the same system. This phenomenon was used to mediate mechanoATRP reactions.[179, 180] Both PMMA-grafted $BaTiO_3$ NPs and ZnO NPs were found to provide a higher equilibrium rate of polymerization than the bare corresponding NPs because of the extra compatibilization with the methyl acrylate/DMSO mixture. However, an induction period was observed in the case of $BaTiO_3$-*g*-PMMA, probably due to the presence of an additional layer of barrier for electron transfer. The induction period was not observed in ZnO-*g*-PMMA-catalyzed mechanoATRP because of a stronger affinity between ZnO NPs and the Cu-complex.

Catalysts should not be limited to inorganic nanoparticles. Organic moieties incorporated in particle brushes created a locally high concentration of the catalyst. For example, particle brush-supported 4-*N*,*N*-dialkylaminopyridine was prepared to be an efficient, recyclable, and tunable organocatalyst for nucleophilic substitution.[540, 541]

6.5 Energy Related Applications

One of the distinctions between polymeric and inorganic materials is that common polymers usually have low permittivity and high breakdown strength while inorganic materials, such as $BaTiO_3$, possess high permittivity but low breakdown strength. Therefore, development of polymer-inorganic hybrid materials with high permittivity and high breakdown strength becomes especially attractive for future energy storage, transmission, and conversion. Such studies began as early as the infancy of nanotechnology. The importance of polymer-NP interfaces for dielectric nanocomposites was emphasized and demonstrated that dispersed small nanoparticles resulted in even distribution of electric stress, and therefore were less likely to fail.[542-544]

One of the most effective methods to achieve well-dispersed inorganic NPs is to disperse polymer-grafted NPs in a compatible polymer matrix. Recent reports demonstrated the significance of NP dispersion and the effectiveness of polymer grafting by both experiments and simulation.[545, 546] While negligible differences in permittivity were observed between $BaTiO_3$-*g*-PS/PMMA and the $BaTiO_3$-PS/PMMA blends, the hybrid particles showed significantly lower dielectric loss and higher breakdown strength, which can be translated to a higher energy storage capacity and a higher charge/discharge efficiency. Simulations revealed that the aggregation of NPs leads to higher local electric field strength thus causing localized material failure, **Fig. 44**. Well-dispersed NPs were able to better achieve a uniform distribution of the electric field. For the same architecture, permittivity of the nanocomposites often increased with the increase of inorganic loading, so did the dielectric loss and probability of failure.[547] However, hybrid materials may sometimes have a higher dielectric strength than pure polymer as the inorganic NPs alter the charge distribution.[548, 549] Independent of the inorganic loading, permittivity and dielectric loss of dielectric nanocomposites increased with the length of polymer grafts. This also resulted in a slight increase in the energy storage density.[550] In addition to conventional combinations of $BaTiO_3$ and glassy PMMA/PS, fluoropolymers are also common choices due to their high intrinsic permittivity being ferroelectric materials.[551-553]. Other high permittivity inorganic nanomaterials, including TiO_2,[554] ZnO,[549] carbon nanotubes,[555, 556] and graphene derivatives[557, 558] were also grafted with polymer brushes and processed into dielectric nanocomposites.

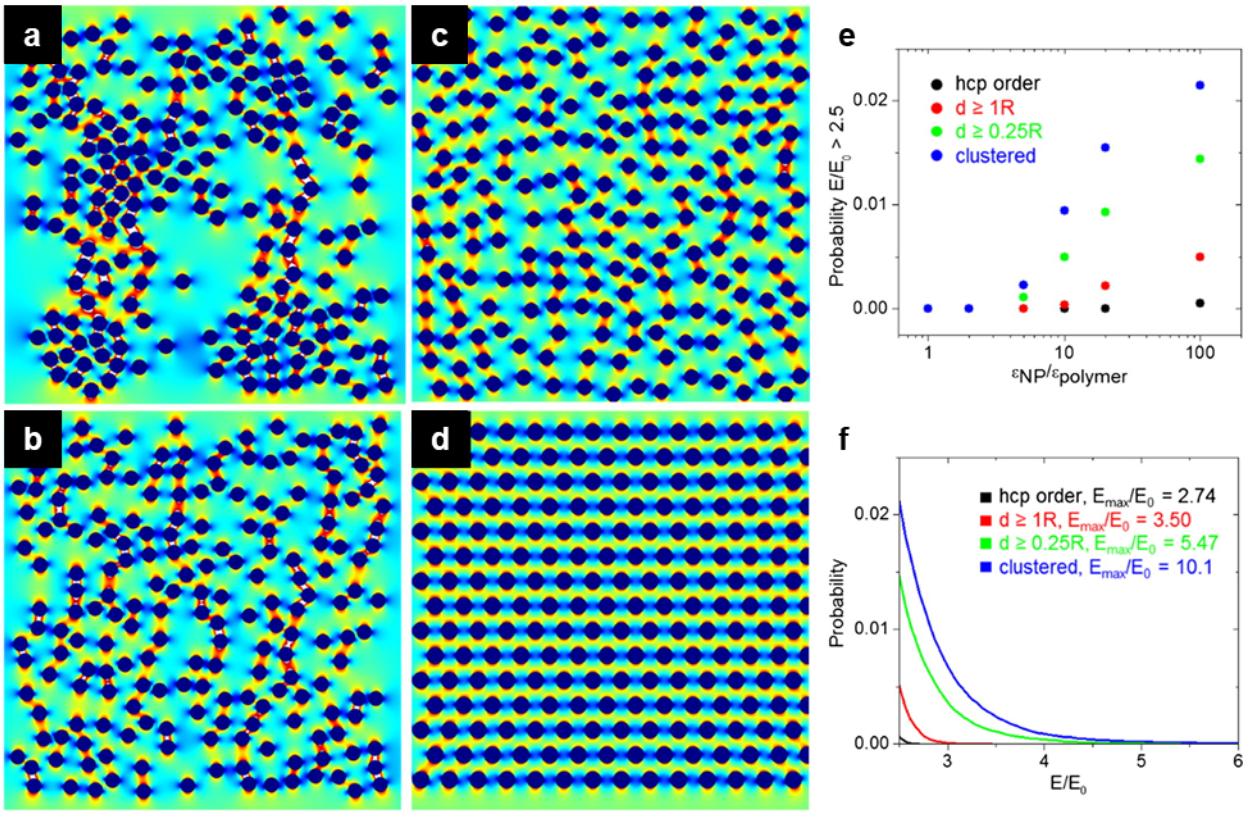

Fig. 44. 2D simulated electric field distributions for 200 particles with permittivity ratio of 100:1. Panel a shows clustered particles, where minimum particle separation, d, is greater than $0.001R$; Panel b shows dispersed particles where $d > 0.25R$ (representing blended films); in Panel c where $d > R$ (representing hybrid NP films); and Panel d demonstrates an idealized hexagonally closed packed structure. Colors correspond to normalized field intensity E/E_0, where white regions are areas where $E/E_0 > 3$. Panel e depicts probability of finding a region where $E/E_0 > 2.5$, as a function of permittivity ratio. Panel f depicts cumulative probability for finding a region with field exclusion greater than E/E_0. [545] Adapted with permission. Open Access distributed under the terms of the Creative Commons Attribution License CC BY 4.0.

As mentioned in the previous section, polymer-brush-based hybrid materials are also excellent precursors for nitrogen-doped carbon materials with high surface areas. In addition to their

catalytic activities in photolysis, oxygen reduction, and hydrogen evolution,[559, 560] these materials are good candidates for high performance pseudocapacitors.[282, 561] An initiator-bearing silsesquioxane core was constructed by crosslinking of 6-(triethoxysilyl)hexyl 2-bromoisobutyrate. PAN brushes were grafted from the core via SI-ATRP and pyrolyze into carbon materials. The silsesquioxane core was etched away by hydrofluoric acid to generate additional surface areas. For PAN brushes with a degree of polymerization $N = 90$, carbons with a specific surface area of 1244 m^2/g and a nitrogen content of 11.9 wt% were achieved. A pseudocapacitor consisted of the resulting nitrogen-doped nanoporous carbon and had a specific capacitance of 160 F/g at a current density of 100 mA/g and 91% of the capacitance was retained after 10,000 cycles.

Recently, polymer brushes were grafted from room-temperature liquid metal, eutectic gallium indium (EGaIn) alloy nanodroplets, instead of solid inorganic nanoparticles.[562] A variety of polymer brushes with different T_g were grafted to produce novel dynamic materials with customizable properties. EGaIn-based polymer nanocomposites were demonstrated to exhibit enhanced dielectric properties and applied as elastomeric actuators and generators with a self-healing capability.[563, 564] Being encapsulated in the polymer matrix, solidification of the EGaIn nanodroplets were significantly suppressed. The material was, thus, fabricated into a self-powered wearable thermoelectric device operable at low temperatures.[565]

7. Summary and Outlook

It has been over a century since inorganic materials and polymers were combined to achieve composites with enhanced and new properties. In the past few decades, the development of methodologies facilitating surface polymerization the synthesis of particle brush-based hybrid

materials has tremendously enriched the versatility of this approach. The preparation of brush-based hybrid materials usually begins with the anchoring of functional groups or polymer chains to the surface. Many different anchoring groups have been developed to accommodate virtually all kinds of inorganic surfaces, including metals, oxides/sulfides/selenides, carbons/silicon, etc. Some of these anchoring groups, such as trialkoxysilanes, carboxylates and polydopamine, are applicable to a wide range of surface chemistries. The outstanding challenges in the application of surface modification are the identification of coupling chemistries to enable sufficiently strong binding as well as the economics of the chemicals involved in the process. Advances in imaging and spectroscopic techniques in combination with modern computational methods should further promote our understanding of inorganic surface chemistries and help design more efficient anchoring agents.

Based on the development of surface modification, four major approaches to tether polymer brushes to inorganic surfaces have been developed: 'grafting-from', 'grafting-onto', 'grafting-through', and 'templated synthesis'. The 'grafting-from' approach enables polymer brushes with tunable grafting densities, but it requires incorporation of initiating groups on the surface prior to polymerization. Currently, a few surface tetherable initiators are commercially available at a reasonable cost. In contrast, the 'grafting-onto' approach does not always need pretreated surfaces, but the achievable grafting density is limited. A derived approach, ligand exchange, however, made higher grafting densities accessible at a price of a limited scope of interchangeable ligands. The 'grafting-through' approach takes surface-immobilized monomers into the chain propagation while combining the features of 'grafting-onto' and 'grafting-from'. However, both the 'grafting-onto' or 'grafting-through' procedures inevitably introduce linear polymers into the final product, demanding additional purification if 'one-component' hybrid particles are needed. The relatively

more recent templated synthesis approach is efficient for the preparation of polymer-brush-based hybrid materials with defined dimensions. Major challenges are the synthesis of the polymeric nanoreactors and selective loading with a high concentration of precursor into the anchoring sites. Besides that, only a narrow selection of polymer brushes is capable of encapsulating precursors while sustaining their conversion into inorganic nanoparticles. There is no single best approach for the preparation of polymer brush-based hybrid materials, the synthetic route should be carefully selected based on the target properties and applications. In general, for the preparation of precisely defined materials, the 'grafting-from' and templated synthesis approaches are most favorable, the latter especially if small nanoparticle dimensions are desired. Although research on polymer-inorganic hybrid materials had an application-driven origin, the majority of work in the past decades was limited to laboratory scale. Vast opportunities can be anticipated from the exploration toward large-scale, low-cost preparation of such materials.

Recent progress in the development of the synthetic strategies has created a library of available architectures of brush particle systems. Many existing polymer architectures have been applied to particle surfaces; however, the realization of specialized architectures, such as polymer loops and molecular bottlebrushes have only been recently accomplished. The architecture of polymer canopy layers has shown to exert a subtle influence on the interactions, assembly behavior and properties of particle brush-based materials. The opportunities for developing innovative material technologies are illustrated by 'one-component hybrid materials', in which the better control of the microstructure provides opportunities for material design.

Based on the successes in controlling particle brush architecture and progression in the understanding of their interactions and properties, a broad spectrum of applications has been developed. Materials with tunable stiffness, increased toughness, and novel phononic and photonic

properties have been reported. Polymer modification has also enabled the application of particle-like materials in biomedicine, for example, in diagnostic imaging, drug/gene delivery, antibacterial/antifouling, and rapid detection of biomolecules. Polymer brushes improve, or moderate, the catalytic activities of inorganic NPs, leading to the development of efficient and 'smart' catalysts for various chemical processes. Furthermore, particle brush-based materials have shown prospect for the development of innovative material solutions for the storage, transport and conversion of energy.

The field of polymer brush-based hybrid materials are still in its infancy stage. Exciting new opportunities for hybrid material science and technology drive research in further advancing chemical methods to control particle-brush architecture and the understanding of structure-property relationships. Establishment of comprehensive structure-property relationships will motivate the development of new synthetic methodologies and facilitate the advancement of materials of unprecedented performances.

Corresponding Author
* bockstaller@cmu.edu (M. R. B.) km3b@andrew.cmu.edu (K. M.)

Conflict of Interest
The authors declare no conflict of interest.

Acknowledgement
The authors acknowledge the financial support from the National Science Foundation (DMR 1501324, CMMI 1663305, DMR 1709344) and the Department of Energy (Basic Energy Sciences) via award DE-SC0018854 is gratefully acknowledged.

References

[1] Ortiz C, Boyce MC. Bioinspired structural materials. Science. 2008;319:1053-4.
[2] Goodyear C. Verfahren zur Fabrication von Gegenständen welche mehr oder weniger hart, biegsam oder elastisch sind, aus Kautschuk und Gutta-percha in Verbindung mit anderen Stoffen. Polytechnisches Journal. 1856;139:376-90.
[3] Baekeland LH. The Synthesis, Constitution, and Uses of Bakelite. Ind Eng Chem. 1909;1:149-61.
[4] Laible R, Hamann K. Polyreaktionen an Pigmentoberflächen. VI. Mitteilung: Radikalisch initiierte Polyreaktionen an SiO2 - Oberflächen. Die Angewandte Makromolekulare Chemie: Applied Macromolecular Chemistry and Physics. 1975;48:97-133.
[5] Laible R, Hamann K. Formation of chemically bound polymer layers on oxide surfaces and their role in colloidal stability. Adv Colloid Interface Sci. 1980;13:65-99.
[6] Mark J, Pan SJ. Reinforcement of polydimethylsiloxane networks by in - situ precipitation of silica: A new method for preparation of filled elastomers. Die Makromolekulare Chemie, Rapid Communications. 1982;3:681-5.
[7] Otsu T, Ogawa T, Yamamoto T. Solid-phase block copolymer synthesis by the iniferter technique. Macromolecules. 1986;19:2087-9.
[8] Matyjaszewski K, Miller PJ, Shukla N, Immaraporn B, Gelman A, Luokala BB, et al. Polymers at Interfaces: Using Atom Transfer Radical Polymerization in the Controlled Growth of Homopolymers and Block Copolymers from Silicon Surfaces in the Absence of Untethered Sacrificial Initiator. Macromolecules. 1999;32:8716-24.
[9] Möller M, Künstle H, Kunz M. Inorganic nanoclusters in organic glasses — Novel materials for electro-optical applications. Synth Met. 1991;41:1159-62.
[10] Colvin V, Goldstein A, Alivisatos A. Semiconductor nanocrystals covalently bound to metal surfaces with self-assembled monolayers. J Am Chem Soc. 1992;114:5221-30.
[11] Spange S, Simon F, Schutz H, Schramm A, Winkelmann H. Preparation and properties of novel cationically active oligo-p-methoxystyryl-silica composites. Journal of Macromolecular Science—Pure and Applied Chemistry. 1992;29:997-1006.
[12] Whitesell JK, Chang HK. Directionally Aligned Helical Peptides on Surfaces. Science. 1993;261:73-6.
[13] Kent M, Factor B, Satija S, Gallagher P, Smith G. Structure of bimodal polymer brushes in a good solvent by neutron reflectivity. Macromolecules. 1996;29:2843-9.
[14] Huang X, Wirth MJ. Surface-initiated radical polymerization on porous silica. Anal Chem. 1997;69:4577-80.

[15] Ejaz M, Yamamoto S, Ohno K, Tsujii Y, Fukuda T. Controlled graft polymerization of methyl methacrylate on silicon substrate by the combined use of the langmuir− blodgett and atom transfer radical polymerization techniques. Macromolecules. 1998;31:5934-6.
[16] Husseman M, Malmström EE, McNamara M, Mate M, Mecerreyes D, Benoit DG, et al. Controlled synthesis of polymer brushes by "living" free radical polymerization techniques. Macromolecules. 1999;32:1424-31.
[17] Weck M, Jackiw JJ, Rossi RR, Weiss PS, Grubbs RH. Ring-opening metathesis polymerization from surfaces. J Am Chem Soc. 1999;121:4088-9.
[18] Sidorenko A, Minko S, Schenk-Meuser K, Duschner H, Stamm M. Switching of polymer brushes. Langmuir. 1999;15:8349-55.
[19] Tsujii Y, Ejaz M, Sato K, Goto A, Fukuda T. Mechanism and kinetics of RAFT-mediated graft polymerization of styrene on a solid surface. 1. Experimental evidence of surface radical migration. Macromolecules. 2001;34:8872-8.
[20] Mori H, Seng DC, Zhang M, Müller AH. Hybrid nanoparticles with hyperbranched polymer shells via self-condensing atom transfer radical polymerization from silica surfaces. Langmuir. 2002;18:3682-93.
[21] Baum M, Brittain WJ. Synthesis of polymer brushes on silicate substrates via reversible addition fragmentation chain transfer technique. Macromolecules. 2002;35:610-5.
[22] Djalali R, Li S-Y, Schmidt M. Amphipolar Core−Shell Cylindrical Brushes as Templates for the Formation of Gold Clusters and Nanowires. Macromolecules. 2002;35:4282-8.
[23] Matyjaszewski K, Dong H, Jakubowski W, Pietrasik J, Kusumo A. Grafting from Surfaces for "Everyone": ARGET ATRP in the Presence of Air. Langmuir. 2007;23:4528-31.
[24] Li B, Yu B, Huck WTS, Zhou F, Liu W. Electrochemically Induced Surface-Initiated Atom-Transfer Radical Polymerization. Angew Chem Int Ed. 2012;51:5092-5.
[25] Yan J, Li B, Zhou F, Liu W. Ultraviolet Light-Induced Surface-Initiated Atom-Transfer Radical Polymerization. ACS Macro Lett. 2013;2:592-6.
[26] Poelma JE, Fors BP, Meyers GF, Kramer JW, Hawker CJ. Fabrication of complex three - dimensional polymer brush nanostructures through light - mediated living radical polymerization. Angew Chem. 2013;125:6982-6.
[27] Usuki A, Kojima Y, Kawasumi M, Okada A, Fukushima Y, Kurauchi T, et al. Synthesis of nylon 6-clay hybrid. J Mater Res. 1993;8:1179-84.
[28] Giannelis EP. Polymer layered silicate nanocomposites. Adv Mater. 1996;8:29-35.
[29] Hayashi H, Sakano K, Suzuki T, Uegakito O, Usuki A. Nylon composite material and production thereof. Espacenet. Japan: Toyota Central R&D Lab Inc; 1987.
[30] Okada A, Kawasumi M, Kohzaki M, Fujimoto M, Kojima Y, Kurauchi T, et al. Composite material and process for producing the same. In: USPTO, editor. USPTO. United States: Toyota Central R&D Labs Inc; 1988.
[31] Usuki A, Mizutani T, Fukushima Y, Fujimoto M, Fukumori K, Kojima Y, et al. Composite material containing a layered silicate. In: USPTO, editor. USPTO. United States: Toyota Central R&D Labs Inc; 1988.
[32] Barbey R, Lavanant L, Paripovic D, Schüwer N, Sugnaux C, Tugulu S, et al. Polymer brushes via surface-initiated controlled radical polymerization: synthesis, characterization, properties, and applications. Chem Rev. 2009;109:5437-527.
[33] Kasemann R, Schmidt HK, Wintrich E. A new type of a sol-gel-derived inorganic-organic nanocomposite. MRS Online Proceedings Library Archive. 1994;346.

[34] Wang J-S, Matyjaszewski K. Controlled/"living" radical polymerization. atom transfer radical polymerization in the presence of transition-metal complexes. J Am Chem Soc. 1995;117:5614-5.
[35] Von Werne T, Patten TE. Preparation of structurally well-defined polymer–nanoparticle hybrids with controlled/living radical polymerizations. J Am Chem Soc. 1999;121:7409-10.
[36] Ohno K, Morinaga T, Koh K, Tsujii Y, Fukuda T. Synthesis of Monodisperse Silica Particles Coated with Well-Defined, High-Density Polymer Brushes by Surface-Initiated Atom Transfer Radical Polymerization. Macromolecules. 2005;38:2137-42.
[37] Matyjaszewski K, Miller PJ, Pyun J, Kickelbick G, Diamanti S. Synthesis and characterization of star polymers with varying arm number, length, and composition from organic and hybrid inorganic/organic multifunctional initiators. Macromolecules. 1999;32:6526-35.
[38] Pyun J, Matyjaszewski K, Kowalewski T, Savin D, Patterson G, Kickelbick G, et al. Synthesis of well-defined block copolymers tethered to polysilsesquioxane nanoparticles and their nanoscale morphology on surfaces. J Am Chem Soc. 2001;123:9445-6.
[39] Pyun J, Matyjaszewski K. Synthesis of Nanocomposite Organic/Inorganic Hybrid Materials Using Controlled/“Living” Radical Polymerization. Chem Mater. 2001;13:3436-48.
[40] Jordan R, Ulman A. Surface initiated living cationic polymerization of 2-oxazolines. J Am Chem Soc. 1998;120:243-7.
[41] Kruk M, Dufour B, Celer EB, Kowalewski T, Jaroniec M, Matyjaszewski K. Synthesis of mesoporous carbons using ordered and disordered mesoporous silica templates and polyacrylonitrile as carbon precursor. J Phys Chem B. 2005;109:9216-25.
[42] Milner S, Witten T, Cates M. Effects of polydispersity in the end-grafted polymer brush. Macromolecules. 1989;22:853-61.
[43] Rungta A, Natarajan B, Neely T, Dukes D, Schadler LS, Benicewicz BC. Grafting Bimodal Polymer Brushes on Nanoparticles Using Controlled Radical Polymerization. Macromolecules. 2012;45:9303-11.
[44] Yan J, Kristufek T, Schmitt M, Wang Z, Xie G, Dang A, et al. Matrix-free Particle Brush System with Bimodal Molecular Weight Distribution Prepared by SI-ATRP. Macromolecules. 2015;48:8208-18.
[45] Ye P, Dong H, Zhong M, Matyjaszewski K. Synthesis of Binary Polymer Brushes via Two-Step Reverse Atom Transfer Radical Polymerization. Macromolecules. 2011;44:2253-60.
[46] Julthongpiput D, Lin Y-H, Teng J, Zubarev ER, Tsukruk VV. Y-shaped polymer brushes: nanoscale switchable surfaces. Langmuir. 2003;19:7832-6.
[47] Zhao B. Synthesis of binary mixed homopolymer brushes by combining atom transfer radical polymerization and nitroxide-mediated radical polymerization. Polymer. 2003;44:4079-83.
[48] Li D, Sheng X, Zhao B. Environmentally responsive “hairy” nanoparticles: Mixed homopolymer brushes on silica nanoparticles synthesized by living radical polymerization techniques. J Am Chem Soc. 2005;127:6248-56.
[49] Antonietti M, Wenz E, Bronstein L, Seregina M. Synthesis and characterization of noble metal colloids in block copolymer micelles. Adv Mater. 1995;7:1000-5.
[50] Yuan J, Xu Y, Walther A, Bolisetty S, Schumacher M, Schmalz H, et al. Water-soluble organo-silica hybrid nanowires. Nat Mater. 2008;7:718-22.

[51] Müllner M, Yuan J, Weiss S, Walther A, Förtsch M, Drechsler M, et al. Water-Soluble Organo−Silica Hybrid Nanotubes Templated by Cylindrical Polymer Brushes. J Am Chem Soc. 2010;132:16587-92.
[52] Pang X, Zhao L, Han W, Xin X, Lin Z. A general and robust strategy for the synthesis of nearly monodisperse colloidal nanocrystals. Nat Nano. 2013;8:426-31.
[53] Lee HJ, Nakayama Y, Matsuda T. Spatio-resolved, macromolecular architectural surface: highly branched graft polymer via photochemically driven quasiliving polymerization technique. Macromolecules. 1999;32:6989-95.
[54] Raula J, Shan J, Nuopponen M, Niskanen A, Jiang H, Kauppinen EI, et al. Synthesis of gold nanoparticles grafted with a thermoresponsive polymer by surface-induced reversible-addition-fragmentation chain-transfer polymerization. Langmuir. 2003;19:3499-504.
[55] Zoppe JO, Ataman NC, Mocny P, Wang J, Moraes J, Klok H-A. Surface-Initiated Controlled Radical Polymerization: State-of-the-Art, Opportunities, and Challenges in Surface and Interface Engineering with Polymer Brushes. Chem Rev. 2017;117:1105-318.
[56] Hui CM, Pietrasik J, Schmitt M, Mahoney C, Choi J, Bockstaller MR, et al. Surface-Initiated Polymerization as an Enabling Tool for Multifunctional (Nano-)Engineered Hybrid Materials. Chem Mater. 2014;26:745-62.
[57] Jakubowski W, Matyjaszewski K. Activators Regenerated by Electron Transfer for Atom-Transfer Radical Polymerization of (Meth)acrylates and Related Block Copolymers. Angew Chem Int Ed. 2006;45:4482-6.
[58] Jakubowski W, Min K, Matyjaszewski K. Activators Regenerated by Electron Transfer for Atom Transfer Radical Polymerization of Styrene. Macromolecules. 2006;39:39-45.
[59] Dunderdale GJ, Urata C, Miranda DF, Hozumi A. Large-Scale and Environmentally Friendly Synthesis of pH-Responsive Oil-Repellent Polymer Brush Surfaces under Ambient Conditions. ACS Appl Mater Interfaces. 2014;6:11864-8.
[60] Sato T, Dunderdale GJ, Urata C, Hozumi A. Sol–Gel Preparation of Initiator Layers for Surface-Initiated ATRP: Large-Scale Formation of Polymer Brushes Is Not a Dream. Macromolecules. 2018;51:10065-73.
[61] Yan W, Fantin M, Ramakrishna S, Spencer ND, Matyjaszewski K, Benetti EM. Growing Polymer Brushes from a Variety of Substrates under Ambient Conditions by Cu0-Mediated Surface-Initiated ATRP. ACS Appl Mater Interfaces. 2019;11:27470-7.
[62] Yan W, Fantin M, Spencer ND, Matyjaszewski K, Benetti EM. Translating Surface-Initiated Atom Transfer Radical Polymerization into Technology: The Mechanism of Cu0-Mediated SI-ATRP under Environmental Conditions. ACS Macro Lett. 2019;8:865-70.
[63] Chmielarz P, Yan J, Krys P, Wang Y, Wang Z, Bockstaller MR, et al. Synthesis of Nanoparticle Copolymer Brushes via Surface-Initiated seATRP. Macromolecules. 2017;50:4151-9.
[64] Li B, Yu B, Huck WT, Liu W, Zhou F. Electrochemically mediated atom transfer radical polymerization on nonconducting substrates: Controlled brush growth through catalyst diffusion. J Am Chem Soc. 2013;135:1708-10.
[65] Yan J, Pan X, Wang Z, Zhang J, Matyjaszewski K. Influence of Spacers in Tetherable Initiators on Surface-Initiated Atom Transfer Radical Polymerization (SI-ATRP). Macromolecules. 2016;49:9283-6.
[66] Pietrasik J, Bombalski L, Cusick B, Huang J, Pyun J, Kowalewski T, et al. Controlling Polymer Chain Topology and Architecture by ATRP from Flat Surfaces. Stimuli-Responsive Polymeric Films and Coatings: American Chemical Society; 2005. p. 28-42.

[67] Song Y, Ye G, Lu Y, Chen J, Wang J, Matyjaszewski K. Surface-initiated ARGET ATRP of poly (glycidyl methacrylate) from carbon nanotubes via bioinspired catechol chemistry for efficient adsorption of uranium ions. ACS Macro Lett. 2016;5:382-6.
[68] Lee H, Dellatore SM, Miller WM, Messersmith PB. Mussel-Inspired Surface Chemistry for Multifunctional Coatings. Science. 2007;318:426-30.
[69] Zeng Z, Wen M, Ye G, Huo X, Wu F, Wang Z, et al. Controlled Architecture of Hybrid Polymer Nanocapsules with Tunable Morphologies by Manipulating Surface-Initiated ARGET ATRP from Hydrothermally Modified Polydopamine. Chem Mater. 2017;29:10212-9.
[70] Wang Z, Mahoney C, Yan J, Lu Z, Ferebee R, Luo D, et al. Preparation of Well-Defined Poly(styrene-co-acrylonitrile)/ZnO Hybrid Nanoparticles by an Efficient Ligand Exchange Strategy. Langmuir. 2016;32:13207-13.
[71] Yan J, Pan X, Wang Z, Lu Z, Wang Y, Liu L, et al. A Fatty Acid-Inspired Tetherable Initiator for Surface-Initiated Atom Transfer Radical Polymerization. Chem Mater. 2017;29:4963-9.
[72] Khabibullin A, Bhangaonkar K, Mahoney C, Lu Z, Schmitt M, Sekizkardes AK, et al. Grafting PMMA Brushes from α-Alumina Nanoparticles via SI-ATRP. ACS Appl Mater Interfaces. 2016;8:5458-65.
[73] Zeng G, Liu M, Shi K, Heng C, Mao L, Wan Q, et al. Surface modification of nanodiamond through metal free atom transfer radical polymerization. Appl Surf Sci. 2016;390:710-7.
[74] Zaborniak I, Chmielarz P, Matyjaszewski K. Modification of wood-based materials by atom transfer radical polymerization methods. Eur Polym J. 2019;120:109253.
[75] Basuki JS, Esser L, Zetterlund PB, Whittaker MR, Boyer C, Davis TP. Grafting of P(OEGA) Onto Magnetic Nanoparticles Using Cu(0) Mediated Polymerization: Comparing Grafting "from" and "to" Approaches in the Search for the Optimal Material, Design of Nanoparticle MRI Contrast Agents. Macromolecules. 2013;46:6038-47.
[76] Dong H, Huang J, Koepsel RR, Ye P, Russell AJ, Matyjaszewski K. Recyclable antibacterial magnetic nanoparticles grafted with quaternized poly (2-(dimethylamino) ethyl methacrylate) brushes. Biomacromolecules. 2011;12:1305-11.
[77] Matrab T, Chehimi MM, Perruchot C, Adenier A, Guillez A, Save M, et al. Novel Approach for Metallic Surface-Initiated Atom Transfer Radical Polymerization Using Electrografted Initiators Based on Aryl Diazonium Salts. Langmuir. 2005;21:4686-94.
[78] Liu T, Jia S, Kowalewski T, Matyjaszewski K, Casado-Portilla R, Belmont J. Grafting Poly(n-butyl acrylate) from a Functionalized Carbon Black Surface by Atom Transfer Radical Polymerization. Langmuir. 2003;19:6342-5.
[79] Kim J-B, Bruening ML, Baker GL. Surface-Initiated Atom Transfer Radical Polymerization on Gold at Ambient Temperature. J Am Chem Soc. 2000;122:7616-7.
[80] Dong H, Zhu M, Yoon JA, Gao H, Jin R, Matyjaszewski K. One-Pot Synthesis of Robust Core/Shell Gold Nanoparticles. J Am Chem Soc. 2008;130:12852-3.
[81] Esteves AC, Bombalski L, Trindade T, Matyjaszewski K, Barros‐Timmons A. Polymer grafting from CdS quantum dots via AGET ATRP in miniemulsion. Small. 2007;3:1230-6.
[82] Kim S-W, Kim S, Tracy JB, Jasanoff A, Bawendi MG. Phosphine Oxide Polymer for Water-Soluble Nanoparticles. J Am Chem Soc. 2005;127:4556-7.
[83] Acres RG, Ellis AV, Alvino J, Lenahan CE, Khodakov DA, Metha GF, et al. Molecular structure of 3-aminopropyltriethoxysilane layers formed on silanol-terminated silicon surfaces. J Phys Chem C. 2012;116:6289-97.

[84] Ryu JH, Messersmith PB, Lee H. Polydopamine surface chemistry: a decade of discovery. ACS Appl Mater Interfaces. 2018;10:7523-40.
[85] Connor PA, Dobson KD, McQuillan AJ. New sol-gel attenuated total reflection infrared spectroscopic method for analysis of adsorption at metal oxide surfaces in aqueous solutions. Chelation of TiO2, ZrO2, and Al2O3 surfaces by catechol, 8-quinolinol, and acetylacetone. Langmuir. 1995;11:4193-5.
[86] Pranantyo D, Xu LQ, Neoh K-G, Kang E-T, Ng YX, Teo SL-M. Tea Stains-Inspired Initiator Primer for Surface Grafting of Antifouling and Antimicrobial Polymer Brush Coatings. Biomacromolecules. 2015;16:723-32.
[87] Kuang J, Messersmith PB. Universal Surface-Initiated Polymerization of Antifouling Zwitterionic Brushes Using a Mussel-Mimetic Peptide Initiator. Langmuir. 2012;28:7258-66.
[88] Allara DL, Nuzzo RG. Spontaneously organized molecular assemblies. 1. Formation, dynamics, and physical properties of n-alkanoic acids adsorbed from solution on an oxidized aluminum surface. Langmuir. 1985;1:45-52.
[89] Zhang L, He R, Gu H-C. Oleic acid coating on the monodisperse magnetite nanoparticles. Appl Surf Sci. 2006;253:2611-7.
[90] Sun S, Murray CB, Weller D, Folks L, Moser A. Monodisperse FePt nanoparticles and ferromagnetic FePt nanocrystal superlattices. science. 2000;287:1989-92.
[91] Leff DV, Brandt L, Heath JR. Synthesis and characterization of hydrophobic, organically-soluble gold nanocrystals functionalized with primary amines. Langmuir. 1996;12:4723-30.
[92] Kumar A, Mandal S, Selvakannan PR, Pasricha R, Mandale AB, Sastry M. Investigation into the Interaction between Surface-Bound Alkylamines and Gold Nanoparticles. Langmuir. 2003;19:6277-82.
[93] Wu N, Fu L, Su M, Aslam M, Wong KC, Dravid VP. Interaction of Fatty Acid Monolayers with Cobalt Nanoparticles. Nano Lett. 2004;4:383-6.
[94] Zhang J, Lee J, Wang Z, Yan J, Lu Z, Liu S, et al. Synthesis and characterization of gibbsite nanoplatelet brushes by surface-initiated atom transfer radical polymerization. Polymer. 2017;126:126-32.
[95] Armes S, Gottesfeld S, Beery J, Garzon F, Agnew S. Conducting polymer-colloidal silica composites. Polymer. 1991;32:2325-30.
[96] Maeda S, Corradi R, Armes SP. Synthesis and characterization of carboxylic acid-functionalized polypyrrole-silica microparticles. Macromolecules. 1995;28:2905-11.
[97] Jung N, Kwon S, Lee D, Yoon D-M, Park YM, Benayad A, et al. Synthesis of Chemically Bonded Graphene/Carbon Nanotube Composites and their Application in Large Volumetric Capacitance Supercapacitors. Adv Mater. 2013;25:6854-8.
[98] Sahoo Y, Pizem H, Fried T, Golodnitsky D, Burstein L, Sukenik CN, et al. Alkyl Phosphonate/Phosphate Coating on Magnetite Nanoparticles: A Comparison with Fatty Acids. Langmuir. 2001;17:7907-11.
[99] Burkett SL, Ko N, Stern ND, Caissie JA, Sengupta D. Covalently Linked Nanocomposites: Poly(methyl methacrylate) Brushes Grafted from Zirconium Phosphonate. Chem Mater. 2006;18:5137-43.
[100] Tsubokawa N. Functionalization of carbon black by surface grafting of polymers. Prog Polym Sci. 1992;17:417-70.
[101] Delamar M, Hitmi R, Pinson J, Saveant JM. Covalent modification of carbon surfaces by grafting of functionalized aryl radicals produced from electrochemical reduction of diazonium salts. J Am Chem Soc. 1992;114:5883-4.

[102] Iruthayaraj J, Chernyy S, Lillethorup M, Ceccato M, Røn T, Hinge M, et al. On surface-initiated atom transfer radical polymerization using diazonium chemistry to introduce the initiator layer. Langmuir. 2010;27:1070-8.
[103] Li Y, Zuilhof H. Photochemical Grafting and Patterning of Organic Monolayers on Indium Tin Oxide Substrates. Langmuir. 2012;28:5350-9.
[104] Colavita PE, Sun B, Tse K-Y, Hamers RJ. Photochemical Grafting of n-Alkenes onto Carbon Surfaces: the Role of Photoelectron Ejection. J Am Chem Soc. 2007;129:13554-65.
[105] Leff DV, Ohara PC, Heath JR, Gelbart WM. Thermodynamic control of gold nanocrystal size: experiment and theory. JPhys Chem. 1995;99:7036-41.
[106] Templeton AC, Wuelfing WP, Murray RW. Monolayer-protected cluster molecules. Acc Chem Res. 2000;33:27-36.
[107] Grönbeck H, Curioni A, Andreoni W. Thiols and disulfides on the Au (111) surface: the headgroup− gold interaction. J Am Chem Soc. 2000;122:3839-42.
[108] Xue Y, Li X, Li H, Zhang W. Quantifying thiol–gold interactions towards the efficient strength control. Nat Commun. 2014;5:4348.
[109] Takahashi A, Kawaguchi M. The structure of macromolecules adsorbed on interfaces. Behavior of Macromolecules. Berlin, Heidelberg: Springer Berlin Heidelberg; 1982. p. 1-65.
[110] Fontana BJ, Thomas JR. The Configuration of Adsorbed Alkyl Methacrylate Polymers by Infrared and Sedimentation Studies. JPhys Chem. 1961;65:480-7.
[111] Koczkur KM, Mourdikoudis S, Polavarapu L, Skrabalak SE. Polyvinylpyrrolidone (PVP) in nanoparticle synthesis. Dalton Transactions. 2015;44:17883-905.
[112] Takashi. A, Yamashit. Y. Morphology, Crystallization, and Surface Properties of Styrene-Tetrahydrofuran Block Copolymers. Abstracts of Papers of the American Chemical Society: Amer Chemical Soc 1155 16th St, Nw, Washington, DC 20036; 1974. p. 32-.
[113] Dawkins JV, Taylor G. Surface layer thickness in non-aqueous polymer dispersions stabilised by AB block copolymers of polystyrene and poly (dimethyl siloxane). Journal of the Chemical Society, Faraday Transactions 1: Physical Chemistry in Condensed Phases. 1980;76:1263-74.
[114] Auschra C, Eckstein E, Mühlebach A, Zink M-O, Rime F. Design of new pigment dispersants by controlled radical polymerization. Prog Org Coat. 2002;45:83-93.
[115] Hadziioannou G, Patel S, Granick S, Tirrell M. Forces between surfaces of block copolymers adsorbed on mica. J Am Chem Soc. 1986;108:2869-76.
[116] Saleh N, Phenrat T, Sirk K, Dufour B, Ok J, Sarbu T, et al. Adsorbed triblock copolymers deliver reactive iron nanoparticles to the oil/water interface. Nano Lett. 2005;5:2489-94.
[117] Costa AC, Geoghegan M, Vlček P, Composto RJ. Block Copolymer Adsorption from a Homopolymer Melt to Silicon Oxide: Effects of Nonadsorbing Block Length and Anchoring Block−Substrate Interaction. Macromolecules. 2003;36:9897-904.
[118] Kelley TW, Schorr PA, Johnson KD, Tirrell M, Frisbie CD. Direct force measurements at polymer brush surfaces by atomic force microscopy. Macromolecules. 1998;31:4297-300.
[119] Kang Y, Taton TA. Controlling Shell Thickness in Core− Shell Gold Nanoparticles via Surface-Templated Adsorption of Block Copolymer Surfactants. Macromolecules. 2005;38:6115-21.
[120] Ding H, Yan J, Wang Z, Xie G, Mahoney C, Ferebee R, et al. Preparation of ZnO hybrid nanoparticles by ATRP. Polymer. 2016;107:492-502.
[121] Lee JH, Kopecek J, Andrade JD. Protein - resistant surfaces prepared by PEO - containing block copolymer surfactants. Journal of biomedical materials research. 1989;23:351-68.

[122] Marra J, Hair ML. Interactions between two adsorbed layers of poly(ethylene oxide)/polystyrene diblock copolymers in heptane—toluene mixtures. Colloids and Surfaces. 1988;34:215-26.
[123] Munch MR, Gast AP. Kinetics of block copolymer adsorption on dielectric surfaces from a selective solvent. Macromolecules. 1990;23:2313-20.
[124] Munch MR, Gast AP. Block copolymers at interfaces. 2. Surface adsorption. Macromolecules. 1988;21:1366-72.
[125] Yerushalmi-Rozen R, Klein J, Fetters LJ. Suppression of Rupture in Thin, Nonwetting Liquid Films. Science. 1994;263:793-5.
[126] Zhu B, Edmondson S. Polydopamine-melanin initiators for Surface-initiated ATRP. Polymer. 2011;52:2141-9.
[127] Fristrup CJ, Jankova K, Hvilsted S. Hydrophilization of poly (ether ether ketone) films by surface-initiated atom transfer radical polymerization. Polym Chem. 2010;1:1696-701.
[128] Yakushiji T, Sakai K, Kikuchi A, Aoyagi T, Sakurai Y, Okano T. Graft Architectural Effects on Thermoresponsive Wettability Changes of Poly(N-isopropylacrylamide)-Modified Surfaces. Langmuir. 1998;14:4657-62.
[129] Labet M, Thielemans W, Dufresne A. Polymer Grafting onto Starch Nanocrystals. Biomacromolecules. 2007;8:2916-27.
[130] Schmidt AM. The synthesis of magnetic core‐shell nanoparticles by surface‐initiated ring‐opening polymerization of ε‐caprolactone. Macromol Rapid Commun. 2005;26:93-7.
[131] Flavel BS, Jasieniak M, Velleman L, Ciampi S, Luais E, Peterson JR, et al. Grafting of Poly(ethylene glycol) on Click Chemistry Modified Si(100) Surfaces. Langmuir. 2013;29:8355-62.
[132] Ingavle GC, Baillie LWJ, Zheng Y, Lis EK, Savina IN, Howell CA, et al. Affinity binding of antibodies to supermacroporous cryogel adsorbents with immobilized protein A for removal of anthrax toxin protective antigen. Biomaterials. 2015;50:140-53.
[133] Beggs KM, Servinis L, Gengenbach TR, Huson MG, Fox BL, Henderson LC. A systematic study of carbon fibre surface grafting via in situ diazonium generation for improved interfacial shear strength in epoxy matrix composites. Compos Sci Technol. 2015;118:31-8.
[134] Luzinov I, Julthongpiput D, Malz H, Pionteck J, Tsukruk VV. Polystyrene Layers Grafted to Epoxy-Modified Silicon Surfaces. Macromolecules. 2000;33:1043-8.
[135] Lummerstorfer T, Hoffmann H. Click Chemistry on Surfaces: 1,3-Dipolar Cycloaddition Reactions of Azide-Terminated Monolayers on Silica. J Phys Chem B. 2004;108:3963-6.
[136] Goldmann AS, Walther A, Nebhani L, Joso R, Ernst D, Loos K, et al. Surface Modification of Poly (divinylbenzene) Microspheres via Thiol– Ene Chemistry and Alkyne–Azide Click Reactions. Macromolecules. 2009;42:3707-14.
[137] Sun X-L, Stabler CL, Cazalis CS, Chaikof EL. Carbohydrate and Protein Immobilization onto Solid Surfaces by Sequential Diels–Alder and Azide–Alkyne Cycloadditions. Bioconjugate Chem. 2006;17:52-7.
[138] Jonkheijm P, Weinrich D, Köhn M, Engelkamp H, Christianen PCM, Kuhlmann J, et al. Photochemical Surface Patterning by the Thiol-Ene Reaction. Angew Chem. 2008;120:4493-6.
[139] Henze M, Mädge D, Prucker O, Rühe J. "Grafting Through": Mechanistic Aspects of Radical Polymerization Reactions with Surface-Attached Monomers. Macromolecules. 2014;47:2929-37.

[140] Khabibullin A, Kopeć M, Matyjaszewski K. Modification of Silica Nanoparticles with Miktoarm Polymer Brushes via ATRP. Journal of Inorganic and Organometallic Polymers and Materials. 2016;26:1292-300.
[141] Guimont A, Beyou E, Alcouffe P, Martin G, Sonntag P, Cassagnau P. Synthesis and characterization of PDMS-grafted graphite oxide sheets. Polymer. 2013;54:4830-7.
[142] Buriak JM. Illuminating silicon surface hydrosilylation: an unexpected plurality of mechanisms. Chem Mater. 2013;26:763-72.
[143] Tedja R, Soeriyadi AH, Whittaker MR, Lim M, Marquis C, Boyer C, et al. Effect of TiO 2 nanoparticle surface functionalization on protein adsorption, cellular uptake and cytotoxicity: the attachment of PEG comb polymers using catalytic chain transfer and thiol–ene chemistry. Polym Chem. 2012;3:2743-51.
[144] Zhu J, Waengler C, Lennox RB, Schirrmacher R. Preparation of water-soluble maleimide-functionalized 3 nm gold nanoparticles: a new bioconjugation template. Langmuir. 2012;28:5508-12.
[145] Gobbo P, Biesinger MC, Workentin MS. Facile synthesis of gold nanoparticle (AuNP)–carbon nanotube (CNT) hybrids through an interfacial Michael addition reaction. Chem Commun. 2013;49:2831-3.
[146] Russell RJ, Sirkar K, Pishko MV. Preparation of Nanocomposite Poly(allylamine)−Poly(ethylene glycol) Thin Films Using Michael Addition. Langmuir. 2000;16:4052-4.
[147] Kim NY, Jeon NL, Choi IS, Takami S, Harada Y, Finnie KR, et al. Surface-Initiated Ring-Opening Metathesis Polymerization on Si/SiO2. Macromolecules. 2000;33:2793-5.
[148] Rowe MD, Hammer BAG, Boyes SG. Synthesis of Surface-Initiated Stimuli-Responsive Diblock Copolymer Brushes Utilizing a Combination of ATRP and RAFT Polymerization Techniques. Macromolecules. 2008;41:4147-57.
[149] Peng Q, Lai DM, Kang E, Neoh K. Preparation of polymer− silicon (100) hybrids via interface-initiated reversible addition-fragmentation chain-transfer (RAFT) polymerization. Macromolecules. 2006;39:5577-82.
[150] Bartholome C, Beyou E, Bourgeat-Lami E, Chaumont P, Zydowicz N. Nitroxide-mediated polymerizations from silica nanoparticle surfaces:“graft from” polymerization of styrene using a triethoxysilyl-terminated alkoxyamine initiator. Macromolecules. 2003;36:7946-52.
[151] Prucker O, Rühe J. Synthesis of poly (styrene) monolayers attached to high surface area silica gels through self-assembled monolayers of azo initiators. Macromolecules. 1998;31:592-601.
[152] Sedjo RA, Mirous BK, Brittain WJ. Synthesis of polystyrene-block-poly (methyl methacrylate) brushes by reverse atom transfer radical polymerization. Macromolecules. 2000;33:1492-3.
[153] Pauloehrl T, Delaittre G, Winkler V, Welle A, Bruns M, Börner HG, et al. Adding Spatial Control to Click Chemistry: Phototriggered Diels–Alder Surface (Bio)functionalization at Ambient Temperature. Angew Chem Int Ed. 2012;51:1071-4.
[154] Tarducci C, Badyal JPS, Brewer SA, Willis C. Diels–Alder chemistry at furan ring functionalized solid surfaces. Chem Commun. 2005:406-8.
[155] Nebhani L, Sinnwell S, Inglis AJ, Stenzel MH, Barner‐Kowollik C, Barner L. Efficient Surface Modification of Divinylbenzene Microspheres via a Combination of RAFT and Hetero Diels‐Alder Chemistry. Macromol Rapid Commun. 2008;29:1431-7.

[156] Ataman NC, Klok H-A. Degrafting of Poly(poly(ethylene glycol) methacrylate) Brushes from Planar and Spherical Silicon Substrates. Macromolecules. 2016;49:9035-47.
[157] Michalek L, Barner L, Barner‐Kowollik C. Polymer on Top: Current Limits and Future Perspectives of Quantitatively Evaluating Surface Grafting. Adv Mater. 2018:1706321.
[158] Liu T, Casado‐Portilla R, Belmont J, Matyjaszewski K. ATRP of butyl acrylates from functionalized carbon black surfaces. J Polym Sci, Part A: Polym Chem. 2005;43:4695-709.
[159] Li C, Han J, Ryu CY, Benicewicz BC. A Versatile Method To Prepare RAFT Agent Anchored Substrates and the Preparation of PMMA Grafted Nanoparticles. Macromolecules. 2006;39:3175-83.
[160] Wu T, Efimenko K, Genzer J. Combinatorial Study of the Mushroom-to-Brush Crossover in Surface Anchored Polyacrylamide. J Am Chem Soc. 2002;124:9394-5.
[161] Wu T, Gong P, Szleifer I, Vlček P, Šubr V, Genzer J. Behavior of surface-anchored poly (acrylic acid) brushes with grafting density gradients on solid substrates: 1. Experiment. Macromolecules. 2007;40:8756-64.
[162] Gong P, Wu T, Genzer J, Szleifer I. Behavior of surface-anchored poly (acrylic acid) brushes with grafting density gradients on solid substrates: 2. Theory. Macromolecules. 2007;40:8765-73.
[163] Polanowski P, Jeszka JK, Matyjaszewski K. Polymer brush relaxation during and after polymerization – Monte Carlo simulation study. Polymer. 2019;173:190-6.
[164] Kang C, Crockett R, Spencer ND. The influence of surface grafting on the growth rate of polymer chains. Polym Chem. 2016;7:302-9.
[165] Matyjaszewski K. Atom Transfer Radical Polymerization (ATRP): Current Status and Future Perspectives. Macromolecules. 2012;45:4015-39.
[166] Wang JS, Matyjaszewski K. Controlled living radical polymierzation - halogen atom-transfer radical polymerization promoted by a Cu(I)Cu(II) redox process. Macromolecules. 1995;28:7901-10.
[167] Matyjaszewski K, Xia J. Atom transfer radical polymerization. Chem Rev. 2001;101:2921-90.
[168] Matyjaszewski K, Tsarevsky NV. Macromolecular engineering by atom transfer radical polymerization. J Am Chem Soc. 2014;136:6513-33.
[169] Matyjaszewski K. Advanced Materials by Atom Transfer Radical Polymerization. Adv Mater. 2018;30:1706441.
[170] Ribelli TG, Lorandi F, Fantin M, Matyjaszewski K. Atom Transfer Radical Polymerization: Billion Times More Active Catalysts and New Initiation Systems. Macromol Rapid Commun. 2019;40:1800616.
[171] Konkolewicz D, Wang Y, Krys P, Zhong M, Isse AA, Gennaro A, et al. SARA ATRP or SET-LRP. End of controversy? Polym Chem. 2014;5:4396-417.
[172] Konkolewicz D, Wang Y, Zhong M, Krys P, Isse AA, Gennaro A, et al. Reversible-deactivation radical polymerization in the presence of metallic copper. A critical assessment of the SARA ATRP and SET-LRP mechanisms. Macromolecules. 2013;46:8749-72.
[173] Matyjaszewski K, Jakubowski W, Min K, Tang W, Huang J, Braunecker WA, et al. Diminishing catalyst concentration in atom transfer radical polymerization with reducing agents. Proc Nat Acad Sci. 2006;103:15309-14.
[174] Pan X, Fantin M, Yuan F, Matyjaszewski K. Externally controlled atom transfer radical polymerization. Chem Soc Rev. 2018.

[175] Magenau AJD, Strandwitz NC, Gennaro A, Matyjaszewski K. Electrochemically Mediated Atom Transfer Radical Polymerization. Science. 2011;332:81-4.
[176] Chmielarz P, Fantin M, Park S, Isse AA, Gennaro A, Magenau AJ, et al. Electrochemically mediated atom transfer radical polymerization (eATRP). Prog Polym Sci. 2017;69:47-78.
[177] Kwak Y, Matyjaszewski K. Photoirradiated Atom Transfer Radical Polymerization with an Alkyl Dithiocarbamate at Ambient Temperature. Macromolecules. 2010;43:5180-3.
[178] Pan X, Tasdelen MA, Laun J, Junkers T, Yagci Y, Matyjaszewski K. Photomediated controlled radical polymerization. Prog Polym Sci. 2016;62:73-125.
[179] Wang Z, Pan X, Li L, Fantin M, Yan J, Wang Z, et al. Enhancing Mechanically Induced ATRP by Promoting Interfacial Electron Transfer from Piezoelectric Nanoparticles to Cu Catalysts. Macromolecules. 2017;50:7940-8.
[180] Wang Z, Pan X, Yan J, Dadashi-Silab S, Xie G, Zhang J, et al. Temporal Control in Mechanically Controlled Atom Transfer Radical Polymerization Using Low ppm of Cu Catalyst. ACS Macro Lett. 2017;6:546-9.
[181] Wang Z, Wang Z, Pan X, Fu L, Lathwal S, Olszewski M, et al. Ultrasonication-Induced Aqueous Atom Transfer Radical Polymerization. ACS Macro Lett. 2018:275-80.
[182] Wang Z, Lorandi F, Fantin M, Wang Z, Yan J, Wang Z, et al. Atom Transfer Radical Polymerization Enabled by Sonochemically Labile Cu-carbonate Species. ACS Macro Lett. 2019:161-5.
[183] Matyjaszewski K, Wei M, Xia J, McDermott NE. Controlled/"Living" Radical Polymerization of Styrene and Methyl Methacrylate Catalyzed by Iron Complexes. Macromolecules. 1997;30:8161-4.
[184] Dadashi-Silab S, Pan X, Matyjaszewski K. Photoinduced iron-catalyzed atom transfer radical polymerization with ppm levels of iron catalyst under blue light irradiation. Macromolecules. 2017;50:7967-77.
[185] Pan X, Malhotra N, Dadashi‐Silab S, Matyjaszewski K. A Simplified Fe‐Based PhotoATRP Using Only Monomers and Solvent. Macromol Rapid Commun. 2017;38:1600651.
[186] Kato M, Kamigaito M, Sawamoto M, Higashimura T. Polymerization of Methyl Methacrylate with the Carbon Tetrachloride/Dichlorotris-(triphenylphosphine)ruthenium(II)/Methylaluminum Bis(2,6-di-tert-butylphenoxide) Initiating System: Possibility of Living Radical Polymerization. Macromolecules. 1995;28:1721-3.
[187] Ando T, Kato M, Kamigaito M, Sawamoto M. Living Radical Polymerization of Methyl Methacrylate with Ruthenium Complex: Formation of Polymers with Controlled Molecular Weights and Very Narrow Distributions. Macromolecules. 1996;29:1070-2.
[188] Fors BP, Hawker CJ. Control of a Living Radical Polymerization of Methacrylates by Light. Angew Chem Int Ed. 2012;51:8850-3.
[189] Treat NJ, Sprafke H, Kramer JW, Clark PG, Barton BE, Read de Alaniz J, et al. Metal-Free Atom Transfer Radical Polymerization. J Am Chem Soc. 2014;136:16096-101.
[190] Pan X, Lamson M, Yan J, Matyjaszewski K. Photoinduced Metal-Free Atom Transfer Radical Polymerization of Acrylonitrile. ACS Macro Lett. 2015;4:192-6.
[191] Pan X, Fang C, Fantin M, Malhotra N, So WY, Peteanu LA, et al. Mechanism of Photoinduced Metal-Free Atom Transfer Radical Polymerization: Experimental and Computational Studies. J Am Chem Soc. 2016;138:2411-25.
[192] Pan X, Lathwal S, Mack S, Yan J, Das SR, Matyjaszewski K. Automated Synthesis of Well-Defined Polymers and Biohybrids by Atom Transfer Radical Polymerization Using a DNA Synthesizer. Angew Chem Int Ed. 2017;56:2740-3.

[193] Chiefari J, Chong YK, Ercole F, Krstina J, Jeffery J, Le TPT, et al. Living Free-Radical Polymerization by Reversible Addition−Fragmentation Chain Transfer: The RAFT Process. Macromolecules. 1998;31:5559-62.
[194] Moad G, Rizzardo E, Thang SH. Living Radical Polymerization by the RAFT Process A Second Update. Aust J Chem. 2009;62:1402-72.
[195] Loiseau J, Doerr N, Suau J, Egraz J, Llauro M, Ladaviere C, et al. Synthesis and characterization of poly (acrylic acid) produced by RAFT polymerization. Application as a very efficient dispersant of CaCO3, kaolin, and TiO2. Macromolecules. 2003;36:3066-77.
[196] Moad G, Chong Y, Postma A, Rizzardo E, Thang SH. Advances in RAFT polymerization: the synthesis of polymers with defined end-groups. Polymer. 2005;46:8458-68.
[197] Taton D, Wilczewska AZ, Destarac M. Direct Synthesis of Double Hydrophilic Statistical Di‐ and Triblock Copolymers Comprised of Acrylamide and Acrylic Acid Units via the MADIX Process. Macromol Rapid Commun. 2001;22:1497-503.
[198] Stenzel MH, Cummins L, Roberts GE, Davis TP, Vana P, Barner‐Kowollik C. Xanthate mediated living polymerization of vinyl acetate: a systematic variation in MADIX/RAFT agent structure. Macromol Chem Phys. 2003;204:1160-8.
[199] Dommanget C, D'Agosto F, Monteil V. Polymerization of Ethylene through Reversible Addition–Fragmentation Chain Transfer (RAFT). Angew Chem Int Ed. 2014;53:6683-6.
[200] Xu J, Jung K, Atme A, Shanmugam S, Boyer C. A Robust and Versatile Photoinduced Living Polymerization of Conjugated and Unconjugated Monomers and Its Oxygen Tolerance. J Am Chem Soc. 2014;136:5508-19.
[201] Xu J, Jung K, Corrigan NA, Boyer C. Aqueous photoinduced living/controlled polymerization: tailoring for bioconjugation. Chemical Science. 2014;5:3568-75.
[202] Xu J, Jung K, Boyer C. Oxygen Tolerance Study of Photoinduced Electron Transfer–Reversible Addition–Fragmentation Chain Transfer (PET-RAFT) Polymerization Mediated by Ru(bpy)3Cl2. Macromolecules. 2014;47:4217-29.
[203] Xu J, Shanmugam S, Duong HT, Boyer C. Organo-photocatalysts for photoinduced electron transfer-reversible addition–fragmentation chain transfer (PET-RAFT) polymerization. Polym Chem. 2015;6:5615-24.
[204] Shanmugam S, Xu J, Boyer C. Utilizing the electron transfer mechanism of chlorophyll a under light for controlled radical polymerization. Chemical science. 2015;6:1341-9.
[205] McKenzie TG, Colombo E, Fu Q, Ashokkumar M, Qiao GG. Sono‐RAFT Polymerization in Aqueous Medium. Angew Chem Int Ed. 2017;56:12302-6.
[206] Wang Y, Fantin M, Park S, Gottlieb E, Fu L, Matyjaszewski K. Electrochemically Mediated Reversible Addition–Fragmentation Chain-Transfer Polymerization. Macromolecules. 2017;50:7872-9.
[207] Lv C, He C, Pan X. Oxygen‐Initiated and Regulated Controlled Radical Polymerization under Ambient Conditions. Angew Chem Int Ed. 2018;57:9430-3.
[208] Solomon DH, Rizzardo E, Cacioli P. Polymerization process and polymers produced thereby. In: USPTO, editor. USPTO. United States: Commonwealth Scientific and Industrial Research Organization; 1986.
[209] Moad G, Rizzardo E. Alkoxyamine-initiated living radical polymerization: factors affecting alkoxyamine homolysis rates. Macromolecules. 1995;28:8722-8.
[210] Guillaneuf Y, Versace D-L, Bertin D, Lalevée J, Gigmes D, Fouassier J-P. Importance of the Position of the Chromophore Group on the Dissociation Process of Light Sensitive Alkoxyamines. Macromol Rapid Commun. 2010;31:1909-13.

[211] Morris J, Telitel S, Fairfull-Smith KE, Bottle SE, Lalevée J, Clément J-L, et al. Novel polymer synthesis methodologies using combinations of thermally- and photochemically-induced nitroxide mediated polymerization. Polym Chem. 2015;6:754-63.
[212] Abreu CMR, Mendonça PV, Serra AC, Noble BB, Guliashvili T, Nicolas J, et al. Nitroxide-Mediated Polymerization of Vinyl Chloride at Low Temperature: Kinetic and Computational Studies. Macromolecules. 2016;49:490-8.
[213] Burguière C, Dourges M-A, Charleux B, Vairon J-P. Synthesis and Characterization of ω-unsaturated poly (styrene-b-n-butyl methacrylate) Block Copolymers using TEMPO-mediated Controlled Radical Polymerization. Macromolecules. 1999;32:3883-90.
[214] Guillaneuf Y, Gigmes D, Marque SRA, Astolfi P, Greci L, Tordo P, et al. First Effective Nitroxide-Mediated Polymerization of Methyl Methacrylate. Macromolecules. 2007;40:3108-14.
[215] Georges MK, Lukkarila JL, Szkurhan AR. TEMPO-mediated n-butyl acrylate polymerizations. Macromolecules. 2004;37:1297-303.
[216] Hui CM, Dang A, Chen B, Yan J, Konkolewicz D, He H, et al. Effect of Thermal Self-Initiation on the Synthesis, Composition, and Properties of Particle Brush Materials. Macromolecules. 2014;47:5501-8.
[217] Pan G, Sudol ED, Dimonie VL, El‐Aasser MS. Thermal self‐initiation of styrene in the presence of TEMPO radicals: Bulk and miniemulsion. J Polym Sci, Part A: Polym Chem. 2004;42:4921-32.
[218] Poli R. Relationship between One-Electron Transition-Metal Reactivity and Radical Polymerization Processes. Angew Chem Int Ed. 2006;45:5058-70.
[219] Wayland BB, Poszmik G, Mukerjee SL, Fryd M. Living Radical Polymerization of Acrylates by Organocobalt Porphyrin Complexes. J Am Chem Soc. 1994;116:7943-4.
[220] Oka M, Tatemoto M. Vinylidene Fluoride—Hexafluoropropylene Copolymer having Terminal Iodines. Contemporary Topics in Polymer Science: Springer; 1984. p. 763-77.
[221] Yamago S, Iida K, Yoshida J-i. Tailored synthesis of structurally defined polymers by organotellurium-mediated living radical polymerization (TERP): synthesis of poly (meth) acrylate derivatives and their di-and triblock copolymers. J Am Chem Soc. 2002;124:13666-7.
[222] Treat NJ, Fors BP, Kramer JW, Christianson M, Chiu C-Y, Alaniz JRd, et al. Controlled Radical Polymerization of Acrylates Regulated by Visible Light. ACS Macro Lett. 2014;3:580-4.
[223] Discekici EH, Pester CW, Treat NJ, Lawrence J, Mattson KM, Narupai B, et al. Simple Benchtop Approach to Polymer Brush Nanostructures Using Visible-Light-Mediated Metal-Free Atom Transfer Radical Polymerization. ACS Macro Lett. 2016;5:258-62.
[224] Yan J, Pan X, Schmitt M, Wang Z, Bockstaller MR, Matyjaszewski K. Enhancing Initiation Efficiency in Metal-Free Surface-Initiated Atom Transfer Radical Polymerization (SI-ATRP). ACS Macro Lett. 2016;5:661-5.
[225] Flory PJ. Molecular size distribution in three dimensional polymers. I. Gelation1. J Am Chem Soc. 1941;63:3083-90.
[226] Stockmayer WH. Theory of molecular size distribution and gel formation in branched polymers II. General cross linking. The Journal of Chemical Physics. 1944;12:125-31.
[227] Pietrasik J, Hui CM, Chaladaj W, Dong H, Choi J, Jurczak J, et al. Silica-Polymethacrylate Hybrid Particles Synthesized Using High-Pressure Atom Transfer Radical Polymerization. Macromol Rapid Commun. 2011;32:295-301.
[228] Bombalski L, Min K, Dong H, Tang C, Matyjaszewski K. Preparation of Well-Defined Hybrid Materials by ATRP in Miniemulsion. Macromolecules (Washington, DC, U S). 2007;40:7429-32.

[229] Gao X, Feng W, Zhu S, Sheardown H, Brash JL. Kinetic Modeling of Surface - Initiated Atom Transfer Radical Polymerization. Macromolecular Reaction Engineering. 2010;4:235-50.
[230] Zhou D, Gao X, Wang W-j, Zhu S. Termination of Surface Radicals and Kinetic Modeling of ATRP Grafting from Flat Surfaces by Addition of Deactivator. Macromolecules. 2012;45:1198-207.
[231] Li C, Benicewicz BC. Synthesis of well-defined polymer brushes grafted onto silica nanoparticles via surface reversible addition– fragmentation chain transfer polymerization. Macromolecules. 2005;38:5929-36.
[232] Zhao Y, Perrier S. Synthesis of Well-Defined Homopolymer and Diblock Copolymer Grafted onto Silica Particles by Z-Supported RAFT Polymerization. Macromolecules. 2006;39:8603-8.
[233] Ohno K, Ma Y, Huang Y, Mori C, Yahata Y, Tsujii Y, et al. Surface-Initiated Reversible Addition–Fragmentation Chain Transfer (RAFT) Polymerization from Fine Particles Functionalized with Trithiocarbonates. Macromolecules. 2011;44:8944-53.
[234] Khani MM, Abbas ZM, Benicewicz BC. Well - defined polyisoprene - grafted silica nanoparticles via the RAFT process. J Polym Sci, Part A: Polym Chem. 2017;55:1493-501.
[235] Niu J, Lunn DJ, Pusuluri A, Yoo JI, O'Malley MA, Mitragotri S, et al. Engineering live cell surfaces with functional polymers via cytocompatible controlled radical polymerization. Nat Chem. 2017;9:537.
[236] Bagheri A, Arandiyan H, Adnan NNM, Boyer C, Lim M. Controlled Direct Growth of Polymer Shell on Upconversion Nanoparticle Surface via Visible Light Regulated Polymerization. Macromolecules. 2017;50:7137-47.
[237] Rahane SB, Kilbey SM, Metters AT. Kinetics of surface-initiated photoiniferter-mediated photopolymerization. Macromolecules. 2005;38:8202-10.
[238] Wang L-P, Dong L-H, Hao J-C, Lv X-H, Li W-Z, Li Y-C, et al. Fabrication of block copolymer brushes on hollow sphere surface via reverse iodine transfer polymerization. J Colloid Interface Sci. 2011;361:400-6.
[239] Yamago S, Yahata Y, Nakanishi K, Konishi S, Kayahara E, Nomura A, et al. Synthesis of Concentrated Polymer Brushes via Surface-Initiated Organotellurium-Mediated Living Radical Polymerization. Macromolecules. 2013;46:6777-85.
[240] Parvole J, Laruelle G, Guimon C, Francois J, Billon L. Initiator-Grafted Silica Particles for Controlled Free Radical Polymerization: Influence of the Initiator Structure on the Grafting Density. Macromol Rapid Commun. 2003;24:1074-8.
[241] Ghannam L, Bacou M, Garay H, Shanahan MER, François J, Billon L. Elastomer monolayers adsorbed on mica surfaces by nitroxide-mediated polymerisation. Polymer. 2004;45:7035-45.
[242] Parvole J, Billon L, Montfort JP. Formation of polyacrylate brushes on silica surfaces. Polym Int. 2002;51:1111-6.
[243] Blas H, Save M, Boissière C, Sanchez C, Charleux B. Surface-Initiated Nitroxide-Mediated Polymerization from Ordered Mesoporous Silica. Macromolecules. 2011;44:2577-88.
[244] Szwarc M, Levy M, Milkovich R. Polymerization Initiated by Electron Transfer to Monomer. A New Method of Formation of Block Polymers. J Am Chem Soc. 1956;78:2656-7.
[245] Higashimura T, Mitsuhashi M, Sawamoto M. Synthesis of p-Methoxystyrene-Isobutyl Vinyl Ether Block Copolymers by Living Cationic Polymerization with Iodine. Macromolecules. 1979;12:178-82.

[246] Quirk RP, Mathers RT. Surface-initiated living anionic polymerization of isoprene using a 1,1-diphenylethylene derivative and functionalization with ethylene oxide. Polym Bull. 2001;45:471-7.
[247] Advincula R, Zhou Q, Park M, Wang S, Mays J, Sakellariou G, et al. Polymer Brushes by Living Anionic Surface Initiated Polymerization on Flat Silicon (SiOx) and Gold Surfaces: Homopolymers and Block Copolymers. Langmuir. 2002;18:8672-84.
[248] Zhao B, Brittain WJ. Synthesis of Polystyrene Brushes on Silicate Substrates via Carbocationic Polymerization from Self-Assembled Monolayers. Macromolecules. 2000;33:342-8.
[249] Carrot G, Rutot-Houzé D, Pottier A, Degée P, Hilborn J, Dubois P. Surface-Initiated Ring-Opening Polymerization: A Versatile Method for Nanoparticle Ordering. Macromolecules. 2002;35:8400-4.
[250] Choi IS, Langer R. Surface-Initiated Polymerization of l-Lactide: Coating of Solid Substrates with a Biodegradable Polymer. Macromolecules. 2001;34:5361-3.
[251] Schneider M, Fetsch C, Amin I, Jordan R, Luxenhofer R. Polypeptoid Brushes by Surface-Initiated Polymerization of N-Substituted Glycine N-Carboxyanhydrides. Langmuir. 2013;29:6983-8.
[252] Tsubokawa N, Funaki A, Hada Y, Sone Y. Grafting onto carbon black: Graft polymerization of β-propiolactone onto carbon black surface. Journal of Polymer Science: Polymer Letters Edition. 1982;20:27-31.
[253] Calderon N. Ring-Opening Polymerization of Cycloolefins AU - Calderon, Nissim. Journal of Macromolecular Science, Part C. 1972;7:105-59.
[254] Bielawski CW, Grubbs RH. Living ring-opening metathesis polymerization. Prog Polym Sci. 2007;32:1-29.
[255] Schrock RR. Living ring-opening metathesis polymerization catalyzed by well-characterized transition-metal alkylidene complexes. Acc Chem Res. 1990;23:158-65.
[256] Grubbs RH, Tumas W. Polymer synthesis and organotransition metal chemistry. Science. 1989;243:907-15.
[257] Ogawa KA, Goetz AE, Boydston AJ. Metal-free ring-opening metathesis polymerization. J Am Chem Soc. 2015;137:1400-3.
[258] Mastan E, Xi L, Zhu S. Factors Affecting Grafting Density in Surface - Initiated ATRP: A Simulation Study. Macromol Theory Simul. 2016;25:220-8.
[259] Chevigny C, Dalmas F, Di Cola E, Gigmes D, Bertin D, Boué F, et al. Polymer-Grafted-Nanoparticles Nanocomposites: Dispersion, Grafted Chain Conformation, and Rheological Behavior. Macromolecules. 2011;44:122-33.
[260] Hayashi S, Naitoh A, Machida S, Okazaki M, Maruyama K, Tsubokawa N. Grafting of polymers onto a carbon black surface by the trapping of polymer radicals. Appl Organomet Chem. 1998;12:743-8.
[261] Tsubokawa N, Kogure A. Surface grafting of polymers onto inorganic ultrafine particles: Reaction of functional polymers with acid anhydride groups introduced onto inorganic ultrafine particles. J Polym Sci, Part A: Polym Chem. 1991;29:697-702.
[262] Hosoya M, Yanadori K, Sone Y. Grafting Onto Carbon Black: Reaction of Functional Groups on Carbon Black with ACYL Chloride-Capped Polymers AU - Tsubokawa, Norio. Journal of Macromolecular Science: Part A - Chemistry. 1990;27:445-57.

[263] Lowe AB, Sumerlin BS, Donovan MS, McCormick CL. Facile preparation of transition metal nanoparticles stabilized by well-defined (co) polymers synthesized via aqueous reversible addition-fragmentation chain transfer polymerization. J Am Chem Soc. 2002;124:11562-3.
[264] Rossner C, Vana P. Planet–Satellite Nanostructures Made To Order by RAFT Star Polymers. Angew Chem Int Ed. 2014;53:12639-42.
[265] Tao P, Viswanath A, Schadler LS, Benicewicz BC, Siegel RW. Preparation and Optical Properties of Indium Tin Oxide/Epoxy Nanocomposites with Polyglycidyl Methacrylate Grafted Nanoparticles. ACS Appl Mater Interfaces. 2011;3:3638-45.
[266] Gao H, Matyjaszewski K. Synthesis of Molecular Brushes by "Grafting onto" Method: Combination of ATRP and Click Reactions. J Am Chem Soc. 2007;129:6633-9.
[267] Leophairatana P, Samanta S, De Silva CC, Koberstein JT. Preventing Alkyne–Alkyne (i.e., Glaser) Coupling Associated with the ATRP Synthesis of Alkyne-Functional Polymers/Macromonomers and for Alkynes under Click (i.e., CuAAC) Reaction Conditions. J Am Chem Soc. 2017;139:3756-66.
[268] Lutz J-F, Börner HG, Weichenhan K. Combining ATRP and "Click" Chemistry: a Promising Platform toward Functional Biocompatible Polymers and Polymer Bioconjugates. Macromolecules. 2006;39:6376-83.
[269] Golas PL, Matyjaszewski K. Click chemistry and ATRP: a beneficial union for the preparation of functional materials. QSAR Comb Sci. 2007;26:1116-34.
[270] Golas PL, Matyjaszewski K. Marrying click chemistry with polymerization: expanding the scope of polymeric materials. Chem Soc Rev. 2010;39:1338-54.
[271] Golas PL, Tsarevsky NV, Matyjaszewski K. Structure–Reactivity Correlation in "Click" Chemistry: Substituent Effect on Azide Reactivity. Macromol Rapid Commun. 2008;29:1167-71.
[272] Yoshimoto K, Hirase T, Madsen J, Armes SP, Nagasaki Y. Non-Fouling Character of Poly[2-(methacryloyloxy)ethyl Phosphorylcholine]-Modified Gold Surfaces Fabricated by the 'Grafting to' Method: Comparison of its Protein Resistance with Poly(ethylene glycol)-Modified Gold Surfaces. Macromol Rapid Commun. 2009;30:2136-40.
[273] Yavuz MS, Cheng Y, Chen J, Cobley CM, Zhang Q, Rycenga M, et al. Gold nanocages covered by smart polymers for controlled release with near-infrared light. Nat Mater. 2009;8:935.
[274] Huang J, Koepsel RR, Murata H, Wu W, Lee SB, Kowalewski T, et al. Nonleaching Antibacterial Glass Surfaces via "Grafting Onto": The Effect of the Number of Quaternary Ammonium Groups on Biocidal Activity. Langmuir. 2008;24:6785-95.
[275] Bulychev NA, Arutunov IA, Zubov VP, Verdonck B, Zhang T, Goethals EJ, et al. Block Copolymers of Vinyl Ethers as Thermo-Responsive Colloidal Stabilizers of Organic Pigments in Aqueous Media. Macromol Chem Phys. 2004;205:2457-63.
[276] Wang X-S, Dykstra TE, Salvador MR, Manners I, Scholes GD, Winnik MA. Surface Passivation of Luminescent Colloidal Quantum Dots with Poly(Dimethylaminoethyl methacrylate) through a Ligand Exchange Process. J Am Chem Soc. 2004;126:7784-5.
[277] Dubois F, Mahler B, Dubertret B, Doris E, Mioskowski C. A Versatile Strategy for Quantum Dot Ligand Exchange. J Am Chem Soc. 2007;129:482-3.
[278] Sardar R, Park J-W, Shumaker-Parry JS. Polymer-Induced Synthesis of Stable Gold and Silver Nanoparticles and Subsequent Ligand Exchange in Water. Langmuir. 2007;23:11883-9.

[279] Ehlert S, Taheri SM, Pirner D, Drechsler M, Schmidt H-W, Förster S. Polymer Ligand Exchange to Control Stabilization and Compatibilization of Nanocrystals. ACS Nano. 2014;8:6114-22.
[280] Wang Z, Lu Z, Mahoney C, Yan J, Ferebee R, Luo D, et al. Transparent and High Refractive Index Thermoplastic Polymer Glasses Using Evaporative Ligand Exchange of Hybrid Particle Fillers. ACS Appl Mater Interfaces. 2017;9:7515-22.
[281] Wang Z, Liu S, Zhang J, Yan J, Zhao Y, Mahoney C, et al. Photocatalytic Active Mesoporous Carbon/ZnO Hybrid Materials from Block Copolymer Tethered ZnO Nanocrystals. Langmuir. 2017.
[282] Zhao Y, Wang Z, Yuan R, Lin Y, Yan J, Zhang J, et al. ZnO/carbon hybrids derived from polymer nanocomposite precursor materials for pseudocapacitor electrodes with high cycling stability. Polymer. 2018;137:370-7.
[283] Gao H, Matyjaszewski K. Synthesis of Miktoarm Star Polymers via ATRP Using the "In–Out" Method: Determination of Initiation Efficiency of Star Macroinitiators. Macromolecules. 2006;39:7216-23.
[284] Espiard P, Guyot A. Poly(ethyl acrylate) latexes encapsulating nanoparticles of silica: 2. Grafting process onto silica. Polymer. 1995;36:4391-5.
[285] Pyun J, Matyjaszewski K. The Synthesis of Hybrid Polymers Using Atom Transfer Radical Polymerization: Homopolymers and Block Copolymers from Polyhedral Oligomeric Silsesquioxane Monomers. Macromolecules. 2000;33:217-20.
[286] Pyun J, Matyjaszewski K, Wu J, Kim G-M, Chun SB, Mather PT. ABA triblock copolymers containing polyhedral oligomeric silsesquioxane pendant groups: synthesis and unique properties. Polymer. 2003;44:2739-50.
[287] Franczyk A, He H, Burdynska J, Hui CM, Matyjaszewski K, Marciniec B. Synthesis of High Molecular Weight Polymethacrylates with Polyhedral Oligomeric Silsesquioxane Moieties by Atom Transfer Radical Polymerization. ACS Macro Lett. 2014;3:799-802.
[288] Alexandris S, Franczyk A, Papamokos G, Marciniec B, Matyjaszewski K, Koynov K, et al. Polymethacrylates with Polyhedral Oligomeric Silsesquioxane (POSS) Moieties: Influence of Spacer Length on Packing, Thermodynamics, and Dynamics. Macromolecules. 2015;48:3376-85.
[289] Alexandris S, Franczyk A, Papamokos G, Marciniec B, Graf R, Matyjaszewski K, et al. Dynamic Heterogeneity in Random Copolymers of Polymethacrylates Bearing Different Polyhedral Oligomeric Silsesquioxane Moieties (POSS). Macromolecules. 2017;50:4043-53.
[290] Park J, Joo J, Kwon SG, Jang Y, Hyeon T. Synthesis of Monodisperse Spherical Nanocrystals. Angew Chem Int Ed. 2007;46:4630-60.
[291] Chan YNC, Craig GSW, Schrock RR, Cohen RE. Synthesis of palladium and platinum nanoclusters within microphase-separated diblock copolymers. Chem Mater. 1992;4:885-94.
[292] Chan YNC, Schrock RR, Cohen RE. Synthesis of single silver nanoclusters within spherical microdomains in block copolymer films. J Am Chem Soc. 1992;114:7295-6.
[293] Möller M, Spatz JP, Roescher A. Gold nanoparticles in micellar poly (styrene) - b - poly (ethylene oxide) films—size and interparticle distance control in monoparticulate films. Adv Mater. 1996;8:337-40.
[294] Moffitt M, McMahon L, Pessel V, Eisenberg A. Size Control of Nanoparticles in Semiconductor-Polymer Composites. 2. Control via Sizes of Spherical Ionic Microdomains in Styrene-Based Diblock Ionomers. Chem Mater. 1995;7:1185-92.

[295] Thomas JR. Preparation and Magnetic Properties of Colloidal Cobalt Particles. J Appl Phys. 1966;37:2914-5.
[296] Hess PH, Parker Jr. PH. Polymers for stabilization of colloidal cobalt particles. J Appl Polym Sci. 1966;10:1915-27.
[297] Burkett SL, Sims SD, Mann S. Synthesis of hybrid inorganic–organic mesoporous silica by co-condensation of siloxane and organosiloxane precursors. Chem Commun. 1996:1367-8.
[298] Spatz JP, Mößmer S, Möller M. Mineralization of Gold Nanoparticles in a Block Copolymer Microemulsion. Chem Eur J. 1996;2:1552-5.
[299] Klingelhöfer S, Heitz W, Greiner A, Oestreich S, Förster S, Antonietti M. Preparation of Palladium Colloids in Block Copolymer Micelles and Their Use for the Catalysis of the Heck Reaction. J Am Chem Soc. 1997;119:10116-20.
[300] Platonova OA, Bronstein LM, Solodovnikov SP, Yanovskaya IM, Obolonkova ES, Valetsky PM, et al. Cobalt nanoparticles in block copolymer micelles: Preparation and properties. Colloid Polym Sci. 1997;275:426-31.
[301] Seregina MV, Bronstein LM, Platonova OA, Chernyshov DM, Valetsky PM, Hartmann J, et al. Preparation of Noble-Metal Colloids in Block Copolymer Micelles and Their Catalytic Properties in Hydrogenation. Chem Mater. 1997;9:923-31.
[302] Zhao H, Douglas EP, Harrison BS, Schanze KS. Preparation of CdS Nanoparticles in Salt-Induced Block Copolymer Micelles. Langmuir. 2001;17:8428-33.
[303] Jaramillo TF, Baeck S-H, Cuenya BR, McFarland EW. Catalytic Activity of Supported Au Nanoparticles Deposited from Block Copolymer Micelles. J Am Chem Soc. 2003;125:7148-9.
[304] Möller M, Spatz JP, Roescher A, Mößmer S, Selvan ST, Klok H-A. Mineralization of gold in block copolymer micelles. Macromolecular Symposia. 1997;117:207-18.
[305] Warren NJ, Armes SP. Polymerization-induced self-assembly of block copolymer nano-objects via RAFT aqueous dispersion polymerization. J Am Chem Soc. 2014;136:10174-85.
[306] Charleux B, Delaittre G, Rieger J, D'Agosto F. Polymerization-induced self-assembly: from soluble macromolecules to block copolymer nano-objects in one step. Macromolecules. 2012;45:6753-65.
[307] Wang G, Schmitt M, Wang Z, Lee B, Pan X, Fu L, et al. Polymerization-Induced Self-Assembly (PISA) Using ICAR ATRP at Low Catalyst Concentration. Macromolecules. 2016;49:8605-15.
[308] Wang G, Wang Z, Lee B, Yuan R, Lu Z, Yan J, et al. Polymerization-induced self-assembly of acrylonitrile via ICAR ATRP. Polymer. 2017;129:57-67.
[309] Zhang Y, Wang Z, Matyjaszewski K, Pietrasik J. Evolution of Morphology of POEGMA-b-PBzMA Nano-Objects Formed by PISA. Macromol Rapid Commun. 2019;40:1800331.
[310] Zhang Y, Filipczak P, He G, Nowaczyk G, Witczak L, Raj W, et al. Synthesis and characterization of Ag NPs templated via polymerization induced self-assembly. Polymer. 2017;129:144-50.
[311] Zhang Y, Wang Z, Matyjaszewski K, Pietrasik J. Versatile PISA templates for tailored synthesis of nanoparticles. Eur Polym J. 2019;110:49-55.
[312] Stenzel MH, Davis TP. Star polymer synthesis using trithiocarbonate functional β - cyclodextrin cores (reversible addition − fragmentation chain - transfer polymerization). J Polym Sci, Part A: Polym Chem. 2002;40:4498-512.
[313] Ohno K, Wong B, Haddleton DM. Synthesis of well - defined cyclodextrin - core star polymers. J Polym Sci, Part A: Polym Chem. 2001;39:2206-14.

[314] Stenzel‐Rosenbaum M, Davis TP, Chen V, Fane AG. Star‐polymer synthesis via radical reversible addition–fragmentation chain‐transfer polymerization. J Polym Sci, Part A: Polym Chem. 2001;39:2777-83.
[315] Costa RO, Vasconcelos WL, Tamaki R, Laine RM. Organic/inorganic nanocomposite star polymers via atom transfer radical polymerization of methyl methacrylate using octafunctional silsesquioxane cores. Macromolecules. 2001;34:5398-407.
[316] Klok HA, Becker S, Schuch F, Pakula T, Müllen K. Fluorescent star‐shaped polystyrenes: "core‐first" synthesis from perylene‐based ATRP initiators and dynamic mechanical solid‐state properties. Macromol Chem Phys. 2002;203:1106-13.
[317] Burdyńska J, Li Y, Aggarwal AV, Höger S, Sheiko SS, Matyjaszewski K. Synthesis and Arm Dissociation in Molecular Stars with a Spoked Wheel Core and Bottlebrush Arms. J Am Chem Soc. 2014;136:12762-70.
[318] Gao H, Matyjaszewski K. Synthesis of Star Polymers by A New "Core-First" Method: Sequential Polymerization of Cross-Linker and Monomer. Macromolecules. 2008;41:1118-25.
[319] Metri V, Louhichi A, Yan J, Baeza GP, Matyjaszewski K, Vlassopoulos D, et al. Physical Networks from Multifunctional Telechelic Star Polymers: A Rheological Study by Experiments and Simulations. Macromolecules. 2018;51:2872-86.
[320] Xia J, Zhang X, Matyjaszewski K. Synthesis of star-shaped polystyrene by atom transfer radical polymerization using an "arm first" approach. Macromolecules. 1999;32:4482-4.
[321] Gao H, Matyjaszewski K. Arm-First Method As a Simple and General Method for Synthesis of Miktoarm Star Copolymers. J Am Chem Soc. 2007;129:11828-34.
[322] Taniguchi T, Inada T, Kashiwakura T, Murakami F, Kohri M, Nakahira T. Preparation of polymer core–shell particles supporting gold nanoparticles. Colloids and Surfaces A: Physicochemical and Engineering Aspects. 2011;377:63-9.
[323] Taniguchi T, Kashiwakura T, Inada T, Kunisada Y, Kasuya M, Kohri M, et al. Preparation of organic/inorganic composites by deposition of silica onto shell layers of polystyrene (core)/poly[2-(N,N-dimethylamino)ethyl methacrylate] (shell) particles. J Colloid Interface Sci. 2010;347:62-8.
[324] Taniguchi T, Murakami F, Kasuya M, Kojima T, Kohri M, Saito K, et al. Preparation of titania hollow particles with independently controlled void size and shell thickness by catalytic templating core–shell polymer particles. Colloid Polym Sci. 2012;291:215-22.
[325] Feng C, Pang X, He Y, Chen Y, Zhang G, Lin Z. A versatile strategy for uniform hybrid nanoparticles and nanocapsules. Polym Chem. 2015;6:5190-7.
[326] Wintermantel M, Gerle M, Fischer K, Schmidt M, Wataoka I, Urakawa H, et al. Molecular bottlebrushes. Macromolecules. 1996;29:978-83.
[327] Dziezok P, Fischer K, Schmidt M, Sheiko SS, Möller M. Cylindrical molecular brushes. Angewandte Chemie International Edition in English. 1997;36:2812-5.
[328] Xie G, Martinez MR, Olszewski M, Sheiko SS, Matyjaszewski K. Molecular Bottlebrushes as Novel Materials. Biomacromolecules. 2019;20:27-54.
[329] Braun E, Eichen Y, Sivan U, Ben-Yoseph G. DNA-templated assembly and electrode attachment of a conducting silver wire. Nature. 1998;391:775.
[330] Fullam S, Cottell D, Rensmo H, Fitzmaurice D. Carbon Nanotube Templated Self-Assembly and Thermal Processing of Gold Nanowires. Adv Mater. 2000;12:1430-2.
[331] Yuan J, Drechsler M, Xu Y, Zhang M, Müller AHE. Cadmium selenide nanowires within core–shell cylindrical polymer brushes: Synthesis, characterization and the double-loading process. Polymer. 2008;49:1547-54.

[332] Yuan J, Lu Y, Schacher F, Lunkenbein T, Weiss S, Schmalz H, et al. Template-Directed Synthesis of Hybrid Titania Nanowires within Core−Shell Bishydrophilic Cylindrical Polymer Brushes. Chem Mater. 2009;21:4146-54.
[333] Yuan J, Schacher F, Drechsler M, Hanisch A, Lu Y, Ballauff M, et al. Stimuli-Responsive Organosilica Hybrid Nanowires Decorated with Metal Nanoparticles. Chem Mater. 2010;22:2626-34.
[334] Müllner M, Lunkenbein T, Breu J, Caruso F, Müller AHE. Template-Directed Synthesis of Silica Nanowires and Nanotubes from Cylindrical Core–Shell Polymer Brushes. Chem Mater. 2012;24:1802-10.
[335] Müllner M, Lunkenbein T, Schieder M, Gröschel AH, Miyajima N, Förtsch M, et al. Template-Directed Mild Synthesis of Anatase Hybrid Nanotubes within Cylindrical Core–Shell–Corona Polymer Brushes. Macromolecules. 2012;45:6981-8.
[336] Zheng Z, Daniel A, Yu W, Weber B, Ling J, Müller AHE. Rare-Earth Metal Cations Incorporated Silica Hybrid Nanoparticles Templated by Cylindrical Polymer Brushes. Chem Mater. 2013;25:4585-94.
[337] Xie G, Ding H, Daniel WFM, Wang Z, Pietrasik J, Sheiko SS, et al. Preparation of titania nanoparticles with tunable anisotropy and branched structures from core–shell molecular bottlebrushes. Polymer. 2016;98:481-6.
[338] Wang Z, Liu T, Lin KC, Li S, Yan J, Olszewski M, et al. Synthesis of Ultra-high Molecular Weight SiO2-g-PMMA Particle Brushes. Journal of Inorganic and Organometallic Polymers and Materials. 2019.
[339] Ojha S, Dang A, Hui CM, Mahoney C, Matyjaszewski K, Bockstaller MR. Strategies for the synthesis of thermoplastic polymer nanocomposite materials with high inorganic filling fraction. Langmuir. 2013;29:8989-96.
[340] Dan N, Tirrell M. Effect of bimodal molecular weight distribution on the polymer brush. Macromolecules. 1993;26:6467-73.
[341] Saphiannikova MG, Pryamitsyn VA, Birshtein TM. Self-Consistent Brownian Dynamics Simulation of Bimodal Polymer Brushes under Shear. Macromolecules. 2000;33:2740-7.
[342] Nair N, Wentzel N, Jayaraman A. Effect of bidispersity in grafted chain length on grafted chain conformations and potential of mean force between polymer grafted nanoparticles in a homopolymer matrix. J Chem Phys. 2011;134:194906.
[343] Li Y, Tao P, Viswanath A, Benicewicz BC, Schadler LS. Bimodal Surface Ligand Engineering: The Key to Tunable Nanocomposites. Langmuir. 2013;29:1211-20.
[344] Natarajan B, Neely T, Rungta A, Benicewicz BC, Schadler LS. Thermomechanical Properties of Bimodal Brush Modified Nanoparticle Composites. Macromolecules. 2013;46:4909-18.
[345] Li Y, Wang L, Natarajan B, Tao P, Benicewicz B, Ullal C, et al. Bimodal “matrix-free” polymer nanocomposites. RSC Adv. 2015;5:14788-95.
[346] Qiao Y, Yin X, Wang L, Islam MS, Benicewicz BC, Ploehn HJ, et al. Bimodal Polymer Brush Core-Shell Barium Titanate Nanoparticles: A Strategy for High-Permittivity Polymer Nanocomposites. Macromolecules. 2015;48:8998-9006.
[347] Burdyńska J, Daniel W, Li Y, Robertson B, Sheiko SS, Matyjaszewski K. Molecular Bottlebrushes with Bimodal Length Distribution of Side Chains. Macromolecules. 2015;48:4813–22.

[348] Whitfield R, Parkatzidis K, Rolland M, Truong NP, Anastasaki A. Tuning Dispersity by Photoinduced Atom Transfer Radical Polymerisation: Monomodal Distributions with ppm Copper Concentration. Angew Chem. 2019;131:13457-62.
[349] Wang Z, Yan J, Liu T, Wei Q, Li S, Olszewski M, et al. Control of Dispersity and Grafting Density of Particle Brushes by Variation of ATRP Catalyst Concentration. ACS Macro Lett. 2019;8:859-64.
[350] Wang Z, Fantin M, Sobieski J, Wang Z, Yan J, Lee J, et al. Pushing the Limit: Synthesis of SiO2-g-PMMA/PS Particle Brushes via ATRP with Very Low Concentration of Initiating Sites. Macromolecules. 2019.
[351] Zhao B, He T. Synthesis of Well-Defined Mixed Poly(methyl methacrylate)/Polystyrene Brushes from an Asymmetric Difunctional Initiator-Terminated Self-Assembled Monolayer. Macromolecules. 2003;36:8599-602.
[352] Goel V, Pietrasik J, Poling-Skutvik R, Jackson A, Matyjaszewski K, Krishnamoorti R. Structure of block copolymer grafted silica nanoparticles. Polymer. 2018;159:138-45.
[353] Mansky P, Liu Y, Huang E, Russell TP, Hawker C. Controlling Polymer-Surface Interactions with Random Copolymer Brushes. Science. 1997;275:1458-60.
[354] Matyjaszewski K, Ziegler MJ, Arehart SV, Greszta D, Pakula T. Gradient copolymers by atom transfer radical copolymerization. J Phys Org Chem. 2000;13:775-86.
[355] Gu B, Sen A. Synthesis of Aluminum Oxide/Gradient Copolymer Composites by Atom Transfer Radical Polymerization. Macromolecules. 2002;35:8913-6.
[356] Xu C, Wu T, Mei Y, Drain CM, Batteas JD, Beers KL. Synthesis and Characterization of Tapered Copolymer Brushes via Surface-Initiated Atom Transfer Radical Copolymerization. Langmuir. 2005;21:11136-40.
[357] Tomlinson MR, Genzer J. Formation of surface-grafted copolymer brushes with continuous composition gradients. Chem Commun. 2003:1350-1.
[358] Tomlinson MR, Genzer J. Formation of Grafted Macromolecular Assemblies with a Gradual Variation of Molecular Weight on Solid Substrates. Macromolecules. 2003;36:3449-51.
[359] Ionov L, Sidorenko A, Stamm M, Minko S, Zdyrko B, Klep V, et al. Gradient Mixed Brushes: "Grafting To" Approach. Macromolecules. 2004;37:7421-3.
[360] Dehghani ES, Du Y, Zhang T, Ramakrishna SN, Spencer ND, Jordan R, et al. Fabrication and Interfacial Properties of Polymer Brush Gradients by Surface-Initiated Cu(0)-Mediated Controlled Radical Polymerization. Macromolecules. 2017;50:2436-46.
[361] Fantin M, Ramakrishna SN, Yan J, Yan W, Divandari M, Spencer ND, et al. The Role of Cu0 in Surface-Initiated Atom Transfer Radical Polymerization: Tuning Catalyst Dissolution for Tailoring Polymer Interfaces. Macromolecules. 2018;51:6825-35.
[362] Chen T, Zhang J, Chang DP, Garcia A, Zauscher S. Fabrication of Micropatterned Stimulus-Responsive Polymer-Brush 'Anemone'. Adv Mater. 2009;21:1825-9.
[363] Rotzoll R, Vana P. Synthesis of poly (methyl acrylate) loops grafted onto silica nanoparticles via reversible addition - fragmentation chain transfer polymerization. J Polym Sci, Part A: Polym Chem. 2008;46:7656-66.
[364] Huang Z, Ji H, Mays JW, Dadmun MD. Understanding the Grafting of Telechelic Polymers on a Solid Substrate to Form Loops. Macromolecules. 2008;41:1009-18.
[365] Morgese G, Shirmardi Shaghasemi B, Causin V, Zenobi-Wong M, Ramakrishna SN, Reimhult E, et al. Next-Generation Polymer Shells for Inorganic Nanoparticles are Highly Compact, Ultra-Dense, and Long-Lasting Cyclic Brushes. Angew Chem. 2017;129:4578-82.

[366] Divandari M, Morgese G, Trachsel L, Romio M, Dehghani ES, Rosenboom J-G, et al. Topology Effects on the Structural and Physicochemical Properties of Polymer Brushes. Macromolecules. 2017;50:7760-9.
[367] Yan W, Divandari M, Rosenboom J-G, Ramakrishna SN, Trachsel L, Spencer ND, et al. Design and characterization of ultrastable, biopassive and lubricious cyclic poly(2-alkyl-2-oxazoline) brushes. Polym Chem. 2018;9:2580-9.
[368] Benetti EM, Divandari M, Ramakrishna SN, Morgese G, Yan W, Trachsel L. Loops and Cycles at Surfaces: The Unique Properties of Topological Polymer Brushes. Chem Eur J. 2017;23:12433-42.
[369] Tsubokawa N, Ichioka H, Satoh T, Hayashi S, Fujiki K. Grafting of 'dendrimer-like' highly branched polymer onto ultrafine silica surface. React Funct Polym. 1998;37:75-82.
[370] Bruening ML, Zhou Y, Aguilar G, Agee R, Bergbreiter DE, Crooks RM. Synthesis and Characterization of Surface-Grafted, Hyperbranched Polymer Films Containing Fluorescent, Hydrophobic, Ion-Binding, Biocompatible, and Electroactive Groups. Langmuir. 1997;13:770-8.
[371] Xu Y, Gao C, Kong H, Yan D, Jin YZ, Watts PCP. Growing Multihydroxyl Hyperbranched Polymers on the Surfaces of Carbon Nanotubes by in Situ Ring-Opening Polymerization. Macromolecules. 2004;37:8846-53.
[372] Kizhakkedathu JN, Janzen J, Le Y, Kainthan RK, Brooks DE. Poly(oligo(ethylene glycol)acrylamide) Brushes by Surface Initiated Polymerization: Effect of Macromonomer Chain Length on Brush Growth and Protein Adsorption from Blood Plasma. Langmuir. 2009;25:3794-801.
[373] Morgese G, Ramakrishna SN, Simic R, Zenobi-Wong M, Benetti EM. Hairy and Slippery Polyoxazoline-Based Copolymers on Model and Cartilage Surfaces. Biomacromolecules. 2018;19:680-90.
[374] Huang W, Baker GL, Bruening ML. Controlled Synthesis of Cross-Linked Ultrathin Polymer Films by Using Surface-Initiated Atom Transfer Radical Polymerization. Angew Chem. 2001;113:1558-60.
[375] Feng W, Li L, Ueda E, Li J, Heißler S, Welle A, et al. Surface Patterning via Thiol-Yne Click Chemistry: An Extremely Fast and Versatile Approach to Superhydrophilic-Superhydrophobic Micropatterns. Advanced Materials Interfaces. 2014;1:1400269.
[376] Chang Y, Shih Y-J, Ko C-Y, Jhong J-F, Liu Y-L, Wei T-C. Hemocompatibility of Poly(vinylidene fluoride) Membrane Grafted with Network-Like and Brush-Like Antifouling Layer Controlled via Plasma-Induced Surface PEGylation. Langmuir. 2011;27:5445-55.
[377] Li A, Ramakrishna SN, Nalam PC, Benetti EM, Spencer ND. Stratified Polymer Grafts: Synthesis and Characterization of Layered 'Brush' and 'Gel' Structures. Advanced Materials Interfaces. 2014;1:1300007.
[378] Lee BS, Lee JK, Kim W-J, Jung YH, Sim SJ, Lee J, et al. Surface-Initiated, Atom Transfer Radical Polymerization of Oligo(ethylene glycol) Methyl Ether Methacrylate and Subsequent Click Chemistry for Bioconjugation. Biomacromolecules. 2007;8:744-9.
[379] Singha NK, Gibson MI, Koiry BP, Danial M, Klok H-A. Side-Chain Peptide-Synthetic Polymer Conjugates via Tandem "Ester-Amide/Thiol–Ene" Post-Polymerization Modification of Poly(pentafluorophenyl methacrylate) Obtained Using ATRP. Biomacromolecules. 2011;12:2908-13.
[380] Kessler D, Roth PJ, Theato P. Reactive Surface Coatings Based on Polysilsesquioxanes: Controlled Functionalization for Specific Protein Immobilization. Langmuir. 2009;25:10068-76.

[381] Hong C-Y, You Y-Z, Pan C-Y. Synthesis of Water-Soluble Multiwalled Carbon Nanotubes with Grafted Temperature-Responsive Shells by Surface RAFT Polymerization. Chem Mater. 2005;17:2247-54.
[382] Li Y, Benicewicz BC. Functionalization of Silica Nanoparticles via the Combination of Surface-Initiated RAFT Polymerization and Click Reactions. Macromolecules. 2008;41:7986-92.
[383] Bach LG, Rafiqul Islam M, Vo T-S, Kim S-K, Lim KT. Poly(allyl methacrylate) functionalized hydroxyapatite nanocrystals via the combination of surface-initiated RAFT polymerization and thiol–ene protocol: A potential anticancer drug nanocarrier. J Colloid Interface Sci. 2013;394:132-40.
[384] Boyer C, Granville A, Davis TP, Bulmus V. Modification of RAFT-polymers via thiol-ene reactions: A general route to functional polymers and new architectures. J Polym Sci, Part A: Polym Chem. 2009;47:3773-94.
[385] Gauthier MA, Gibson MI, Klok H-A. Synthesis of Functional Polymers by Post-Polymerization Modification. Angew Chem Int Ed. 2009;48:48-58.
[386] Sides SW, Kim BJ, Kramer EJ, Fredrickson GH. Hybrid particle-field simulations of polymer nanocomposites. Phys Rev Lett. 2006;96:250601.
[387] Ohno K, Morinaga T, Takeno S, Tsujii Y, Fukuda T. Suspensions of Silica Particles Grafted with Concentrated Polymer Brush: Effects of Graft Chain Length on Brush Layer Thickness and Colloidal Crystallization. Macromolecules. 2007;40:9143-50.
[388] Ohno K, Morinaga T, Takeno S, Tsujii Y, Fukuda T. Suspensions of Silica Particles Grafted with Concentrated Polymer Brush: A New Family of Colloidal Crystals. Macromolecules. 2006;39:1245-9.
[389] Dukes D, Li Y, Lewis S, Benicewicz B, Schadler L, Kumar SK. Conformational Transitions of Spherical Polymer Brushes: Synthesis, Characterization, and Theory. Macromolecules. 2010;43:1564-70.
[390] Daoud M, Cotton J. Star shaped polymers: a model for the conformation and its concentration dependence. J Phys. 1982;43:531-8.
[391] Choi J, Hui CM, Pietrasik J, Dong H, Matyjaszewski K, Bockstaller MR. Toughening fragile matter: mechanical properties of particle solids assembled from polymer-grafted hybrid particles synthesized by ATRP. Soft Matter. 2012;8:4072-82.
[392] Milner ST, Witten T, Cates M. Theory of the grafted polymer brush. Macromolecules. 1988;21:2610-9.
[393] Wijmans CM, Zhulina EB. Polymer brushes at curved surfaces. Macromolecules. 1993;26:7214-24.
[394] Hore MJ, Ford J, Ohno K, Composto RJ, Hammouda B. Direct measurements of polymer brush conformation using small-angle neutron scattering (SANS) from highly grafted iron oxide nanoparticles in homopolymer melts. Macromolecules. 2013;46:9341-8.
[395] Jiao Y, Tibbits A, Gillman A, Hsiao M-S, Buskohl P, Drummy LF, et al. Deformation Behavior of Polystyrene-Grafted Nanoparticle Assemblies with Low Grafting Density. Macromolecules. 2018;51:7257-65.
[396] Dodd PM, Jayaraman A. Monte carlo simulations of polydisperse polymers grafted on spherical surfaces. J Polym Sci, Part B: Polym Phys. 2012;50:694-705.
[397] Hakem IF, Leech AM, Johnson JD, Donahue SJ, Walker JP, Bockstaller MR. Understanding ligand distributions in modified particle and particlelike systems. J Am Chem Soc. 2010;132:16593-8.

[398] Bachhar N, Kumaraswamy G, Kumar SK. Core-Size Dispersity Dominates the Self-Assembly of Polymer-Grafted Nanoparticles in Solution. Macromolecules. 2019.
[399] Shan J, Zhao Y, Granqvist N, Tenhu H. Thermoresponsive properties of N-isopropylacrylamide oligomer brushes grafted to gold nanoparticles: effects of molar mass and gold core size. Macromolecules. 2009;42:2696-701.
[400] Seifpour A, Spicer P, Nair N, Jayaraman A. Effect of monomer sequences on conformations of copolymers grafted on spherical nanoparticles: A Monte Carlo simulation study. The Journal of chemical physics. 2010;132:164901.
[401] Pai SS, Hammouda B, Hong K, Pozzo DC, Przybycien TM, Tilton RD. The conformation of the poly (ethylene glycol) chain in mono-PEGylated lysozyme and mono-PEGylated human growth hormone. Bioconjugate Chem. 2011;22:2317-23.
[402] Ferebee R, Hakem IF, Koch A, Chen M, Wu Y, Loh D, et al. Light scattering analysis of mono-and multi-PEGylated bovine serum albumin in solution: Role of composition on structure and interactions. J Phys Chem B. 2016;120:4591-9.
[403] Le Cœur Cm, Combet S, Carrot Gr, Busch P, Teixeira J, Longeville Sp. Conformation of the Poly (ethylene Glycol) chains in DiPEGylated hemoglobin specifically probed by SANS: correlation with PEG length and in vivo efficiency. Langmuir. 2015;31:8402-10.
[404] Yu X, Yue K, Hsieh I-F, Li Y, Dong X-H, Liu C, et al. Giant surfactants provide a versatile platform for sub-10-nm nanostructure engineering. Proc Nat Acad Sci. 2013;110:10078-83.
[405] Zhu X, Wang L, Lin J, Zhang L. Ordered nanostructures self-assembled from block copolymer tethered nanoparticles. Acs Nano. 2010;4:4979-88.
[406] Iacovella CR, Horsch MA, Zhang Z, Glotzer SC. Phase diagrams of self-assembled mono-tethered nanospheres from molecular simulation and comparison to surfactants. Langmuir. 2005;21:9488-94.
[407] Likos C, Löwen H, Watzlawek M, Abbas B, Jucknischke O, Allgaier J, et al. Star polymers viewed as ultrasoft colloidal particles. Phys Rev Lett. 1998;80:4450.
[408] Likos CN. Effective interactions in soft condensed matter physics. Physics Reports. 2001;348:267-439.
[409] Kim JU, Matsen MW. Interaction between polymer-grafted particles. Macromolecules. 2008;41:4435-43.
[410] Voudouris P, Choi J, Dong H, Bockstaller MR, Matyjaszewski K, Fytas G. Effect of Shell Architecture on the Static and Dynamic Properties of Polymer-Coated Particles in Solution. Macromolecules. 2009;42:2721-8.
[411] Goel V, Pietrasik J, Dong H, Sharma J, Matyjaszewski K, Krishnamoorti R. Structure of polymer tethered highly grafted nanoparticles. Macromolecules. 2011;44:8129-35.
[412] Modica KJ, Martin TB, Jayaraman A. Effect of polymer architecture on the structure and interactions of polymer grafted particles: theory and simulations. Macromolecules. 2017;50:4854-66.
[413] Watzlawek M, Likos CN, Löwen H. Phase diagram of star polymer solutions. Phys Rev Lett. 1999;82:5289.
[414] Iacovella CR, Glotzer SC. Complex crystal structures formed by the self-assembly of ditethered nanospheres. Nano Lett. 2009;9:1206-11.
[415] Jayaraman A, Schweizer KS. Effect of the number and placement of polymer tethers on the structure of concentrated solutions and melts of hybrid nanoparticles. Langmuir. 2008;24:11119-30.

[416] Choueiri RM, Galati E, Thérien-Aubin H, Klinkova A, Larin EM, Querejeta-Fernández A, et al. Surface patterning of nanoparticles with polymer patches. Nature. 2016;538:79.
[417] Koerner H, Drummy LF, Benicewicz B, Li Y, Vaia RA. Nonisotropic self-organization of single-component hairy nanoparticle assemblies. ACS Macro Lett. 2013;2:670-6.
[418] Midya J, Cang Y, Egorov SA, Matyjaszewski K, Bockstaller MR, Nikoubashman A, et al. Disentangling the Role of Chain Conformation on the Mechanics of Polymer Tethered Particle Materials. Nano Lett. 2019;19:2715-22.
[419] Leibler L. Theory of microphase separation in block copolymers. Macromolecules. 1980;13:1602-17.
[420] Hore MJ. Polymers on nanoparticles: structure & dynamics. Soft matter. 2019;15:1120-34.
[421] Buenning E, Jestin J, Huang Y, Benicewicz BC, Durning CJ, Kumar SK. Location of imbibed solvent in polymer-grafted nanoparticle membranes. ACS Macro Lett. 2018;7:1051-5.
[422] Koerner H, Opsitnick E, Grabowski CA, Drummy LF, Hsiao M-S, Che J, et al. Physical aging and glass transition of hairy nanoparticle assemblies. J Polym Sci, Part B: Polym Phys. 2016;54:319-30.
[423] Cang Y, Reuss AN, Lee J, Yan J, Zhang J, Alonso-Redondo E, et al. Thermomechanical Properties and Glass Dynamics of Polymer-Tethered Colloidal Particles and Films. Macromolecules. 2017;50:8658-69.
[424] Voudouris P, Choi J, Gomopoulos N, Sainidou R, Dong H, Matyjaszewski K, et al. Anisotropic elasticity of quasi-one-component polymer nanocomposites. ACS nano. 2011;5:5746-54.
[425] Schmitt M, Choi J, Hui CM, Chen B, Korkmaz E, Yan J, et al. Processing fragile matter: Effect of polymer graft modification on the mechanical properties and processibility of (nano-) particulate solids. Soft matter. 2016;12:3527-37.
[426] Lee J, Wang Z, Zhang J, Yan J, Deng T, Matyjaszewski K, et al. Molecular Parameters Governing the Elastic Properties of Brush Particle Films. Macromolecules. 2019.
[427] Podsiadlo P, Krylova G, Lee B, Critchley K, Gosztola DJ, Talapin DV, et al. The role of order, nanocrystal size, and capping ligands in the collective mechanical response of three-dimensional nanocrystal solids. J Am Chem Soc. 2010;132:8953-60.
[428] Schneider D, Schmitt M, Hui CM, Sainidou R, Rembert P, Matyjaszewski K, et al. Role of Polymer Graft Architecture on the Acoustic Eigenmode Formation in Densely Polymer-Tethered Colloidal Particles. ACS Macro Lett. 2014;3:1059-63.
[429] Kramer EJ, Berger LL. Fundamental processes of craze growth and fracture. Berlin, Heidelberg: Springer Berlin Heidelberg; 1990. p. 1-68.
[430] Henkee CS, Kramer EJ. Loss of entanglement density during crazing. Journal of materials science. 1986;21:1398-404.
[431] Tchoul MN, Fillery SP, Koerner H, Drummy LF, Oyerokun FT, Mirau PA, et al. Assemblies of titanium dioxide-polystyrene hybrid nanoparticles for dielectric applications. Chem Mater. 2010;22:1749-59.
[432] Choi J, Dong H, Matyjaszewski K, Bockstaller MR. Flexible Particle Array Structures by Controlling Polymer Graft Architecture. J Am Chem Soc. 2010;132:12537-9.
[433] Schmitt M, Zhang J, Lee J, Lee B, Ning X, Zhang R, et al. Polymer ligand–induced autonomous sorting and reversible phase separation in binary particle blends. Science advances. 2016;2:e1601484.
[434] Russell K, Tobolsky A. Thermal Initiation of Styrene Polymerization. J Am Chem Soc. 1953;75:5052-4.

[435] Tchoul MN, Dalton M, Tan L-S, Dong H, Hui CM, Matyjaszewski K, et al. Enhancing the fraction of grafted polystyrene on silica hybrid nanoparticles. Polymer. 2012;53:79-86.
[436] Schmitt M, Hui CM, Urbach Z, Yan J, Matyjaszewski K, Bockstaller MR. Tailoring structure formation and mechanical properties of particle brush solids via homopolymer addition. Faraday Discuss. 2016;186:17-30.
[437] Gast AP, Leibler L. Interactions of sterically stabilized particles suspended in a polymer solution. Macromolecules. 1986;19:686-91.
[438] Meng D, Kumar SK, D. Lane JM, Grest GS. Effective interactions between grafted nanoparticles in a polymer matrix. Soft Matter. 2012;8:5002-10.
[439] Fowler ME, Barlow JW, Paul DR. Kinetics of adhesion development at PMMA-SAN interfaces. Polymer. 1987;28:2145-50.
[440] Paul DR. Polymer-polymer interactions. Pure Appl Chem1995. p. 977.
[441] Dang A, Ojha S, Hui CM, Mahoney C, Matyjaszewski K, Bockstaller MR. High-Transparency Polymer Nanocomposites Enabled by Polymer-Graft Modification of Particle Fillers. Langmuir. 2014;30:14434-42.
[442] Bombalski L, Dong H, Listak J, Matyjaszewski K, Bockstaller MR. Null - Scattering Hybrid Particles Using Controlled Radical Polymerization. Adv Mater. 2007;19:4486-90.
[443] Garnett JCM. Colours in Metal Glasses and in Metallic Films. Philosophical Transactions of the Royal Society of London A: Mathematical, Physical and Engineering Sciences. 1904;203:385-420.
[444] Akcora P, Liu H, Kumar SK, Moll J, Li Y, Benicewicz BC, et al. Anisotropic self-assembly of spherical polymer-grafted nanoparticles. Nat Mater. 2009;8:354-9.
[445] Pryamtisyn V, Ganesan V, Panagiotopoulos AZ, Liu H, Kumar SK. Modeling the anisotropic self-assembly of spherical polymer-grafted nanoparticles. The Journal of Chemical Physics. 2009;131:221102.
[446] Keng PY, Shim I, Korth BD, Douglas JF, Pyun J. Synthesis and Self-Assembly of Polymer-Coated Ferromagnetic Nanoparticles. ACS Nano. 2007;1:279-92.
[447] Charlesby A, Morris J, Montague P. Mechanisms of reinforcement of silicone rubbers crosslinked by radiation. Journal of Polymer Science Part C: Polymer Symposia. 1967;16:4505-13.
[448] Novak BM. Hybrid Nanocomposite Materials—between inorganic glasses and organic polymers. Adv Mater. 1993;5:422-33.
[449] Moll JF, Akcora P, Rungta A, Gong S, Colby RH, Benicewicz BC, et al. Mechanical Reinforcement in Polymer Melts Filled with Polymer Grafted Nanoparticles. Macromolecules. 2011;44:7473-7.
[450] Akcora P, Kumar SK, Moll J, Lewis S, Schadler LS, Li Y, et al. "Gel-like" Mechanical Reinforcement in Polymer Nanocomposite Melts. Macromolecules. 2010;43:1003-10.
[451] Maillard D, Kumar SK, Fragneaud B, Kysar JW, Rungta A, Benicewicz BC, et al. Mechanical properties of thin glassy polymer films filled with spherical polymer-grafted nanoparticles. Nano Lett. 2012;12:3909-14.
[452] Shah T, Gupta C, Ferebee RL, Bockstaller MR, Washburn NR. Extraordinary toughening and strengthening effect in polymer nanocomposites using lignin-based fillers synthesized by ATRP. Polymer. 2015;72:406-12.
[453] Kubiak JM, Yan J, Pietrasik J, Matyjaszewski K. Toughening PMMA with fillers containing polymer brushes synthesized via atom transfer radical polymerization (ATRP). Polymer. 2017;117:48-53.

[454] Maldovan M. Sound and heat revolutions in phononics. Nature. 2013;503:209.
[455] Alonso-Redondo E, Schmitt M, Urbach Z, Hui CM, Sainidou R, Rembert P, et al. A new class of tunable hypersonic phononic crystals based on polymer-tethered colloids. Nat Commun. 2015;6:8309.
[456] Briscoe WH, Titmuss S, Tiberg F, Thomas RK, McGillivray DJ, Klein J. Boundary lubrication under water. Nature. 2006;444:191.
[457] Nomura A, Okayasu K, Ohno K, Fukuda T, Tsujii Y. Lubrication Mechanism of Concentrated Polymer Brushes in Solvents: Effect of Solvent Quality and Thereby Swelling State. Macromolecules. 2011;44:5013-9.
[458] Bielecki RM, Benetti EM, Kumar D, Spencer ND. Lubrication with oil-compatible polymer brushes. Tribology Letters. 2012;45:477-87.
[459] Banquy X, Burdyńska J, Lee DW, Matyjaszewski K, Israelachvili J. Bioinspired Bottle-Brush Polymer Exhibits Low Friction and Amontons-like Behavior. J Am Chem Soc. 2014;136:6199-202.
[460] Faivre J, Shrestha BR, Xie G, Delair T, David L, Matyjaszewski K, et al. Unraveling the Correlations between Conformation, Lubrication, and Chemical Stability of Bottlebrush Polymers at Interfaces. Biomacromolecules. 2017;18:4002-10.
[461] Liu G, Liu Z, Li N, Wang X, Zhou F, Liu W. Hairy Polyelectrolyte Brushes-Grafted Thermosensitive Microgels as Artificial Synovial Fluid for Simultaneous Biomimetic Lubrication and Arthritis Treatment. ACS Appl Mater Interfaces. 2014;6:20452-63.
[462] Wright RAE, Wang K, Qu J, Zhao B. Oil-Soluble Polymer Brush Grafted Nanoparticles as Effective Lubricant Additives for Friction and Wear Reduction. Angew Chem Int Ed. 2016;55:8656-60.
[463] Seymour BT, Wright RAE, Parrott AC, Gao H, Martini A, Qu J, et al. Poly(alkyl methacrylate) Brush-Grafted Silica Nanoparticles as Oil Lubricant Additives: Effects of Alkyl Pendant Groups on Oil Dispersibility, Stability, and Lubrication Property. ACS Appl Mater Interfaces. 2017;9:25038-48.
[464] Kawata Y, Yamamoto T, Kihara H, Ohno K. Dual Self-Healing Abilities of Composite Gels Consisting of Polymer-Brush-Afforded Particles and an Azobenzene-Doped Liquid Crystal. ACS Appl Mater Interfaces. 2015;7:4185-91.
[465] Williams GA, Ishige R, Cromwell OR, Chung J, Takahara A, Guan Z. Mechanically Robust and Self-Healable Superlattice Nanocomposites by Self-Assembly of Single-Component "Sticky" Polymer-Grafted Nanoparticles. Adv Mater. 2015;27:3934-41.
[466] Bohren CF, Huffman DR. Absorption and scattering of light by small particles: John Wiley & Sons; 2008.
[467] Small A, Hong S, Pine D. Scattering properties of core–shell particles in plastic matrices. J Polym Sci, Part B: Polym Phys. 2005;43:3534-48.
[468] Sato T, Morinaga T, Marukane S, Narutomi T, Igarashi T, Kawano Y, et al. Novel Solid - State Polymer Electrolyte of Colloidal Crystal Decorated with Ionic - Liquid Polymer Brush. Adv Mater. 2011;23:4868-72.
[469] Lee WA, Pernodet N, Li B, Lin CH, Hatchwell E, Rafailovich MH. Multicomponent polymer coating to block photocatalytic activity of TiO2 nanoparticles. Chem Commun. 2007:4815-7.
[470] Du J, Sun H. Polymer/TiO2 Hybrid Vesicles for Excellent UV Screening and Effective Encapsulation of Antioxidant Agents. ACS Appl Mater Interfaces. 2014;6:13535-41.

[471] Xiao J, Chen W, Wang F, Du J. Polymer/TiO2 Hybrid Nanoparticles with Highly Effective UV-Screening but Eliminated Photocatalytic Activity. Macromolecules. 2013;46:375-83.
[472] Farmer SC, Patten TE. Photoluminescent Polymer/Quantum Dot Composite Nanoparticles. Chem Mater. 2001;13:3920-6.
[473] Zorn M, Bae WK, Kwak J, Lee H, Lee C, Zentel R, et al. Quantum Dot−Block Copolymer Hybrids with Improved Properties and Their Application to Quantum Dot Light-Emitting Devices. ACS Nano. 2009;3:1063-8.
[474] Tao P, Li Y, Siegel RW, Schadler LS. Transparent luminescent silicone nanocomposites filled with bimodal PDMS-brush-grafted CdSe quantum dots. J Mater Chem C. 2013;1:86-94.
[475] Yeh J-M, Liou S-J, Lai C-Y, Wu P-C, Tsai T-Y. Enhancement of Corrosion Protection Effect in Polyaniline via the Formation of Polyaniline−Clay Nanocomposite Materials. Chem Mater. 2001;13:1131-6.
[476] Bourbigot S, Devaux E, Flambard X. Flammability of polyamide-6/clay hybrid nanocomposite textiles. Polym Degrad Stab. 2002;75:397-402.
[477] Priolo MA, Gamboa D, Grunlan JC. Transparent Clay−Polymer Nano Brick Wall Assemblies with Tailorable Oxygen Barrier. ACS Appl Mater Interfaces. 2010;2:312-20.
[478] Tsai T-Y, Li C-H, Chang C-H, Cheng W-H, Hwang C-L, Wu R-J. Preparation of Exfoliated Polyester/Clay Nanocomposites. Adv Mater. 2005;17:1769-73.
[479] Priolo MA, Gamboa D, Holder KM, Grunlan JC. Super Gas Barrier of Transparent Polymer−Clay Multilayer Ultrathin Films. Nano Lett. 2010;10:4970-4.
[480] Kim D, Park S, Lee JH, Jeong YY, Jon S. Antibiofouling Polymer-Coated Gold Nanoparticles as a Contrast Agent for in Vivo X-ray Computed Tomography Imaging. J Am Chem Soc. 2007;129:7661-5.
[481] Oh MH, Lee N, Kim H, Park SP, Piao Y, Lee J, et al. Large-Scale Synthesis of Bioinert Tantalum Oxide Nanoparticles for X-ray Computed Tomography Imaging and Bimodal Image-Guided Sentinel Lymph Node Mapping. J Am Chem Soc. 2011;133:5508-15.
[482] Rabin O, Manuel Perez J, Grimm J, Wojtkiewicz G, Weissleder R. An X-ray computed tomography imaging agent based on long-circulating bismuth sulphide nanoparticles. Nat Mater. 2006;5:118.
[483] Peng C, Zheng L, Chen Q, Shen M, Guo R, Wang H, et al. PEGylated dendrimer-entrapped gold nanoparticles for in vivo blood pool and tumor imaging by computed tomography. Biomaterials. 2012;33:1107-19.
[484] Yan J, Li S, Cartieri F, Wang Z, Hitchens TK, Leonardo J, et al. Iron Oxide Nanoparticles with Grafted Polymeric Analogue of Dimethyl Sulfoxide as Potential Magnetic Resonance Imaging Contrast Agents. ACS Appl Mater Interfaces. 2018;10:21901-8.
[485] Park YC, Smith JB, Pham T, Whitaker RD, Sucato CA, Hamilton JA, et al. Effect of PEG molecular weight on stability, T2 contrast, cytotoxicity, and cellular uptake of superparamagnetic iron oxide nanoparticles (SPIONs). Colloids and Surfaces B: Biointerfaces. 2014;119:106-14.
[486] Lee H, Lee E, Kim DK, Jang NK, Jeong YY, Jon S. Antibiofouling Polymer-Coated Superparamagnetic Iron Oxide Nanoparticles as Potential Magnetic Resonance Contrast Agents for in Vivo Cancer Imaging. J Am Chem Soc. 2006;128:7383-9.
[487] Yoo M-K, Park I-K, Lim H-T, Lee S-J, Jiang H-L, Kim Y-K, et al. Folate–PEG–superparamagnetic iron oxide nanoparticles for lung cancer imaging. Acta Biomaterialia. 2012;8:3005-13.

[488] Sun C, Sze R, Zhang M. Folic acid-PEG conjugated superparamagnetic nanoparticles for targeted cellular uptake and detection by MRI. Journal of Biomedical Materials Research Part A. 2006;78A:550-7.
[489] Beija M, Li Y, Duong HT, Laurent S, Elst LV, Muller RN, et al. Polymer–gold nanohybrids with potential use in bimodal MRI/CT: enhancing the relaxometric properties of Gd(iii) complexes. J Mater Chem. 2012;22:21382-6.
[490] Lee N, Cho HR, Oh MH, Lee SH, Kim K, Kim BH, et al. Multifunctional Fe3O4/TaOx Core/Shell Nanoparticles for Simultaneous Magnetic Resonance Imaging and X-ray Computed Tomography. J Am Chem Soc. 2012;134:10309-12.
[491] Xiao Q, Bu W, Ren Q, Zhang S, Xing H, Chen F, et al. Radiopaque fluorescence-transparent TaOx decorated upconversion nanophosphors for in vivo CT/MR/UCL trimodal imaging. Biomaterials. 2012;33:7530-9.
[492] Wang Y, Bansal V, Zelikin AN, Caruso F. Templated Synthesis of Single-Component Polymer Capsules and Their Application in Drug Delivery. Nano Lett. 2008;8:1741-5.
[493] Cui J, Yan Y, Wang Y, Caruso F. Templated Assembly of pH-Labile Polymer-Drug Particles for Intracellular Drug Delivery. Adv Funct Mater. 2012;22:4718-23.
[494] Brown SD, Nativo P, Smith J-A, Stirling D, Edwards PR, Venugopal B, et al. Gold Nanoparticles for the Improved Anticancer Drug Delivery of the Active Component of Oxaliplatin. J Am Chem Soc. 2010;132:4678-84.
[495] Xu H, Cheng L, Wang C, Ma X, Li Y, Liu Z. Polymer encapsulated upconversion nanoparticle/iron oxide nanocomposites for multimodal imaging and magnetic targeted drug delivery. Biomaterials. 2011;32:9364-73.
[496] Nasongkla N, Bey E, Ren J, Ai H, Khemtong C, Guthi JS, et al. Multifunctional Polymeric Micelles as Cancer-Targeted, MRI-Ultrasensitive Drug Delivery Systems. Nano Lett. 2006;6:2427-30.
[497] Lee J-H, Lee K, Moon SH, Lee Y, Park TG, Cheon J. All-in-One Target-Cell-Specific Magnetic Nanoparticles for Simultaneous Molecular Imaging and siRNA Delivery. Angew Chem Int Ed. 2009;48:4174-9.
[498] Pan B, Cui D, Sheng Y, Ozkan C, Gao F, He R, et al. Dendrimer-Modified Magnetic Nanoparticles Enhance Efficiency of Gene Delivery System. Cancer Research. 2007;67:8156-63.
[499] Majewski AP, Stahlschmidt U, Jérôme V, Freitag R, Müller AHE, Schmalz H. PDMAEMA-Grafted Core–Shell–Corona Particles for Nonviral Gene Delivery and Magnetic Cell Separation. Biomacromolecules. 2013;14:3081-90.
[500] Averick S, Mehl RA, Das SR, Matyjaszewski K. Well-defined biohybrids using reversible-deactivation radical polymerization procedures. J Controlled Release. 2015;205:45-57.
[501] Liu C, Guo J, Yang W, Hu J, Wang C, Fu S. Magnetic mesoporous silica microspheres with thermo-sensitive polymer shell for controlled drug release. J Mater Chem. 2009;19:4764-70.
[502] Liu R, Liao P, Liu J, Feng P. Responsive Polymer-Coated Mesoporous Silica as a pH-Sensitive Nanocarrier for Controlled Release. Langmuir. 2011;27:3095-9.
[503] Li W, Cai X, Kim C, Sun G, Zhang Y, Deng R, et al. Gold nanocages covered with thermally-responsive polymers for controlled release by high-intensity focused ultrasound. Nanoscale. 2011;3:1724-30.
[504] Jain TK, Morales MA, Sahoo SK, Leslie-Pelecky DL, Labhasetwar V. Iron Oxide Nanoparticles for Sustained Delivery of Anticancer Agents. Molecular Pharmaceutics. 2005;2:194-205.

[505] Lee H, Yu MK, Park S, Moon S, Min JJ, Jeong YY, et al. Thermally Cross-Linked Superparamagnetic Iron Oxide Nanoparticles: Synthesis and Application as a Dual Imaging Probe for Cancer in Vivo. J Am Chem Soc. 2007;129:12739-45.
[506] Yang Y, Liu J, Liang C, Feng L, Fu T, Dong Z, et al. Nanoscale Metal–Organic Particles with Rapid Clearance for Magnetic Resonance Imaging-Guided Photothermal Therapy. ACS Nano. 2016;10:2774-81.
[507] Von Maltzahn G, Park J-H, Agrawal A, Bandaru NK, Das SK, Sailor MJ, et al. Computationally guided photothermal tumor therapy using long-circulating gold nanorod antennas. Cancer research. 2009;69:3892-900.
[508] Sharker SM, Lee JE, Kim SH, Jeong JH, In I, Lee H, et al. pH triggered in vivo photothermal therapy and fluorescence nanoplatform of cancer based on responsive polymer-indocyanine green integrated reduced graphene oxide. Biomaterials. 2015;61:229-38.
[509] Kang T, Li F, Baik S, Shao W, Ling D, Hyeon T. Surface design of magnetic nanoparticles for stimuli-responsive cancer imaging and therapy. Biomaterials. 2017;136:98-114.
[510] Wang J, Zhou Z, Wang L, Wei J, Yang H, Yang S, et al. CoFe 2 O 4@ MnFe 2 O 4/polypyrrole nanocomposites for in vitro photothermal/magnetothermal combined therapy. RSC Adv. 2015;5:7349-55.
[511] Espinosa A, Di Corato R, Kolosnjaj-Tabi J, Flaud P, Pellegrino T, Wilhelm C. Duality of Iron Oxide Nanoparticles in Cancer Therapy: Amplification of Heating Efficiency by Magnetic Hyperthermia and Photothermal Bimodal Treatment. ACS Nano. 2016;10:2436-46.
[512] Brazel CS. Magnetothermally-responsive nanomaterials: combining magnetic nanostructures and thermally-sensitive polymers for triggered drug release. Pharm Res. 2009;26:644-56.
[513] Zheng M, Yue C, Ma Y, Gong P, Zhao P, Zheng C, et al. Single-step assembly of DOX/ICG loaded lipid-polymer nanoparticles for highly effective chemo-photothermal combination therapy. ACS nano. 2013;7:2056-67.
[514] Anyaogu KC, Fedorov AV, Neckers DC. Synthesis, Characterization, and Antifouling Potential of Functionalized Copper Nanoparticles. Langmuir. 2008;24:4340-6.
[515] Krystosiak P, Tomaszewski W, Megiel E. High-density polystyrene-grafted silver nanoparticles and their use in the preparation of nanocomposites with antibacterial properties. J Colloid Interface Sci. 2017;498:9-21.
[516] Jennings MC, Minbiole KPC, Wuest WM. Quaternary Ammonium Compounds: An Antimicrobial Mainstay and Platform for Innovation to Address Bacterial Resistance. ACS Infectious Diseases. 2015;1:288-303.
[517] Tiller JC, Liao C-J, Lewis K, Klibanov AM. Designing surfaces that kill bacteria on contact. Proc Nat Acad Sci. 2001;98:5981-5.
[518] Lin J, Tiller JC, Lee SB, Lewis K, Klibanov AM. Insights into bactericidal action of surface-attached poly(vinyl-N-hexylpyridinium) chains. Biotechnol Lett. 2002;24:801-5.
[519] Lee SB, Koepsel RR, Morley SW, Matyjaszewski K, Sun Y, Russell AJ. Permanent, Nonleaching Antibacterial Surfaces. 1. Synthesis by Atom Transfer Radical Polymerization. Biomacromolecules. 2004;5:877-82.
[520] Murata H, Koepsel RR, Matyjaszewski K, Russell AJ. Permanent, non-leaching antibacterial surfaces—2: How high density cationic surfaces kill bacterial cells. Biomaterials. 2007;28:4870-9.

[521] Huang J, Murata H, Koepsel RR, Russell AJ, Matyjaszewski K. Antibacterial Polypropylene via Surface-Initiated Atom Transfer Radical Polymerization. Biomacromolecules. 2007;8:1396-9.
[522] Wang L, Chen YP, Miller KP, Cash BM, Jones S, Glenn S, et al. Functionalised nanoparticles complexed with antibiotic efficiently kill MRSA and other bacteria. Chem Commun. 2014;50:12030-3.
[523] Pageni P, Yang P, Chen YP, Huang Y, Bam M, Zhu T, et al. Charged Metallopolymer-Grafted Silica Nanoparticles for Antimicrobial Applications. Biomacromolecules. 2018;19:417-25.
[524] Kobayashi M, Terayama Y, Yamaguchi H, Terada M, Murakami D, Ishihara K, et al. Wettability and Antifouling Behavior on the Surfaces of Superhydrophilic Polymer Brushes. Langmuir. 2012;28:7212-22.
[525] Yang WJ, Cai T, Neoh K-G, Kang E-T, Dickinson GH, Teo SL-M, et al. Biomimetic Anchors for Antifouling and Antibacterial Polymer Brushes on Stainless Steel. Langmuir. 2011;27:7065-76.
[526] Zhang G, Lu S, Zhang L, Meng Q, Shen C, Zhang J. Novel polysulfone hybrid ultrafiltration membrane prepared with TiO2-g-HEMA and its antifouling characteristics. Journal of Membrane Science. 2013;436:163-73.
[527] Shi H, Yuan L, Wu Y, Liu S. Colorimetric immunosensing via protein functionalized gold nanoparticle probe combined with atom transfer radical polymerization. Biosens Bioelectron. 2011;26:3788-93.
[528] Otsuka H, Akiyama Y, Nagasaki Y, Kataoka K. Quantitative and Reversible Lectin-Induced Association of Gold Nanoparticles Modified with α-Lactosyl-ω-mercapto-poly(ethylene glycol). J Am Chem Soc. 2001;123:8226-30.
[529] Nam J-M, Thaxton CS, Mirkin CA. Nanoparticle-Based Bio-Bar Codes for the Ultrasensitive Detection of Proteins. Science. 2003;301:1884-6.
[530] Fang S, Lee HJ, Wark AW, Corn RM. Attomole Microarray Detection of MicroRNAs by Nanoparticle-Amplified SPR Imaging Measurements of Surface Polyadenylation Reactions. J Am Chem Soc. 2006;128:14044-6.
[531] You C-C, Miranda OR, Gider B, Ghosh PS, Kim I-B, Erdogan B, et al. Detection and identification of proteins using nanoparticle–fluorescent polymer 'chemical nose' sensors. Nature Nanotechnology. 2007;2:318.
[532] Li D, Dunlap JR, Zhao B. Thermosensitive Water-Dispersible Hairy Particle-Supported Pd Nanoparticles for Catalysis of Hydrogenation in an Aqueous/Organic Biphasic System. Langmuir. 2008;24:5911-8.
[533] Wang Y, Wei G, Zhang W, Jiang X, Zheng P, Shi L, et al. Responsive catalysis of thermoresponsive micelle-supported gold nanoparticles. J Mol Catal A: Chem. 2007;266:233-8.
[534] He H, Averick S, Mandal P, Ding H, Li S, Gelb J, et al. Multifunctional Hydrogels with Reversible 3D Ordered Macroporous Structures. Advanced Science. 2015;2:1500069.
[535] Beija M, Palleau E, Sistach S, Zhao X, Ressier L, Mingotaud C, et al. Control of the catalytic properties and directed assembly on surfaces of MADIX/RAFT polymer-coated gold nanoparticles by tuning polymeric shell charge. J Mater Chem. 2010;20:9433-42.
[536] Mogha NK, Gosain S, Masram DT. Gold nanoworms immobilized graphene oxide polymer brush nanohybrid for catalytic degradation studies of organic dyes. Appl Surf Sci. 2017;396:1427-34.

[537] Kong H, Song J, Jang J. Photocatalytic Antibacterial Capabilities of TiO2−Biocidal Polymer Nanocomposites Synthesized by a Surface-Initiated Photopolymerization. Environmental Science & Technology. 2010;44:5672-6.
[538] Ulku I, Morlet-Savary F, Lalevée J, Yagci Acar H. Homogenous photopolymerization of acrylic monomers initiated with ZnO-methacrylate in non-aqueous medium and production of luminescent nanocomposites. Polym Chem. 2018;9:828-33.
[539] Yoon M, Lee J-E, Jang YJ, Lim JW, Rani A, Kim DH. Comprehensive Study on the Controlled Plasmon-Enhanced Photocatalytic Activity of Hybrid Au/ZnO Systems Mediated by Thermoresponsive Polymer Linkers. ACS Appl Mater Interfaces. 2015;7:21073-81.
[540] Zhao B, Jiang X, Li D, Jiang X, O'Lenick TG, Li B, et al. Hairy particle-supported 4-N,N-dialkylaminopyridine: An efficient and recyclable nucleophilic organocatalyst. J Polym Sci, Part A: Polym Chem. 2008;46:3438-46.
[541] Jiang X, Wang B, Li CY, Zhao B. Thermosensitive polymer brush-supported 4-N,N-dialkylaminopyridine on silica particles as catalyst for hydrolysis of an activated ester in aqueous buffers: Comparison of activity with linear polymer-supported version and effect of LCST transition. J Polym Sci, Part A: Polym Chem. 2009;47:2853-70.
[542] Lewis TJ. Interfaces and nanodielectrics are synonymous. Proceedings of the 2004 IEEE International Conference on Solid Dielectrics, 2004 ICSD 20042004. p. 792-5 Vol.2.
[543] Nelson JK. Dielectric Polymer Nanocomposites: Springer US; 2009.
[544] Yan J, Pietrasik J, Wypych-Puszkarz A, Ciekanska M, Matyjaszewski K. Synthesis of high k nanoparticles by CRP. In: Beata Łuszczyńska, Matyjaszewski K, Ulański J, editors. Solution-Processable Components for Organic Electronic Devices. Weinheim Wiley-VCH; 2019. p. 181-226.
[545] Grabowski CA, Fillery SP, Koerner H, Tchoul M, Drummy L, Beier CW, et al. Dielectric performance of high permitivity nanocomposites: impact of polystyrene grafting on BaTiO3 and TiO2. Nanocomposites. 2016;2:117-24.
[546] Grabowski CA, Koerner H, Meth JS, Dang A, Hui CM, Matyjaszewski K, et al. Performance of Dielectric Nanocomposites: Matrix-Free, Hairy Nanoparticle Assemblies and Amorphous Polymer–Nanoparticle Blends. ACS Appl Mater Interfaces. 2014;6:21500-9.
[547] Xie L, Huang X, Wu C, Jiang P. Core-shell structured poly(methyl methacrylate)/BaTiO3 nanocomposites prepared by in situ atom transfer radical polymerization: a route to high dielectric constant materials with the inherent low loss of the base polymer. J Mater Chem. 2011;21:5897-906.
[548] Paniagua SA, Kim Y, Henry K, Kumar R, Perry JW, Marder SR. Surface-Initiated Polymerization from Barium Titanate Nanoparticles for Hybrid Dielectric Capacitors. ACS Appl Mater Interfaces. 2014;6:3477-82.
[549] Wahlander M, Nilsson F, Andersson RL, Sanchez CC, Taylor N, Carlmark A, et al. Tailoring dielectric properties using designed polymer-grafted ZnO nanoparticles in silicone rubber. J Mater Chem A. 2017;5:14241-58.
[550] Yang K, Huang X, Zhu M, Xie L, Tanaka T, Jiang P. Combining RAFT Polymerization and Thiol–Ene Click Reaction for Core–Shell Structured Polymer@BaTiO3 Nanodielectrics with High Dielectric Constant, Low Dielectric Loss, and High Energy Storage Capability. ACS Appl Mater Interfaces. 2014;6:1812-22.
[551] Yang K, Huang X, Huang Y, Xie L, Jiang P. Fluoro-Polymer@BaTiO3 Hybrid Nanoparticles Prepared via RAFT Polymerization: Toward Ferroelectric Polymer

Nanocomposites with High Dielectric Constant and Low Dielectric Loss for Energy Storage Application. Chem Mater. 2013;25:2327-38.
[552] Zhang X, Chen H, Ma Y, Zhao C, Yang W. Preparation and dielectric properties of core–shell structural composites of poly(1H,1H,2H,2H-perfluorooctyl methacrylate)@BaTiO3 nanoparticles. Appl Surf Sci. 2013;277:121-7.
[553] Zhang X, Zhao S, Wang F, Ma Y, Wang L, Chen D, et al. Improving dielectric properties of BaTiO3/poly(vinylidene fluoride) composites by employing core-shell structured BaTiO3@Poly(methylmethacrylate) and BaTiO3@Poly(trifluoroethyl methacrylate) nanoparticles. Appl Surf Sci. 2017;403:71-9.
[554] Crippa M, Bianchi A, Cristofori D, D'Arienzo M, Merletti F, Morazzoni F, et al. High dielectric constant rutile-polystyrene composite with enhanced percolative threshold. J Mater Chem C. 2013;1:484-92.
[555] Zhang W, Zhou Z, Li Q, Chen G-X. Controlled Dielectric Properties of Polymer Composites from Coating Multiwalled Carbon Nanotubes with Octa-acrylate Silsesquioxane through Diels–Alder Cycloaddition and Atom Transfer Radical Polymerization. Industrial & Engineering Chemistry Research. 2014;53:6699-707.
[556] Chen Z, Xie L, Huang X, Li S, Jiang P. Achieving large dielectric property improvement in polymer/carbon nanotube composites by engineering the nanotube surface via atom transfer radical polymerization. Carbon. 2015;95:895-903.
[557] Song S, Zhai Y, Zhang Y. Bioinspired Graphene Oxide/Polymer Nanocomposite Paper with High Strength, Toughness, and Dielectric Constant. ACS Appl Mater Interfaces. 2016;8:31264-72.
[558] Chen Y, Zhang S, Liu X, Pei Q, Qian J, Zhuang Q, et al. Preparation of Solution-Processable Reduced Graphene Oxide/Polybenzoxazole Nanocomposites with Improved Dielectric Properties. Macromolecules. 2015;48:365-72.
[559] Zhang J, Song Y, Kopeć M, Lee J, Wang Z, Liu S, et al. Facile Aqueous Route to Nitrogen-Doped Mesoporous Carbons. J Am Chem Soc. 2017;139:12931-4.
[560] Zhang J, Yuan R, Natesakhawat S, Wang Z, Zhao Y, Yan J, et al. Individual Nanoporous Carbon Spheres with High Nitrogen Content from Polyacrylonitrile Nanoparticles with Sacrificial Protective Layers. ACS Appl Mater Interfaces. 2017;9:37804-12.
[561] Zhang J, Song Y, Zhao Y, Zhao S, Yan J, Lee J, et al. Organosilica with Grafted Polyacrylonitrile Brushes for High Surface Area Nitrogen-Enriched Nanoporous Carbons. Chem Mater. 2018;30:2208-12.
[562] Yan J, Malakooti MH, Lu Z, Wang Z, Kazem N, Pan C, et al. Solution processable liquid metal nanodroplets by surface-initiated atom transfer radical polymerization. Nature Nanotechnology. 2019.
[563] Pan C, Markvicka EJ, Malakooti MH, Yan J, Hu L, Matyjaszewski K, et al. A Liquid-Metal–Elastomer Nanocomposite for Stretchable Dielectric Materials. Adv Mater. 2019;31:1900663.
[564] Markvicka EJ, Bartlett MD, Huang X, Majidi C. An autonomously electrically self-healing liquid metal–elastomer composite for robust soft-matter robotics and electronics. Nat Mater. 2018:1.
[565] Malakooti MH, Kazem N, Yan J, Pan C, Markvicka EJ, Matyjaszewski K, et al. Liquid Metal Supercooling for Low-Temperature Thermoelectric Wearables. Adv Funct Mater.1906098.